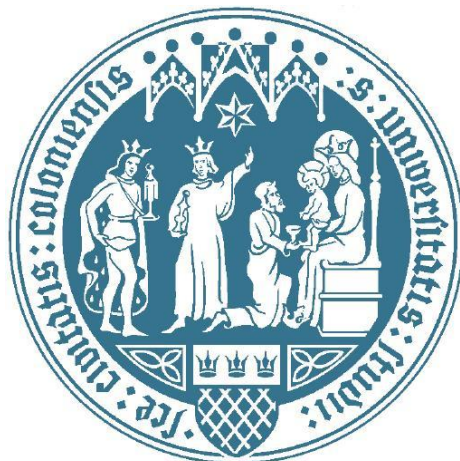# GMS proteins shield endocellular membranes from accumulation of effector Immunity-Related GTPases

Inaugural-Dissertation
zur
Erlangung des Doktorgrades
der Mathematisch-Naturwissenschaftlichen Fakultät
der Universität zu Köln

vorgelegt von
Jelena Marić
aus Novi Sad, Serbien
Köln 2014

Berichterstatter: Prof. Dr. Jonathan Howard

Prof. Dr. Kay Hofmann

Tag der mündlichen Prüfung: 26.1.2015

The scientists of today think deeply instead of clearly.

One must be sane to think clearly, but one can think deeply and be quite insane.

Nikola Tesla

Table of contents

LIST OF ABREVIATIONS

AB	Antibody
ADAR1	Adenosine deaminase, RN-specific 1
APOBEC3	Apolipoproten B mRNA-editing enzyme, catalytic polypeptide 3
AS	Antiserum
BAF	Bafilomycin
BCA	bicinchoninic acid
BMDM	Bone marrow derived macrophage
BrdU	Bromodeoxyuridine
BSA	Bovine serun albumin
CFSE	Carboxyfluorescein succinimidyl ester
DALIS	Dendritic cell aggresome like structures
DAPI	4',6-Diamidino-2-phenylindol
DDC	Diaphragm-derived cells
DMEM	Dulbecco's modified Eagle's medium
DMSO	Dimethyl-sufoxide
DNA	Desoxyribonucleic acid
DUOX	Dual oxydases
EAE	Experimental autoimmune encephalomyelitis
ECL	Enhanced chemiluminiscence
EDTA	Ethylenediaminetetraacetic acid
ER	Endoplasmic reticulum
FCS	Fetal calf serum
GAP	GTPase activating proteins
GBP	Guanylate-binding protein
GDI	Guanine nucleotide dissociation inhibitors
GDP	Guanosine diphosphate
GEF	Guanine nucleotide exchange factors
GFP	Green fluorescent protein
GM130	Cis-Golgi matrix protein
GS	Gene Switch
GTP	Gunosine triphosphate
HRP	Horse radish peroxidase
HSC	Hematopoetic stem cells
IDO	Indoleamine 2,3-dioxygenase
IF	Immunofluorescence
IFITM	IFN-inducible transmembrane proteins
IFN	Interferon
IRF	IFN Regulatory Factor
IRGs	Immunity-related GTPases
ISGF3	IFN-Stimulated Gene Factor 3
ISRE	IFN-Stimulated response element
JAK	Janus kinase
KO	Knock out
LAMP1	Lysosomal-Associated Membrane Protein 1
LC3	Microtubule associated protein 1 light chain 3

LD	Lipid droplet
LMP	Lysosomal membrane permeabilization
LPS	Lipopolysaccharide
MEF	Mouse embryonic fibroblast
MIF	Mifepristone
NOX	NAPDH oxidases
NRAMP-1	Natural Resistance-Associated Macrophage Protein-1
OAS	2'-5' oligoadenylate synthases
ORF	Open reading frame
OVA	Ovalbumine
PAMPs	Pathogen associated molecular patterns
PBS	Phosphate buffer saline
PhaCo	Phase contrast
PI	Propidium iodide
PitIns	Phosphatydil inositol
PMCAO	Permanent middle cerebral artery occlusion
PRR	Pattern recognition receptor
PVM	Parasitophorous vacuolar membrane
RAP	Rapamycin
RIPA	Radio-Immunoprecipitation Assay
RNA	Ribonucleic acid
RNS	Ractive nitrogen species
ROS	Reactive oxygen species
RPMI	Roswell Park Memorial Institute medium
SDS	Sodium dodecyl sulphate
SDS-PAGE	Sodium dodecyl sulphate polyacrylamide gel electrophoresis
STAT	Signal Transducer and Activator of Transcription
TBST	Tris-Buffered Saline and Tween 20
TLR	Toll-like receptor
TNFα	Tumor necrosis factor alpha
TRIM	Tripartite-motif
TYK 2	Tyrosine kinase 2
VLIG	Very Large Inducible GTPases
WB	Western blot
WT	Wild type
YFP	Yellow fluoresent protein

1. INTRODUCTION

1.1. Host recognition of pathogen

For a long time, mechanisms of action that are used by organisms causing infectious diseases, collectively called pathogens, have been a target of investigation. However, mechanisms that evolved to protect host from the pathogen infection, called immune responses, are also extensively researched.

In order to successfully invade the host, pathogens need to overcome host's mechanisms of protection. The first lines of defense that pathogens need to face during infection are the surface barriers of the host. These barriers can be: mechanical, like skin or cuticle; chemical, like gastric acid or defensins; and biological, like commensal flora. The second line of immunity represents non-specific, but relatively immediate defense, named the innate immune system. The third layer of defense comprises the more sophisticated adaptive immune system that is specific for the particular pathogen and provides long lasting protection once activated (Reviewed in (Murphy et al., 2012)).

Vertebrate host defense is often seen as a defense by specialized sets of professional immune cells. However, this view greatly underestimates a capacity of most cell lineages, the majority of which fall outside of traditional immune system cells, to defend themselves against infection. This ancient and ubiquitous form of host protection is called cell-autonomous immunity (Howard, 2007) (Randow et al., 2013).

Discrimination between the components of the host and the pathogen is crucial for host defense. Charles Janeway and colleagues proposed three strategies that vertebrates use to distinguish pathogens: (1) recognition of "microbial non-self", (2) recognition of "induced or altered self" and (3) recognition of "missing self" (Medzhitov and Janeway, 2002).

Recognition of "microbial non-self" is based on the detection of conserved molecular patterns that are essential microbial products, but are not produced by the host, named pathogen associated molecular patterns (PAMPs) (reviewed in (Medzhitov and Janeway, 2002)). Lipopolysaccharides (LPS) or peptidoglycan that are exclusively produced by bacteria are prominent examples of PAMPs. The PAMPs are recognized by the receptors of the innate immune system called pattern recognition receptors (PRRs), like for example Toll-like receptors (TLRs) (Trinchieri and Sher, 2007) (Kawai and Akira, 2010).

Recognition of "induced self" is based on detection of markers of abnormal self that are expressed only upon infection and can tag the affected cells for elimination by the immune system. For example, viral infection is followed by cellular transformation and expression of particular self-proteins that can be recognized by the immune system as altered self (Medzhitov and Janeway, 2002).

Recognition of "missing self" relies on the detection of markers of normal self, namely gene products and products of metabolic pathways that are unique to the host and absent from the pathogen. Therefore, host immunity effectors can target non-labeled structures for destruction (Medzhitov and Janeway, 2002) (Coers, 2013). The most prominent example of the "missing self" recognition are natural killer cells (NK cells). MHC class I protein is constitutively expressed on all nucleated cells and often downregulated as a consequence of viral infection. Hence, recognition of cells lacking MHC class I proteins on the surface targets them for destruction by NK cells (Karre et al., 1986).

IFNγ-inducible Immunity-related GTPases (IRGs), which are further investigated in this study, represent one of the weapons of cell-autonomous immunity in vertebrates (Reviewed in (Martens and Howard, 2006)). Recently, it has been proposed that IRGs also recognize the pathogens by the "missing self" principle (Martens, 2004) (Hunn and Howard, 2010) (Coers, 2013) (da Fonseca Ferreira-da-Silva et al., 2014). Therefore, further properties of these interferon-stimulated genes will be discussed.

1.2.   Interferon-stimulated genes in cell-autonomous immunity

Interferons (IFN) are pro-inflammatory cytokines secreted by immune and non-immune cells in a brief and self limiting manner. According to their sequence homology and receptor specificity, interferons can be classified into three groups: Type I interferons, which include IFNα, IFNβ, IFNω, IFNκ, IFNε, IFNδ and IFNτ; Type II interferon, which includes only IFNγ; and Type III interferons encompassing IFNλ1, IFNλ2 and IFNλ3. Type I Interferons are produced by almost every cell type, while IFNγ, a type II interferon, is mainly produced by professional immune cells (Reviewed in (Borden et al., 2007)).

Interferons are among the most potent vertebrate-derived signals for mobilizing antimicrobial effector functions against intracellular pathogens (Nathan et al., 1983) (Schroder et al., 2004). Up to now, more than 2000 human and mouse interferon-stimulated

genes (ISG) have been identified (Hertzog et al., 2011) (Rusinova et al., 2013), with most of them still being uncharacterized.

Interferons induce cell-autonomous host defense genes through three receptor complexes with high affinities for their ligands, which are named Interferon Type I, Type II and Type III receptor complexes. Following receptor-ligand engagement, Signal Transducer and Activator of Transcription 1 (STAT1) and/or STAT2 form dimers and localize to the receptor complexes. STAT molecules at receptor complexes are phosphorylated by receptor-bound tyrosine kinases: Janus kinases (JAK) and Tyrosine kinase 2 (TYK2). In Type I signaling, phosphorylated STAT1-STAT2 heterodimers form a complex with IRF9 to produce IFN-stimulated gene factor 3 (ISGF3). ISGF3 translocates to the nucleus and binds to IFN-stimulated response elements (ISREs) that further induce IFN-stimulated effector genes. In Type II signaling, phosphorylated STAT1 homodimers translocate to the nucleus and bind to IFNγ-activated site (GAS) promoter elements to stimulate IFN-induced expression of antimicrobial effector genes (Reviewed in (MacMicking, 2012)).

IFN-stimulated genes (ISGs) contribute to cell-autonomous immunity by very different mechanisms:

a) IFN-induced oxidative and nitrosative defense

Cytotoxic gases, collectively called Reactive Oxygen Species (ROS) and Reactive Nitrogen Species (RNS), are one of the most ancient forms of cell-autonomous defense. They are generated by oxidoreductases and target bacterial DNA, lipids, and haem-groups or iron-sulphur clusters within bacterial enzymes. A large proportion of the redox damage caused by these gases can be traced to derivatives of O_2^- and NO (Nathan and Shiloh, 2000) (Nathan and Ding, 2010). In mammals, three classes of IFN-inducible oxidoreductases control ROS and RNS production: (1) NAPDH oxidases (NOXs) that catalyze production of O_2^-; (2) dual oxidases (DUOXs) that mediate H_2O_2 production; and (3) nitric oxide synthases (NOSs) that are involved in NO production. These enzymes are either directly inducible by interferons, like NOS2, NOX1 and DUOX2, or indirectly require IFN-induced components for its activity, like NOX2 (Reviewed in (MacMicking, 2012)).

b) Competing for intracellular cations and nutrients

Intracellular pathogens often require particular metal cation concentrations for their proliferation in the host. IFN-mediated mechanisms have evolved to restrict phagosomal or cytosolic availability of Mn^{2+}, Fe^{2+} and Zn^{2+}. IFNγ inducible Natural Resistance-Associated Macrophage Protein-1 (NRAMP-1) is a proton-dependent Mn^{2+} and Fe^{2+} efflux pump that prevents sequestration of these ions by phagosomal pathogens (Jabado et al., 2000). Fe^{2+}

exporter ferroportin 1 and transferring receptor expression are also both influenced by IFNγ (Nairz et al., 2008). IFNγ also stimulates relocation of Cu^+ pump ATP7A to the phagosome. Cu^+ in the phagosome enhances production of hydroxyl radicals and therefore intraphagosomal killing of bacteria (White et al., 2009).

Interferon inducible Indoleamine-2,3-dioxygenases (IDOs) are oxidoreductases responsible for the initial rate-limiting step of the kynurenine pathway. In this pathway L-Tryptophan, which some pathogens cannot produce, and thus have to exploit from the cell, is degraded. Therefore growth of a large number of pathogens, including *Toxoplasma gondii*, is inhibited (Pfefferkorn, 1984).

c) Blocking viral entry, replication, assembly and budding

IFN-inducible proteins, especially type I IFN inducible proteins, are also involved in anti-viral immune responses. IFN-inducible transmembrane (IFITM) proteins and Tripartite-motif (TRIM) proteins interfere with viral entry (Brass et al., 2009) (Stremlau et al., 2004). Moreover, RNA-activated protein kinase (PKR), 2'-5' oligoadenylate synthases (OAS), APOBEC3 (apolipoproten B mRNA-editing enzyme, catalytic polypeptide 3) and ADAR1 (adenosine deaminase, RN-specific 1) manipulate viral RNA (Sadler and Williams, 2008). In addition, tetherin and viperin interfere with viral release (Neil et al., 2008) (Evans et al., 2010) (Hinson and Cresswell, 2009) (Wang et al., 2007).

IFN-inducible GTPases named Myxoma resistance proteins (Mx) (chapter 1.3.) are involved in defense against orthomyxoviruses, bunyaviruses, togaviruses and rhabdoviruses (Haller and Kochs, 2011). It has been proposed that these proteins, analogously to dynamins, form oligomer ring-like structures which trap nucleocapsids and associated polymerases (Gao et al., 2010) (Haller and Kochs, 2011).

d) Targeting parasitophorous vacuole

Immunity-related GTPases (IRGs), which are further investigated in this study, play a crucial role in host response to a heterogeneous subset of intracellular pathogens in a heterogeneous subset of vertebrates (chapters 1.4., 1.5. and 1.6.). This interferon-γ (IFNγ) inducible resistance system accumulates at the parasitophorous vacuolar membrane (PVM) of *Toxoplasma gondii*, inclusions of *Chlamydia trachomatis*, vacuolar membranes of *Encephalitozoon cuniculi* and *Neospora Caninum* (Boehm et al., 1998) (Bekpen et al., 2005) (Martens et al., 2005) (Coers et al., 2008) (Reid et al., 2012) (Spekker et al., 2013) (da Fonseca Ferreira-da-Silva et al., 2014). IRG loading to the PVM of *T. gondii* is shortly followed by PVM disruption and necrotic cell death (Zhao et al., 2009b).

Guanylate-binding proteins (GBPs) (chapter 1.3.) also accumulate at the membranes of *Listeria monocytogenes* and *Toxoplasma gondii* and play a role in the resistance to these pathogens (Kim et al., 2011) (Degrandi et al., 2007). The mechanism of GBP action in pathogen resistance remains to be investigated.

1.3.   The Interferon-inducible GTPases

Guanosine triphosphatases (GTPases) are enzymes that can bind and hydrolyze guanosine 5'-triphosphate (GTP). They are involved in diverse cellular functions: signal transduction, endocytosis, vesicle trafficking, nuclear transport, cytoskeleton regulation, synthesis and translocation of proteins and cell division (Leipe et al., 2002) (Takai et al., 2001).

Nearly all GTPases have a more or less modified Ras-like GTPase domain (G-domain). A classical G-domain, with a molecular mass of roughly 20 kDa, is composed of six β-strands which are surrounded by five α-helices. The G-domain harbors five (G1 to G5) nucleotide-binding motifs and two flexible regions, switch I and II, which undergo nucleotide-dependent conformational rearrangements (Leipe et al., 2002).
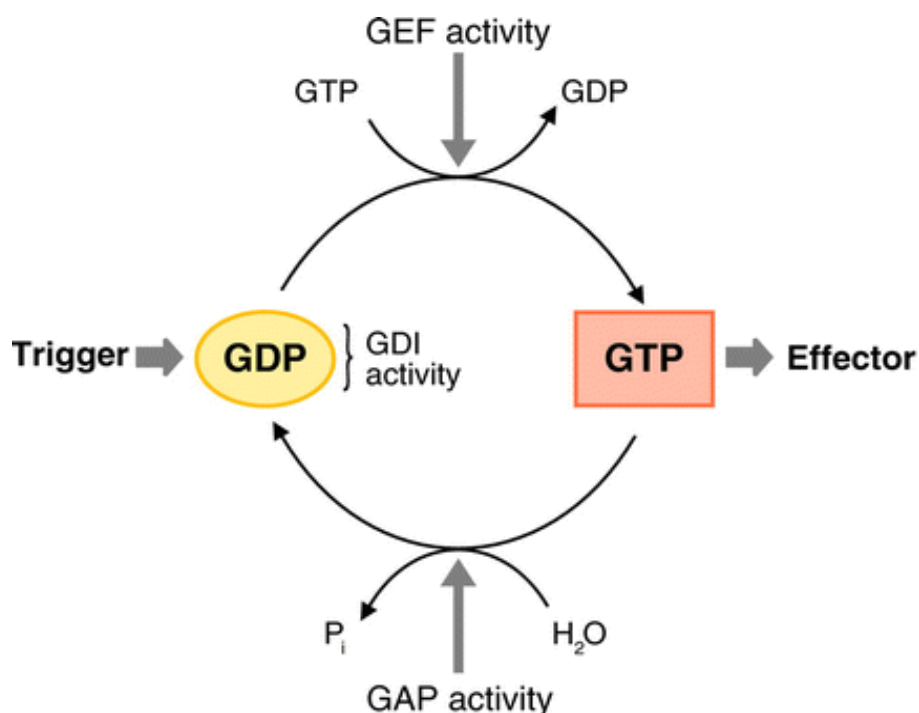
Figure 1.   The GTPase cycle. The transition between the GDP- and GTP-bound states of GTPases can be regulated by various reactions that are often, but not exclusively, influenced by other proteins. GDI activity inhibits dissociation of GDP and keeps the GTPase in the inactive form. GEF activity enhances the release of bound GDP from the GTPase. Contrary, GAP activity triggers GTP hydrolysis and restores the inactive GDP form (Modified from (Martens and Howard, 2006)).

GTPases often work as molecular switches. They cycle between two alternative conformations: the guanosine 5'-diphosphate (GDP) bound form, which is considered to be inactive; and GTP bound form, which is considered to be active. A conformational rearrangement between the GDP- and GTP-bound form, which primarily happens in the switch regions, enables GTPases to interact specifically with different downstream factors. Other molecules, such as guanine nucleotide exchange factors (GEFs), GTPase activating proteins (GAPs) and guanine nucleotide dissociation inhibitors (GDIs) can regulate the GTPase cycle at various positions (Figure 1) (Reviewed in (Martens and Howard, 2006)).

The IFN-inducible GTPases share certain structural and mechanistical features with dynamins (Martens and Howard, 2006), which are able to deform and tubulate cellular membranes and are involved in vesicular processing (Praefcke and McMahon, 2004).

Up to this point, four GTPase families were reported to be IFN-inducible: Mx proteins (Staeheli et al., 1986), (Haller et al., 2007); Guanylate binding proteins (GBPs) (Cheng et al., 1983); Immunity-related GTPases (IRGs) (Chapter 1.4.); and Very Large Inducible GTPases (VLIG) (Klamp et al., 2003).

a) Mx proteins

Mx proteins (Lindenmann et al., 1963) are Type I and Type III Interferon inducible dynamin-like GTPases that are present in nearly all vertebrate genomes, including mouse (*Mx1* and *Mx2*) and human (*MxA*), and play an important role in anti-viral defense (reviewed in (Martens and Howard, 2006) (Haller and Kochs, 2011) (Verhelst et al., 2013)). Mx proteins are members of the family of large GTPases and their primary aminoacid sequence suggests existence of N-terminal GTPase domain, a middle domain (MD) and C-terminal GTPase effector domain (GED) (Haller and Kochs, 2002). Unlike dynamins, Mx proteins lack pleckstrin-like homologly domain, which is involved in membrane targeting, and proline rich domain, which is involved in protein-protein interactions (Praefcke and McMahon, 2004). The crystal structure of GTP-free human MxA protein, which was resolved in 2011, shows three-domain structure that does not coincide with the domains identified in the primary aminoacid sequence: the GTP domain is connected to the bundle signaling element (BSE) and then to stalk (Gao et al., 2011).

At low protein concentrations Mx proteins form tetramers in solution and in higher protein concentrations, these tetramers form ring-like oligomers with characteristic criss-cross pattern between stalk domains. The interaction of adjacent rings is GTP-dependent (Di Paolo et al., 1999) (Gao et al., 2010).

Mx genes play an important role in the immune response to many RNA viruses including the ones from *Orthomyxoviridae* (Mx1 was firstly identified in response to Influenza), *Rhabdoviridae*, *Bunyaviridae* and *Paramyxoviridae* families (Reviewed at (Verhelst et al., 2013)). Even though the mechanism of their action is not fully understood, in general, Mx proteins recognize the capsid proteins of different viruses and interfere with the activity of viral polymerases (Reviewed at (Verhelst et al., 2013)), in the case of influenza by targeting of the viral ribonucleoprotein (vRNP) (Huang et al., 1992) .

b) Guanylate binding proteins (GBPs)

GBPs, with molecular weight of 65-72 kDa, were among first IFN-inducible proteins identified (Cheng et al., 1983). These proteins can be directly or indirectly induced with IFNγ, IFNα, interleukin-1β (IL-1β), tumor necrosis factor α (TNFα) and Lipopolysaccharide (LPS). They are well conserved through most of the vertebrates and a number of GBPs are described in mouse and human genome (Cheng et al., 1991) (Luan et al., 2002) (Fellenberg et al., 2004) (Olszewski et al., 2006) (Boehm et al., 1998) (Wynn et al., 1991) (Robertsen et al., 2006).

Although the structure and biochemical properties of GBPs are reasonably well understood, their role in the pathogen resistance is not fully clarified (Martens and Howard, 2006). siRNA knock-down of 11 mouse GBPs had revealed that the cells lacking Gbp1, Gbp6, Gbp7 or Gbp10 show increased susceptibility to *Listeria monocytogenes* and *Mycobacterium bovis*. The growth of these pathogens was additionally enhanced in the cells which had multiple GBPs silenced and it was reported that different GBPs accumulate at Listerial and Mycobacterial phagosomes (Kim et al., 2011). Moreover, it has been shown that *Gbp1* KO mice (Kim et al., 2011) and *Gbp5* KO mice (Shenoy et al., 2012) are susceptible to *Listeria monocytogenes* infection, while *Gbp2* KO mice are not (Degrandi et al., 2013). In contrast, it has been also shown that *Gbp*$^{Chr3-/-}$ (*Gbp1/2/3/5/7* KO) mice are not susceptible to *L. monocytogenes*, disputing the importance of these GBPs in *Listeria* response (Yamamoto et al., 2012).

Recently, it has been proposed that GBP proteins are required for Caspase-11-dependent pyroptosis upon infection with intracellular pathogens. In these reports, it has been suggested that after phagosomal accumulation, GBPs can kill the bacteria and lyse the phagosome itself. Exposure of LPS to the cytosol would then trigger Caspase-11-dependent pyroptosis of the host cell bacteria (Meunier et al., 2014) (Pilla et al., 2014).

Together with IRGs, GBPs are also known to accumulate at the parasitophorous vacuolar membrane of *Toxoplasma gondii* (Degrandi et al., 2007). In addition, *Gbp*$^{Chr3-/-}$ (*Gbp1/2/3/5/7* KO) mice are reported to be susceptible to *T. gondii* infection with over 80

percent of $Gbp^{Chr3-/-}$ mice succumbing to the infection. The reintroduction of Gbp1, Gbp5 or Gbp7 into $Gbp^{Chr3-/-}$ cell had partially restored IFNγ-induced anti-*T. gondii* response (Yamamoto et al., 2012).

It has been questioned whether human GBP proteins, analogously to IRG proteins in mice, are involved in *T. gondii* resistance (Virreira Winter et al., 2011). However, recent CRISPR/Cas9 knock out of *hGbp1-7* in human cells had revealed that *T. gondii* growth in these cells is not affected, indicating that these GBPs do not play a role in *T. gondii* resistance in humans (Ohshima et al., 2014).

c) Very Large Inducible GTPase (VLIG)

Very Large Inducible GTPases have molecular mass of about 200-280 kDa. In C57BL/6 mice, a representative VLIG-1 is a member of a cluster of at least six similar genes on chromosome 7 (Klamp et al., 2003). However, gene and copy number in VLIG family greatly varies between mouse strains (Lilue, personal communication). In humans, VLIG family is represented by a single close VLIG-1 homologue on chromosome 11 (Klamp et al., 2003). Up to now, it has been shown that VLIG-1 is strongly induced by IFNγ and IFNβ. Basally expressed VLIG-1 is predominantly located at the nucleus, while induced one is located at the nucleus and the cytoplasm (Klamp et al., 2003). The further biological role of VLIG protein family is not understood and remains to be investigated.

d) Immunity-related GTPases (IRGs)

IRG proteins are 47kDa GTPases shown to be crucial in resistance to a variety of pathogens. These proteins will be further discussed in the rest of the manuscript.

1.4. Immunity-related GTPases (IRGs)

1.4.1. *IRG* gene presence in different species

a) *IRG* genes in mouse

The immunity-related GTPases (IRGs) or p47-GTPases are Interferon-inducible guanine nucleotide binding proteins (Boehm et al., 1998). Up to date, 23 *IRG* genes are identified in the C57BL/6 laboratory mouse genome and they are localized on chromosomes 11 (*Irgm1-3, Irgb1-10, Irgd*), 18 (*Irga1-8*) and 7 (*Irgc*) (Bekpen et al., 2005) (Figure 2). Striking protein polymorphism, copy number variation and presence/absence polymorphism have been reported in different wild mouse strains (Lilue et al., 2013).
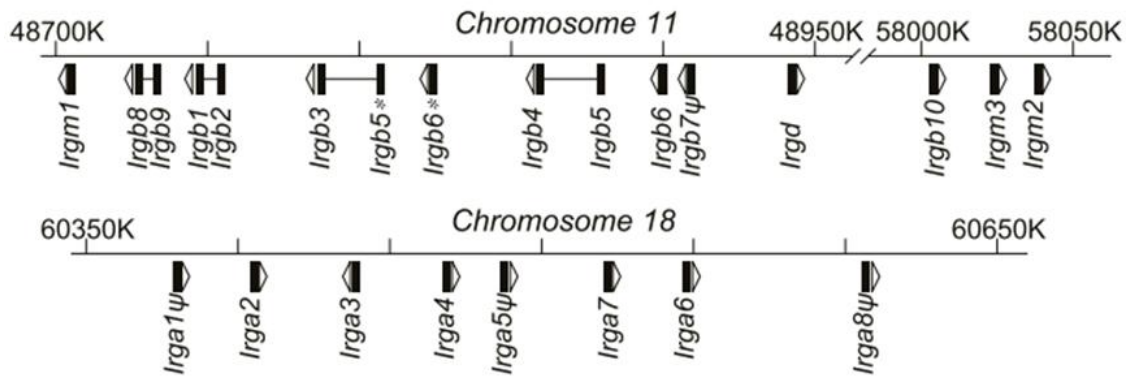
Figure 2. Linear order of *IRG* gene clusters on Chromosome 11 and Chromosome 18 of mouse strain C57BL/6 (Modified from (Lilue et al., 2013)).

The open reading frame of *Irg* genes is typically encoded on a single 3' exon that follows one or more 5' untranslated exons (Bekpen et al., 2005). *Irgm1-3* genes are encoded on two alternative 5' exons and one 3' exon, which yield two isoforms of both Irgm1 and Irgm2 (Bekpen et al., 2005). *Irgb2* and *Irgb1*, as well as *Irgb5* and *Irgb3*; *Irgb5* and *Irgb4*; and *Irgb9* and *Irgb8* are transcribed together leading to expression of so called tandem IRG proteins with apparent molecular weight of about 94 kDa (Bekpen et al., 2005), (Lilue et al., 2013).

Mouse Irga1-6, Irgb1-10, Irgc and Irgd proteins posses the universally conserved sequence (GXXXXGKS) in the G1 motif of the GTP binding site and are informally called GKS proteins. However, Irgm1, Irgm2 and Irgm3 proteins contain the non-canonical GXXXXGMS sequence in the G1 motif and are therefore named GMS proteins (Boehm et al., 1998) (Bekpen et al., 2005).

In addition to conventional IRG genes, a family unconventionally called *quasi-IRG* genes was identified in mouse (Irgq), in human (IRGQ) and other vertebrates (Bekpen et al., 2005) (Martens and Howard, 2006) (Hunn, 2008). Typical for this family is the disruption of the universally conserved G1 motif, which leads to a radically modified GTP-binding site. Therefore, these proteins are almost certainly not functional as GTPases (Bekpen et al., 2005) (Martens and Howard, 2006).

Most of the *IRG* genes contain GAS and ISRE elements, but no other motifs in their promoter region. Thus, they can be induced by Interferon Type I and Type II, with IFNγ being their strongest inducer and LPS or TNFα as secondary inducers (Bekpen et al., 2005) (Boehm et al., 1998) (Bekpen et al., 2005, Gilly et al., 1996) (Taylor et al., 1996) (Bafica et al., 2007). However, the promoter of Irgc does not contain an ISRE or GAS sequences and is not inducible by IFNs. Mouse Irgc is expressed exclusively in haploid spermatids in the

mature testis, but a genomic disruption of *Irgc* gene in mice did not lead to any obvious abnormality or to male sterility (Bekpen et al., 2005) (Rhode, 2007).

In healthy mouse tissues, IRG proteins, with exception of Irgc, are expressed at very low levels, with their expression levels drastically increased after induction (Taylor et al., 1996) (Collazo et al., 2001). However, bone marrow derived hematopoetic stem cells (HSCs) show high expression levels of IRG proteins without external induction (Ivanova et al., 2002) (Ramalho-Santos et al., 2002).

b) *IRG* genes in human

In humans, only two *IRG* genes are described: *IRGM* on chromosome 5 and *IRGC* on chromosome 19 (Bekpen et al., 2005) (Hunn, 2008). In addition, *quasi-IRG* gene *IRGQ* is also located at chromosome 19. Human *IRGC* is 90 percent identical to mouse *Irgc* and human *IRGQ* is over 80 percent identical to mouse *Irgq* at the amino acid level (Hunn, 2008). However, human *IRGM* encodes only an N- and C-terminally truncated G-domain homologous to mouse GMS proteins (Bekpen et al., 2005) (Hunn, 2008). While mouse GMS proteins are about 400 amino acids long, human IRGM is truncated to 183 amino acids and is only 54 %, 53 % and 51 % identical to Irgm1, Irgm2 and Irgm3 respectively (Bekpen et al., 2005). Interestingly, none of the human IRGs is interferon inducible (Bekpen et al., 2005) and the role of these proteins is not fully understood.

c) *IRG* genes in other species

IRG genes have been identified in many vertebrates (Figure 3), including mammals, reptiles, amphibians and fish (Bekpen et al., 2005) (Hunn, 2008) (Li et al., 2009) (Lilue, 2012) (Gazzinelli et al., 2014). All rodents analyzed so far, like rat, Guinea pig and squirrel have a number of IRG representatives from GKS and GMS subfamiles. Domestic dog, cattle, zebrafish and reptiles, like lizard also have representatives of both GKS and GMS IRG proteins. However, only *IRGC* and *IRGQ*-related sequences could be identified in the domestic cat, only IRGC could be identified in pig and no IRGs could be found in chicken (Hunn, 2008).

Not only humans, but also many other higher primates, have lost full length IFN-inducible *IRG* genes. For example, chimpanzee, orangutan and rhesus monkey posses only *IRGM*, *IRGC* and *IRGQ* sequences, which are similar to human ones. However, lower primates like bushbaby (*Otolemur garnettii*) and grey mouse lemur (*Microcebus murinus*) have *IRG* genes from IRGA and IRGD subfamilies (Hunn, 2008).

		GMS IRG	GKS IRG
House mouse	*Mus musculus*	3	16
Algerian mouse	*Mus spretus*	3	18
Rat	*Rattus norvegicus*	3	11
Chinese hamster	*Cricetulus griseus*	3	18
Golden hamster	*Mesocricetus auratus*	3	19
Degu	*Octodon degus*	1	3
Chinchilla	*Chinchilla lanigera*	1	7
Rabbit	*Oryctolagus cuniculus*	1	1
Pika	*Ochotona princeps*	1	2
Hedgehog	*Erinaceus europaeus*	0	3
Star-nosed mole	*Condylura cristata*	0	0
Horse	*Equus caballus*	0	0
White Rhino	*Ceratotherium simum*	1	1
Armadillo	*Dasypus novemcinctus*	1	4
Elephant	*Loxodonta africana*	2	5
Manatees	*Trichechus manatus*	2	6
Platypus	*Ornithorhynchus anatinus*	0	6
Orca	*Orcinus orca*	0	0
Human	*Homo sapiens*	1	0
Bonobo	*Pan paniscus*	1	0
Panda	*Ailuropoda melanoleuca*	6	7
Dog	*Canis lupus familiaris*	3	3
Cat	*Felis catus*	0	0

Figure 3. Distribution of IRG genes in certain mammalian species (Modified from (Gazzinelli et al., 2014)).

As for the presence of other IRGs, presence of IRGM also varies from species to species and is, for example, not expressed in the Old and New world monkeys due to the open reading frame (ORF) disruption by AluSc sequence insertion. Human and African great apes restore an ORF of about 20 kD in length, possibly due to insertion of the retroviral promoter element ERV9. Hence, it has been proposed that the IRGM gene became non-functional about 40 million years ago, but was resurrected about 20 million years ago in the common ancestor of humans and apes (Bekpen et al., 2009). Whether the function of IRGM remained the same before and after "resurrection" remains to be investigated.

1.4.2. Nucleotide binding and structural properties of IRG proteins

The first biochemical studies of IRG proteins were performed on Irgm3 and Irgb6 and demonstrated their ability to hydrolyse GTP to GDP (Taylor et al., 1996) (Taylor et al., 1997) (Carlow et al., 1998). It has been also shown that Irga6 is stable in the absence of nucleotides and shows a relatively low affinity for guanine nucleotides in the micromolar range (Uthaiah et al., 2003). Recombinant Irga6 has 10-15 fold higher affinity for GDP-, than for GTP. The basal GTP-ase activity of Irga6 is low, but it is elevated at higher concentrations of the protein, indicating cooperative behavior of Irga6 molecules. A GMS protein Irgm3 can bind to GTP and hydrolyze it to GDP only at minor extent, indicating that GXXXXGKS to GXXXXGMS mutation does not fully abolish GTPase activity (Taylor et al.,

1996) (Taylor et al., 1997). In solution, in the presence of GDP or in the absence of nucleotides, Irga6 is monomeric, whereas in the presence of GTP it forms oligomers. The oligomers are largely resolved upon GTP hydrolysis (Uthaiah et al., 2003), with low levels of remaining Irga6 oligomers that probably represent denatured Igra6 proteins (Howard, personal communication).

The crystal structure of Irga6 reveals that this protein is built of three domains: a Ras-like G-domain and N- and C-terminal helical domains (Ghosh et al., 2004) (Figure 4A). The G-domain consists of six stranded β-sheets (S1-S6) and six α-helices (H1-H5 and d). The H1-S2 loop corresponds to the switch I region and is extended in Irga6, while the switch II region is located between H1 and H2 helix. The helical domain of Irga6 comprises ten helices (αA-L). αA, αB and αC form the N-terminal region preceding the G-domain, whereas αF-L constitute the C-terminal region following the G-domain and linker helix αE connects the G-domain to αF. The first 13 amino acids of Igra6 could not be properly resolved in the crystal structure. Thus, little information concerning the structure of Irga6 N-terminus is available (Ghosh et al., 2004).
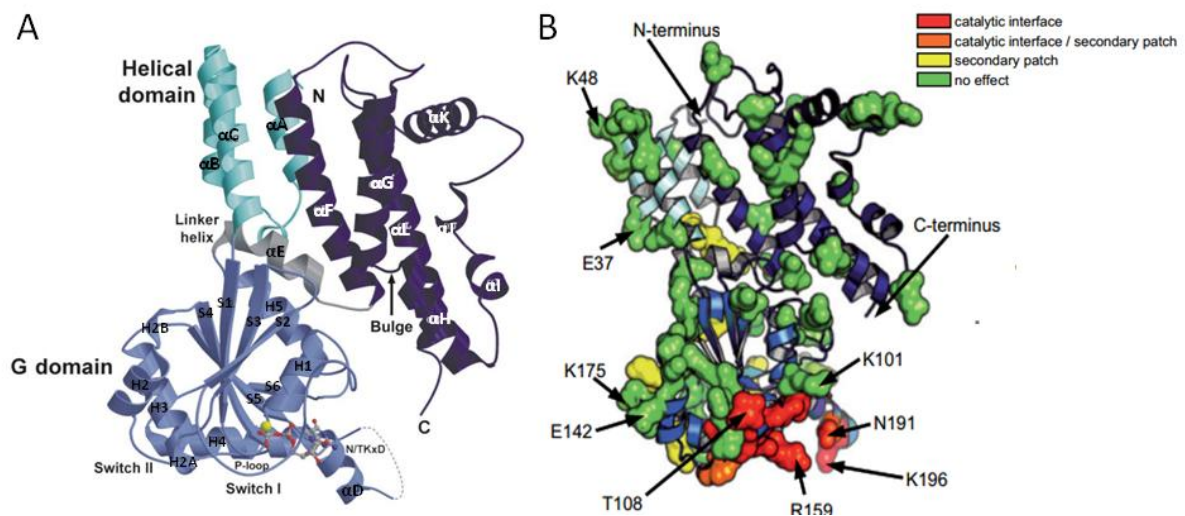
Figure 4. Crystal structure and catalytic interface of Irga6 protein A) Ribbon presentation of the GDP/Mg^{2+}-bound Irga6 crystal consisting of a Ras-like G-domain (S1-H5 helix) in blue; N-terminal (αA-C helix) and C-terminal (αF-αL helix) helical regions in cyan and dark blue; and a linker αE helix in grey (modified from (Ghosh et al., 2004)). **B)** The catalytic interface of Irga6 protein which was determined by the mutation of the depicted amino acids (modified from (Pawlowski et al., 2011)).

It has been shown that Irga6 forms GTP-dependent oligomeric complexes *in vitro* (Uthaiah et al., 2003), and that it forms at least dimers *in vivo* (Papic et al., 2008). The interface of Irga6, which is responsible for Irga6 oligomerization and accelerated hydrolysis of the GTP is identified on the G-domain and includes the nucleotide-binding site and the switch regions the bound GTP substrate (Figure 4B). The engagement of the catalytic

interface is also crucial for the activating interaction between Irga6 and Irgb6 and for the inhibitory interaction between Irga6 and the GMS protein Irgm3 (Pawlowski et al., 2011).

1.4.3. Intracellular localization of the IRG proteins

IRG proteins are distributed over different sub-cellular compartments. In non-infected, IFNγ-induced cells, GKS proteins Irgb6, Irgb10 and Irgd are predominantly cytosolic and Irga6 partitions between endoplasmic reticulum (ER) and the cytosol in a 60:40 ratio (Martens et al., 2004) (Coers et al., 2008).
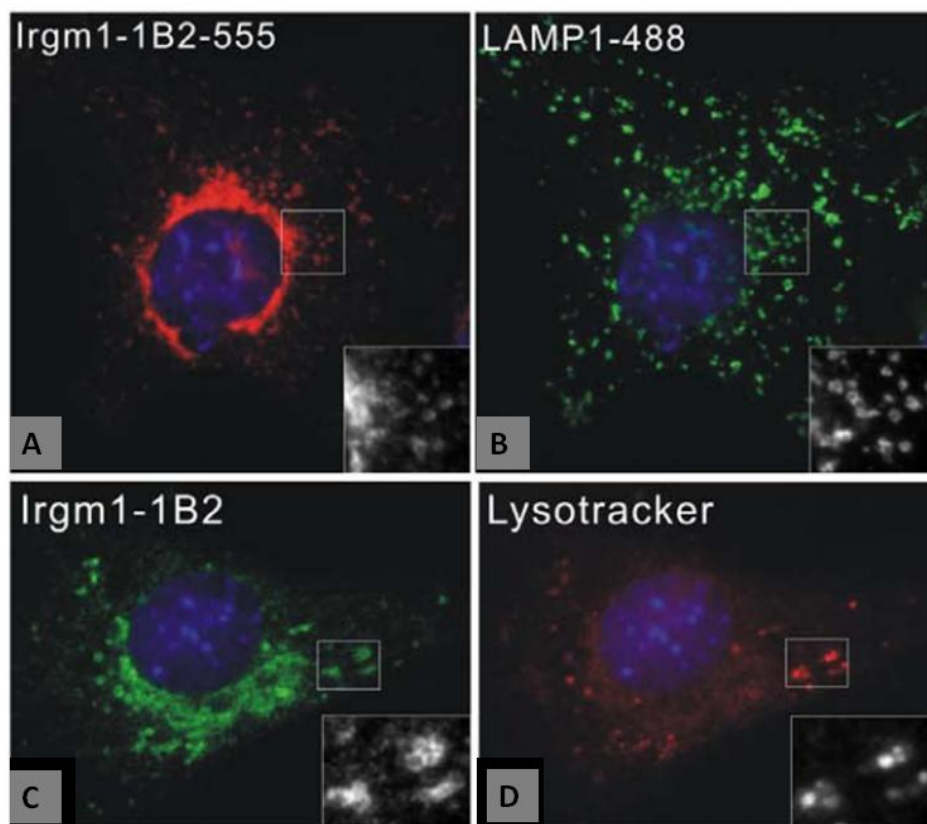
Figure 5. Irgm1 co-localizes with lysosomes. Mouse embryonic fibroblasts (MEFs) were treated with 200 U/ml IFNγ for 24 hours. Cells were either fixed and stained for Irgm1 and LAMP1 (A, B) or incubated with 50 nM LysoTracker Red DND-99 for 30 minutes and stained for Irgm1 (C, D). Irgm1 was found to co-localize with LAMP1 positive compartments (A, B) and with the LysoTracker positive compartments (C, D) (Modified from (Zhao et al., 2010)).

In contrast, GMS proteins are mainly membrane-bound (Martens et al., 2004). In IFNγ-induced cells Irgm1 localizes mainly to Golgi (Martens et al., 2004) (Butcher et al., 2005) (Tiwari et al., 2009) and to lysosomes (Figure 5) (Butcher et al., 2005) (Zhao et al., 2010), and has also been reported to localize to mitochondria (Tiwari et al., 2009) (Chang et al., 2011) (Springer et al., 2013), lipid droplets (Haldar et al., 2013), endosomes and

peroxisomes (Tiwari et al., 2009) (Haldar et al., 2013). Irgm2 was reported to localize to Golgi (Hunn et al., 2008) (Martens and Howard, 2006) and Irgm3 localizes to the ER and lipid droplets (Taylor et al., 1997) (Martens et al., 2004) (Hunn et al., 2008) (Bougneres et al., 2009). Thus, endogenously expressed GMS proteins probably localize to every endocellular membrane.

Interestingly, in IFNγ-induced wild-type cells, none of the GMS proteins were observed to localize to the plasma membrane. Therefore, plasma membrane probably represents the only membrane in the cell which is not GMS-coated (further discussed in chapter 4.2.). GMS proteins were found to target this membrane only under the following conditions: Firstly, upon phagocytosis of latex beads, Irgm1 was found to co-localize with the phagocytic cups (Martens et al., 2004); Secondly, truncated Irgm1, that includes only the G-domain and C-terminus of this protein, was shown to exclusively co-localize with the plasma membrane (Martens et al., 2004).

Targeting of Golgi and lysosomal membranes by Irgm1 is highly dependent on a sequence in the C-terminal domain, which corresponds to the amphipathic αK-helix of Irga6 (Martens et al., 2004) (Martens and Howard, 2006) (Zhao et al., 2010). It has been also shown that a similar sequence is essential for intracellular membrane targeting of the other GMS proteins (Zhao et al., 2010).

The mechanism of association of the GKS proteins with the sub-cellular compartments is also not completely understood. It has been reported that a myristoyl group, which is attached to the N-terminal Glycine-2 of Irga6 protein, is important for the membrane binding of Irga6 (Martens et al., 2004) (Steinfeldt et al., 2010). Mutations of the Glycine-2 abolished presence of Irga6 in the membrane-bound fraction (Zhao et al., 2010). Non-myristoylated Irga6 is also described to show defects in conformational transition associated with GTP-dependent activation (Papic et al., 2008).

1.4.4. GMS proteins regulate GKS protein interaction

When Irga6 is expressed in the IFNγ-induced cell, immunofluorescence staining of these cells reveals a smooth pattern of non-aggregated Irga6 (Martens et al., 2004). However, when Irga6 is transfected in unstimulated mouse cells, it accumulates in aggregate-like structures. In *T. gondii* infected IFNγ-induced cells, Irga6 accumulates at the parasitophorous vacuolar membrane (PVM) resulting in membrane disintegration and parasite death. Aggregated Irga6 cannot accumulate at the PVM. To this end, it has been suggested that correct cellular localization of Irga6 requires concomitant expression of

additional IFNγ-inducible factors, which possibly could be other IRG proteins (Hunn et al., 2008).

Indeed, when mouse cells that stably express Irga6 with an inducible promoter were co-transfected with Irgm1, Irgm2 and Irgm3, smooth, non-aggregated pattern of Irga6 was restored. When these GMS-transfected cells were infected with *T. gondii*, Irga6 could accumulate on the PVM, as in IFNγ-induced cells (Hunn et al., 2008). Therefore, all three GMS proteins are necessary for the proper localization and function of Irga6.

The nucleotide-bound status of Irga6 is apparently crucial for its proper function. The constitutively active Irga6-K82A mutant forms aggregate-like structures when expressed in non-induced cells. These structures do not resolve upon IFNγ-induction or GMS transfection. In contrast, constitutively inert mutant, Igra6-S83N does not form aggregates in non-induced or induced cells and does not accumulate at the *T. gondii* PVM.

Immunofluorescence microscopy analysis with the monoclonal antibody 10D7, which *in vivo* detects specifically the GTP-bound form of Irga6, and 10E7, which detects both GTP- and GDP-bound Irga6, revealed that in IFNγ-induced uninfected cells Irga6 is in an inactive GDP-bound state. Irga6 that accumulates on the *T. gondii* PVM is in activated, GTP-bound and probably oligomerized state (Papic et al., 2008). 10D7 staining had also revealed that aggregate-like accumulations of Irga6 are GTP-bound, indicating off-target activation of this protein (Papic et al., 2008) (Hunn et al., 2008).

The nucleotide-binding status of the GMS proteins is also crucial for Irga6 localization and function. Mutations that are homologous to Irga6-S83N, that also prevent GTP-binding, were introduced into the GMS proteins: Irgm1-S90N, Irgm2-S78N and Irgm3-S98N. When these mutated proteins, called GMN proteins, were transfected into the Irga6 expressing uninduced cells, Irga6 aggregate-like structures were not resolved and Irga6 could not accumulate at the *T. gondii* PVM (Hunn et al., 2008).

As previously described, purified Irga6 forms enzymatically active GTP-dependent oligomers in solution (Uthaiah et al., 2003). Irga6 oligomers could not be isolated from IFNγ-induced wild-type mouse cells (Papic et al., 2008). In contrast, when the cells containing overexpressed Irga6, in the absence of GMS proteins, were treated with GTPγS or Aluminum-Fluoride (AlFx), the substances that prevent the shifts between GTP- and GDP-bound state of the GTPases, the dimmers of Irga6 could be isolated (Papic et al., 2008). In accordance to that, Irga6 aggregate-like structures formed in GMS-deficient cells could represent transient GTP-dependent dimmers and possibly oligomers.

The yeast two-hybrid (Y2H) analysis of the GKS and GMS proteins showed homologous and heterologous interactions between the IRG proteins. Strong homotypic interaction was observed for Irga6, strengthening the reports concerning Irga6 oligomerization (Uthaiah et al., 2003) (Papic et al., 2008). Irga6 was shown to interact with Irgm1, Irgm2 and Irgm3 and this interaction was abolished with respective GMN mutants. Likewise, Irga6-S83N did not interact with IRG proteins (Hunn et al., 2008). In addition, the GDP-dependent interaction of Irga6 and Irgm3 was also shown in pull-down assays (Hunn et al., 2008).

Similarly to Irga6, overexpressed Irgb6 also forms aggregate-like structures that cannot accumulate at the PVM. These aggregates are also resolved upon GMS expression (Hunn et al., 2008). Homotypic interaction of Irgb6, as well as Irgb6 interaction with Irgm2, were also revealed by Y2H analysis (Hunn et al., 2008) and Irga6 and Irgb6 were also shown to interact in pull-down assays (Pawlowski et al., 2011).

1.4.5. IRG and GBP protein aggregation

Living cells employ a sophisticated machinery for maintaining their proteome. Proteostasis refers to control of concentration, conformation, binding interactions and location of individual proteins. It is influenced by the chemistry of protein folding/misfolding and by numerous regulated networks of interacting and competing biological pathways (reviewed in (Balch et al., 2008)). Mismanagement of the protein folding and function by the proteostasis network is responsible for the wide range of diseases that include, among others, lysosomal storage disease, myelination diseases, cystic fibrosis and neurodegenerative diseases including Alzheimer's disease. One of the outcomes of the proteostasis network failure is the aggregation of permanently or temporary non-functional proteins, which can have toxic effects for the individual aggregate producing cell (cell autonomous toxicity) and/or for the other cells in the system (non-autonomous toxicity), thereby playing a role in many of previously numbered diseases (Reviewed in (Hutt et al., 2009)).

In 2004, it has been reported that Irga6 forms filamenous aggregate-like structures when expressed in unstimulated L929 fibroblasts (Martens et al., 2004). Thus far, it has been reported that the GKS aggregates are also formed in Irga6-transfected non-induced mouse cells; mifepristone-induced Irga6 expressing GS 3T3 cells; IFNγ-induced *Irgm1* KO, *Irgm3* KO or *Irgm1/Irgm3* KO mouse embryonic fibroblasts (MEFs) and other IFNγ-induced cells which lack at least one of the GMS proteins (Martens et al., 2004) (Hunn, 2008) (Hunn

and Howard, 2010) (Haldar et al., 2013). As previously described (chapter 1.4.4.), GKS protein aggregation is GTP-dependent and regulated by the GMS proteins. The presence of all Irgm1, Irgm2 and Irgm3 is necessary to obtain smooth non-aggregated appearance of Irga6 or Irgb6 in the cell.

To this end, localization of most of the GKS aggregate-like structures is not clarified. Electron-microscopy images had shown that overexpressed Irga6 partially co-localizes with the ER (Kaiser, 2005) (Hunn et al., 2008). Recent reports had alsoshown that Irgb10 and Irga6 aggregate-like structures co-localize with the lipid droplets in IFNγ-induced *Irgm1/Irgm3* KO cells (Haldar et al., 2013), but the localization of Irga6 and other GKS proteins in other GMS-deficient cells has not been investigated.

Interestingly, GKS protein aggregate-like structures are formed not only in the absence of the GMS proteins, but also in the absence of certain autophagy-related proteins. IFNγ-induced *Atg5* KO cells were shown to contain Irga6, Irgb6, Irgd and Irgb10 aggregate-like structures and Irgb10 accumulations were reported in IFNγ-induced *Atg3* KO cells (Khaminets et al., 2010) (Traver et al., 2011) (Haldar et al., 2014). Similarly to Irga6 in GMS-deficient cells, Irga6 aggregate-like structures in *Atg5* KO cells are also GTP-bound and unable to accumulate at the *T. gondii* PVM (Khaminets et al., 2010). Aggregated Irgb10 in *Atg3* and *Atg5* KO cells cannot accumulate at *Chlamydia trachomatis* inclusions (Haldar et al., 2014). Irgb6 was also not able to load to the *T. gondii* PVM in IFNγ-induced *Atg7* KO and *Atg16L* KO cells, probably due to aggregate formation (Ohshima et al., 2014). However, in the cells lacking *Atg9a* or *Atg14* did not encounter this problem (Ohshima et al., 2014). Further yycharacteristics of these aggregate-like structures and their similarity to the aggregate-like structures in GMS deficient cells remain to be investigated.

Not only IRG proteins, but also GBP-proteins are prone to aggregation in the absence of the GMS proteins. It has been shown that mouse Gbp2 protein forms aggregate-like structures in *Irgm1* KO or *Irgm3* KO MEFs and bone marrow-derived macrophages (BMDMs). Interestingly, over 80% of GBP aggregate-like structures were reported to co-localize with Irga6 aggregate-structures, indicating that these accumulations are made of both IRG and GBP proteins (Traver et al., 2011). GBP proteins also form aggregate-like structures in Atg-deficient cells: Gbp2 accumulations could also be detected in IFNγ-induced *Atg5* and *Atg3* KO mouse cells (Traver et al., 2011) (Haldar et al., 2014). Whether the GBP proteins are also regulated by GMS and Atg proteins, remains to be clarified.

1.5. Parasite control by the IRG resistance system

The analysis of IRG-deficient mouse resistance had suggested that IRG proteins are implicated in resistance against particular intracellular pathogens, namely against *Toxoplasma gondii* (Taylor et al., 2000) (Collazo et al., 2001) (Butcher et al., 2005) (Martens et al., 2005) (Zhao et al., 2009b) (Khaminets et al., 2010), *Chlamydia trachomatis* (Coers et al., 2008) (Al-Zeer et al., 2009) (Nelson et al., 2005) (Coers et al., 2011), *Chlamydia psittaci* (Miyairi et al., 2007), *Encephalitozoon cuniculi* (da Fonseca Ferreira-da-Silva et al., 2014) and *Neospora caninum* (Spekker et al., 2013) (Reid et al., 2012) (chapters 1.5.1. and 1.5.2.). In addition to these pathogens, *Irgm1* knock-out (KO) mice have been reported to succumb to infection with *Leishmania major*, *Trypanosoma cruzi*, *Listeria monocytogenes*, *Mycobacterium avium*, *M. tuberculosis* and *M. bovis, Salmonella typhimurium* and other (chapter 1.6.1). However, it has been proposed that the susceptibility of *Irgm1* KO mice might be a consequence of dysregulation of the other IRG proteins in the absence of Irgm1 (Hunn and Howard, 2010) (chapter 1.6.3.).

1.5.1. IRG resistance to *Toxoplasma gondii*

Toxoplasma gondii is a obligate intracellular protozoan parasite which belongs to the phylum *Apicomplexa.* It has a broad host range and can infect most nucleated cells of any warm blooded animal (Levine, 1988) (Black and Boothroyd, 2000) (Sibley, 2003).

The life cycle of *T. gondii* is complex and it includes sexual and asexual phase of reproduction (Boothroyd and Grigg, 2002). The sexual reproduction of *Toxoplasma* occurs only in members of the *Felidae* family, nowadays to a large extent in the domestic cat (*Felis silvestris catus*) (Hutchison, 1965). The cat gets infected by carnivorism and, after the sexual process, sheds environmentally resistant cysts of *T. gondii*, which can get taken up by any foraging warm-blooded animal (Dubey and Frenkel, 1972) (Dubey, 1995). After the asexual phase in any warm-blooded animal, *T. gondii* encysts in the tissues and resides there until the animal dies or gets eaten by another animal (Dubey and Frenkel, 1972) (Sims et al., 1989) (Dubey et al., 1997).

In the immunocompetent human hosts the acute phase of the disease toxoplasmosis is often asymptomatic and sometimes followed by flu-like symptoms. However, in immunocompromised individuals *T. gondii* infection can result in severe toxoplasmosis, which predominantly attacks the nervous system and can lead to fatal encephalitis (Lieberman and Hunter, 2002) (Suzuki et al., 1988).

For a long time, *T. gondii* population of Europe and North America was classified into three clonal lineages, named type I, II and III (Howe and Sibley, 1995). Although these lineages show less than 1 percent of genomic variation, there is a striking difference concerning their virulence in laboratory strains of mice. Nowdays, over 200 different genotypes of *T. gondii* (Shwab et al., 2013) with striking differences in virulence have been distinguished (Lilue et al., 2013). The highest *Toxoplasma* population diversity is reported in South America, especially in Brazil (Shwab et al., 2013).

IFNγ is crucial in controlling replication and dissemination of avirulent *T. gondii* in both myeloid and non-myeloid cells, which can both develop IFNγ-induced cell autonomous resistance mechanism to *T. gondii* (Suzuki et al., 1988) (Scharton-Kersten et al., 1996) (Halonen et al., 2001) (Butcher et al., 2005) (Martens et al., 2005). Thus, IFNγ-deficient mice die even after infection with avirulent *T. gondii* (Scharton-Kersten et al., 1996).

IRG proteins represent IFNγ-inducible factors that play an essential role in mouse resistance to *T. gondii.* Namely, 100 percent of *Irgm1* KO (Collazo et al., 2001), *Irgm3* KO (Taylor et al., 2000) or *Irgm1/Irgm3* KO mice (Henry et al., 2009) and about 50 percent of infected *Irga6* KO (Liesenfeld et al., 2011) or *Irgd* KO (Collazo et al., 2001) die 10-12 days after infection with avirulent *T. gondii* strains.

On a subcellular level *T. gondii* can actively invade any nucleated cell of the host and resides in it in a parasitophorous vacuole (PV) (Morisaki et al., 1995). The parasitophorus vacuolar membrane (PVM) is formed from the invaginated and modified host cell plasma membrane (Suss-Toby et al., 1996) and provides an intracellular niche, which shields the parasite from endogenous host defense mechanisms (Sibley, 2011). The PV does not fuse with the endolysosomal compartment and therefore its acidification is blocked (Sibley et al., 1985).

Immediately after *Toxoplasma* entry into an IFNγ-induced cell, effector IRG proteins, called GKS proteins, accumulate and activate at the PVM in a nucleotide-dependent manner (Martens et al., 2005) (Ling et al., 2006) (Zhao et al., 2009b) (Hunn et al., 2008) (Papic et al., 2008). IRG proteins load onto the PVM in a cooperative and hierarchical manner with Irgb6 and Irgb10 being the most efficient and also first to load (Khaminets et al., 2010). It has been proposed that, during this process, GTP-dependent heterooligomers are formed at the PVM (Khaminets et al., 2010) (Pawlowski et al., 2011) (Hermanns et al., manuscript in preparation). Regulatory IRG proteins, called GMS proteins, do not target the PVM (Irgm1), or target it only in a marginal extent (Irgm2, Irgm3), probably being brought there in complex with GKS proteins (Butcher et al., 2005) (Martens et al., 2005) (Khaminets et al., 2010)

(Haldar et al., 2013). After accumulation of the IRG proteins to the *T. gondii* PVM, the effective surface area of the PVM is reduced by vesiculation and ruffling (Martens et al., 2005) (Ling et al., 2006) (Zhao et al., 2009b). Therefore, it has been proposed, that created membrane tension ultimately leads to PVM rupture (Zhao et al., 2009b) (Howard et al., 2011). Once exposed to the cytosol, the parasite dies, followed by death of the host cell (Martens et al., 2005) (Ling et al., 2006) (Melzer et al., 2008) (Zhao et al., 2009b).

The mechanism of parasite death and subsequent death of the host cell are not yet clarified. The host cell death is characterized by plasma membrane permeabilization and the release of the high-mobility group protein 1 (HMGB1) (Zhao et al., 2009b). Cytochrome C is not released from the mitochondria prior to death and no cleavage of caspase-3 or its substrate PARP could be seen (Zhao et al., 2009b). The cell death is also not caspase-1 dependent (Zhao et al., 2009b), but preliminary data show that death of *T. gondii* infected cells can be inhibited by the inactivation of lysosomal cathepsins (Carolina Alves, unpublished data). Taken together, host cell death is currently characterized as necrosis-like cell death.

In human, *T. gondii* control is also IFNγ-dependent. The mechanism behind the IFNγ-dependent response to *T. gondii* is not well understood. It has been shown that human IRG proteins do not accumulate at the PVM. However, *T. gondii* proliferation in human cells depends on IFNγ-inducible indoleamine-2,3-dioxygenase (IDO), which degrades amino acid tryptophan to kynurenine (chapter 1.2.). Since *T. gondii* cannot synthesize tryptophan on its own and scavenges it from the host cell, depletion of tryptophan by IDO inhibits *T. gondii* replication (Pfefferkorn, 1984).

1.5.2. IRG resistance to *C. trachomatis*, *E. cuniculi* and *N. caninum*

a) IRG response to *Chlamydia*

Chlamydiae are bacteria with obligatory intracellular lifestyle and biphasic life cycle (Moulder, 1991). The entry mechanism of *Chamydia* is not well understood, but it comprises some properties of clathrin-mediated endocytosis, and differs from conventional phagocytosis, calveolar-mediated endocytosis and macropinocytosis (Hybiske and Stephens, 2007). Early modifications of the nascent chlamydial vacuole prevent vacuolar fusion with the lysosomes (Hackstadt et al., 1995).

Chlamydiae exibit a broad spectrum of natural host infection tropism (Morrison and Caldwell, 2002). *Chlamydia trachomatis* is prevalently human pathogen and *Chlamydia*

muridarum mainly infects the mouse (Cotter and Byrne, 1996). In contrast to the mouse response to *C. muridarum*, which is not IFNγ-mediated, response to *Chlamydia trachomatis* in mouse is mediated by IFNγ and IRG proteins (Nelson et al., 2005).

Firstly, it has been shown that *Irgm1* KO and *Irgm3* KO, but not *Irga6* KO mice are susceptible to *C. trachomatis* infection (Coers et al., 2008). Secondly, it has been shown that Irga6 and Irgb10 proteins accumulate at *C. trachomatis* inclusions (Coers et al., 2008). Thirdly, Irgb10 ectopic expression reduces the number of inclusions (Coers et al., 2008). Fourthly, the inclusions in *Irga6* KO cells were larger than in the WT cells. however, *Irgm1/Irgm3* double KO mice rescued myeloid cell defects in *C. trachomatis* response that exist in *Irgm1* KO mouse myeloid cells (Coers et al., 2011). *C. muridarum* probably can overcome IRG response due to gene *TC438*, whose homologue *YopT* is involved in Rho GTPase inactivation by removal of lipid modification in *Yersinia*. Thus, it has been proposed that *TC438* is responsible for the inactivation of IRG proteins and therefore evasion of IRG response in mice (Nelson et al., 2005).

IRG proteins are also shown to be involved in the response to *Chlamydia psittaci*, bacteria that cause severe pulmonary infections in humans. All *Irgm3* KO mice that were infected with *C. psittaci* died several days after infection. These mice had also shown post-infection weight loss and the cross sections of their spleen were coated with fibrin and infiltrated with inflammatory cells. All wild type C57BL/6 mice had survived *C. psittaci* infection and did not show the weight loss, but all the 129S1/SvImJ mice suffered from the weight loss and succumbed to infection. Since 129S1/SvImJ mice have low expression levels of Irgb10 protein, these data indicated that this protein might play important role in *C. Psittaci* resistance (Miyairi et al., 2007). Further linkage analysis using BXD recombinant inbred stains revealed a single effector locus at chromosome 11 encoding a cluster of three IRG proteins, Irgb10, Irgm2 and Irgm3 that plays a role in the resistance to *C. psittaci* (Miyairi et al., 2007).

b) IRG response to *Encephalitozoon cuniculi*

The microsporidian, *Encephalitozoon cuniculi* is an abundant obligate intracellular pathogen, infecting primarily rodents, but is also pathogenic in immunologically deficient humans (Didier, 2005). Microsporidia have a very peculiar entry mechanism into host cell: it employs a filamentous tube, named the polar tube, which, upon an unknown trigger, can be suddenly extruded creating a deep and narrow invagination in any adjacent host cell plasma membrane. The *E. cuniculi* sporoplasm is transferred through the tube and resides in the host cytoplasm in a PVM derived from the invaginated plasma membrane (Bohne et al., 2011).

The proliferation of *E. cuniculi* is also inhibited by IFNγ. IFNγ restriction suppresses *E. cuniculi* growth in murine peritoneal macrophages, mouse embryonic fibroblasts, human enterocyte cell lines and human monocyte-derived macrophages (Didier, 2005) (Choudhry et al., 2009) (Fischer et al., 2008) (da Fonseca Ferreira-da-Silva et al., 2014). Moreover, *IFNγ* KO mice are susceptible to *E. cuniculi* (Khan and Moretto, 1999). Recently, it has been shown that IRG proteins mediate *E. cuniculi* resistance in mouse cells: Irga6, Irgb6, Irgd and Irgm2 were detected at the *E. cuniculi* parasitophorus vacuole, as on the *T. gondii* PVM. IFNγ-mediated inhibitory effects on *E. cuniculi* are lost in GMS-deficient cells, emphasizing an essential role of IRG proteins (da Fonseca Ferreira-da-Silva et al., 2014).

c) IRG response to *Neospora caninum*

A close relative of *T. gondii,* prevalently dog pathogen *Neospora caninum*, is also proposed to be controlled by the IRG resistance system. Irga6, Irgb6 and Irgd have been reported to accumulate on the PVM of *N. caninum* in infected murine cells (Spekker et al., 2013) (Reid et al., 2012).

1.6. GMS proteins: the role and the mechanism of action

1.6.1. Susceptibility of *GMS* knock-out mice to infection

Opinions about the mechanism of action of GMS proteins, especially of Irgm1, are divided (Chapter 1.6.4.). The lifespan and the weight of *Irgm3* KO and *Irgm1/Irgm3* KO mice, which are raised under SPF conditions, are indistinguishable from corresponding wild-type (WT) mice (Taylor et al., 2000). *Irgm1* KO mice, which are grown under SPF conditions, weight slightly less than wild-type mice, but their life span is not affected (Collazo et al., 2001) (personal communication with Gregory A. Taylor).

In contrast to *Irgm3* KO and *Irgm1/Irgm3* KO mice, which are susceptible to the infection with *T. gondii* and *C. trachomatis, Irgm1* KO mice succumb to infection with not only these, but also with variety of other very different pathogens, which will be described in this chapter. *Irgm1* KO mice also die due to various non-pathogen induced inflammations, which do not have severe consequences in WT mice or in *Irgm3* and *Irgm1/Irgm3* KO mice (chapter 1.6.2.). Thus, Irgm1 is often proposed to have pan-anti-inflammatory and pan-defensive roles.

a) Susceptibility to *Listeria monocytogenes* infection

Experiments monitoring the survival of *GMS* KO mice after *Listeria monocytogenes* infection have shown that *Irgm1* KO mice are fully susceptible to this infection. They die 4-5 days after infection and have high parasite burdens in spleen and liver (Collazo et al., 2001). Contrary, *Irgm3* KO mice survive and fully recover from the *L. monocytogenes* challenge (Taylor et al., 2000).

b) Susceptibility to *Trypanosoma cruzi*

Irgm1 KO mice were also reported to be susceptible to *Trypanosoma cruzi* and die 14-19 days after infection (Santiago et al., 2005). The increased parasite burden is found in spleen, liver and heart of these mice. Infected *Irgm1* KO animals also suffer from characteristic severe anemia, lymphopenia and thrombocytopenia together with lymphoid organ atrophy and bone marrow cell depletion (Santiago et al., 2005). In contrast, *Irgm3* KO mice were reported to be fully resistant to *T. cruzi* infection (de Souza et al., 2003).

c) Susceptibility to *Mycobacteria* infection

The most extensive study on *Irgm1* KO mouse resistance was performed with *Mycobacterium avium* infection by Carl Feng and his coworkers (Feng et al., 2004). *M. avium* infected *Irgm1* KO mice die 10-20 days post infection and show increased bacterial burden in the lungs and liver. *Irgm1* KO macrophages respond to *M. avium* infection by production of normal levels of pro-inflammatory mediators like tumor necrosis factor α (TNFα) and nitric oxide (NO). However, granuloma formation in these mice is impaired and, interestingly, infected *Irgm1* KO mice suffer from striking lymphopenia. Splenic lymphocyte counts of these mice are a third of those in infected WT mice and both CD4 and CD8 T cell pools are depleted. Peripheral lymphocyte and thymocytes counts are also severely decreased (Feng et al., 2004).

To investigate whether the lymphocyte depletion observed in *M. avium* infected *Irgm1* KO mice is exclusively caused by a lymphocyte defect, or also by defects in non-lymphoid compartments, naive T-lymphocytes from WT or *Irgm1* KO donors were transferred into *M. avium* infected *RAG-2* KO recipients, which lack mature lymphocytes, but express Irgm1 (Shinkai et al., 1992). The bacterial growth was assayed 6 weeks post infection and both *RAG-2* KO mice with naïve WT and *Irgm1* KO lymphocytes showed equivalent infection control (Feng et al., 2004). Similar results were also reported when 2 week infected WT or *Irgm1* KO mice were used as T-lymphocyte donors, indicating that the defective lymphocytes alone are not the cause of the death of *Irgm1* KO mice after *M. avium* infection (Feng et al., 2004).

Irgm1 KO mice are also highly susceptible to infection with *Mycobacterium tuberculosis* (Erdman-strain), while *Irgm3* KO survive this infection as well as WT mice (MacMicking et al., 2003). In IFNγ-induced *Irgm1* KO BMDMs, *M. tuberculosis* grows faster than in IFNγ-induced WT BMDMs and it has been shown that acidification of the Mycobacterial phagosome is impaired in *Irgm1* KO BMDMs (MacMicking et al., 2003).

d) Susceptibility to *Salmonella typhimurium*

Infection of *Irgm1* KO mice with *Salmonella typhimurium* also resulted in increased pathogen burden in spleen and liver and impaired granuloma formation, and finally in death of the animals (Henry et al., 2007). Again, *Irgm3* KO mice were fully resistant to *S. typhimurium* (Henry et al., 2007). Surprisingly, *Irgm1/Irgm3* KO mice were also fully resistant to *S. typhimurium,* with pathogen burden, spleen weight and granuloma formation similar to WT and *Irgm3* KO mice (Henry et al., 2009).

In *vitro* analysis confirmed that *S. typhimurium* proliferation in induced *Irgm1* KO BMDMs is increased in comparison to WT BMDMs (Henry et al., 2007).

e) Susceptibility to other pathogens

Irgm1 KO mice were also reported to be susceptible to *Leishmania major* (Taylor et al., 2004). All the pathogens that caused *Irgm1* KO mouse death have in common to induce IFNγ response and thereby IRG proteins, which then could act toxically in the absence of Irgm1 (Taylor et al., 2004). In accordance to that, Th-2 response to the helminth *Schistosoma mansoni*, which does not induce IFNγ responses, and does not stimulate IRG protein expression, did not cause death of *Irgm1* KO mouse, indicating that the *Irgm1* KO phenotype requires IFNγ induction (Feng et al., 2008b).

1.6.2. Susceptibility of *GMS* KO mice to non-infective inflammation

Irgm1 KO mice are also susceptible to a variety of inflammatory stimuli that are not directly induced by infection with a pathogen, but all directly or indirectly stimulate IFNγ production. Intraperitoneal LPS injection in concentrations resisted by all of the wild type mice, had caused death of all *Irgm1* KO mice within 2 days post injection (Bafica et al., 2007).

Induction of colitis by addition of dextran sulfate-sodium (DSS) to drinking water had caused a severe phenotype in the *Irgm1* KO mice. These mice exhibit greater degree of weight loss, altered stool consistency and rectal bleeding than WT mice. They also suffer

from significant atypical ileal injury including increased infiltration by lamina propria inflammatory cells, local epithelial denudation, mild goblet cell depletion and crypt epithelial cell hyperplasia. Paneth cells of these mice are morphologically changed and showed increased number of autophagosomes (Liu et al., 2013).

The role of Irgm1 in experimental autoimmune encephalomyelitis (EAE), a mouse model of multiple sclerosis, and permanent middle cerebral artery occlusion (pMCAO), a mouse model for stroke, was also investigated. It was reported that *Irgm1* KO mice treated with EAE inducer, myelin basic protein (MBP), had shown milder neuro-inflammatory phenotype of EAE and simultaneously increased death of CD4 positive cells in comparison to the induced WT mice (Xu et al., 2010) (Wang et al., 2013). In the mouse model of stroke, infarct area in the *Irgm1* KO mice was reported to be significantly larger than in the WT mice after pMCAO induction (He et al., 2012).

Irgm1 was also proposed to be involved in the regulation of the oxLDL uptake by macrophages, suggesting the importance of this gene in artherosclerosis (Xia et al., 2013).

Even though these preliminary reports in the involvement of the Irgm1 in a variety of diseases remain to be further investigated, it seems that every inflammatory disease that induces IRG protein expression has severe consequences for the *Irgm1* KO mouse.

1.6.3. Susceptibility of *GMS* KO cells to inflammation

Analysis of *Irgm1* KO-derived cells that express IRG proteins strengthens the hypothesis that *Irgm1* KO mice can die after treatment with any stimulus that induces expression of other IRG proteins (chapters 1.6.1. and 1.6.2).

After IFNγ induction, *Irgm1* KO BMDMs have decreased adhesion and motility properties compared with WT BMDMs (Henry et al., 2007). However, even though the morphology of these cells is changed, their proliferation and cell death rate are similar to WT BMDMs (Henry et al., 2007).

Analysis of isolated *Irgm1* KO lymphocytes had shown that these cells encounter proliferation and survival problems after induction. Isolated CD4 positive lymphocytes from *Irgm1* KO mice, induced with agonistic monoclonal antibodies (mAb) to CD3, display a growth defect shown by a thymidine incorporation test. Similarly, when splenic dendritic cells of *Irgm1* KO OT-II mouse, which was created by crossing of *Irgm1* KO and ovalbumin (OVA) TCR-transgenic mice, were stimulated by either OVA protein or OVA 323-339 peptide, the incorporation of thymidine and cell counts were lower. BrdU incorporation test showed that

DNA synthesis in individual cells was not impaired, but the proliferation of these cells, as shown with CFSE staining, was decreased. The number of dead (Propidium-iodide (PI) stained) cells was increased in OVA-induced *Irgm1* KO OT-II cells. EHej lectron-microscopy analysis showed an increase in autophagosome size and number in *Irgm1* KO lymphocytes after IFNγ induction (Feng et al., 2008b). Lymphocyte survival and proliferation were fully rescued in *Irgm1/Ifng* double KO mice, indicating that these phenomena are indeed IFN-dependent (Feng et al., 2008b).

Hematopoietic stem cells (HSCs) of *Irgm1* KO mice, which express IRG proteins without IFN-induction, were also analyzed (Ivanova et al., 2002) (Ramalho-Santos et al., 2002) (Feng et al., 2008a) (King et al., 2011). After exposure to sublethal dose or irradiation, *Irgm1* KO mice showed impaired recovery of bone marrow and thymic cellularity. In competitive and non-competitive bone marrow transplantation assays, *Irgm1* KO HSC had failed to properly repopulate the hematopoetic system (Feng et al., 2008a). When challenged with hematopoetic ablation by 5-fluorouracil (5-FU) or by infection with *M. avium*, *Irgm1* KO mice did not achieve the expected expansion response in stem and progenitor cell populations (Feng et al., 2008a). However, these self-renewal and repopulation defects were fully restored in *Irgm1/Irgm3* double KO mice (King et al., 2011).

Taken together, it seems that the IFNγ response and IRG protein expression affect cell survival and proliferation of *Irgm1* KO lymphocytes and hematopoetic stem cells. However, the survival and proliferation of BMDMs are not affected, indicating that the phenotype of *Irgm1* KO mice is not caused by the failure of every cell in the mouse, but rather particular cell groups.

1.6.4. Models of Irgm1 function

Due to its importance in the protective response to various pathogens, involvement in inflammation and maintenance of the HSC pool, different mechanisms of action have been suggested for Irgm1. In principle, three models concerning the molecular function of Irgm1 have been proposed: the first one suggests Irgm1 involvement in the acidification of bacterial phagosome, the second one describes Irgm1 as an autophagy regulator and the third one proposes that Irgm1 is an essential negative regulator of other IRG proteins whose absence leads to pathological defects.

a) Irgm1 as a regulator of phagosomal acidification

Irgm1 was firstly proposed to target the bacterial phagosome, to facilitate its transfer to lysosomes and induces phagosomal acidification (reviewed in (MacMicking, 2012)). This model is based on studies that analyzed the response of *Irgm1* KO cells and mice to *Mycobacterium tuberculosis* infection (MacMicking et al., 2003). *Irgm1* KO mice were reported to be highly susceptible to infection with *Mycobacterium* and *Listeria* (chapter 1.6.1.) and it has been claimed that Irgm1 localizes to mycobacterial and listerial phagosomes (Shenoy et al., 2007) (Tiwari et al., 2009). In WT macrophages, fusion of mycobacterial phagosomes and lysosome is enhanced in the presence of IFNγ and phagosomal acidification that follows. However, the pH drop could not be detected in infected, IFNγ-induced *Irgm1* KO macrophages, indicating that the fusion of phagosomes and lysosomes in these cells is impaired (MacMicking et al., 2003). Furthermore, Irgm1 was proposed to have a preference to bind lipids that are present, although not exclusively, at the nascent phagosomal membrane: phosphatidylinositol-3,4-biphosphate (PitIns(3,4)P_2), phosphatidylinositol-3,4,5-triphosphate (PitIns(3,4,5)P_3) and diphosphatydil-glycerol (DPG) (Tiwari et al., 2009).

Therefore, it has been proposed that Irgm1 targets bacterial phagosomes and with the help of autophagic machinery, mediates their fusion with lysosomes (MacMicking et al., 2003) (Shenoy et al., 2007) (Tiwari et al., 2009) (MacMicking, 2012). Recently, the claimed localization of Irgm1 to the Mycobacterial and Listerial phagosome has been disputed (Springer et al., 2013) and therefore the model of Irgm1 as a regulator of phagosomal processing needs to be re-evaluated.

b) Irgm1 as an autophagy regulator

A role of Irgm1 in the regulation of autophagy was proposed in several different models.

On the one hand, the role of Irgm1 as an IFNγ-dependent direct effector and inducer of autophagic elimination of *M. tuberculosis* in macrophages has been suggested (Gutierrez et al., 2004) (Deretic, 2011). This model is based on the report that transfection of Irgm1 in non-IFNγ induced macrophages increased the amount of autophagosomes in the cell and that transfected GFP-Irgm1 accumulates at the autophagosomes (Gutierrez et al., 2004) (Singh et al., 2006). It has been shown that autophagic induction in WT cells can increase the fusion of Mycobacterial phagosomes with lysosomes and enhance *M. tuberculosis* clearance (Gutierrez et al., 2004). However, one should keep in mind that GFP-tagged Irgm1

was shown to mislocalize in comparison to endogenous Irgm1 and therefore the indicated observations might be misinterpreted (Zhao et al., 2010).

It has been also suggested that Irgm1 and Irgm3 are involved in autophagic degradation of the ubiquitinated GKS protein aggregates and therefore, GKS aggregates are formed in their absence (Traver et al., 2011). In addition, co-localization of IRG proteins and autophagic LC3-structures was observed in *Irgm1/Irgm3* KO MEFs, suggesting involvement of autophagy in the IRG protein degradation (Haldar et al., 2013).

On the other hand, it was proposed that autophagy increase can induce the death of *Irgm1* KO cells and thus that Irgm1 might inhibit autophagic cell death (Feng et al., 2008b) (Feng et al., 2009) (King et al., 2011). This model was based on the reports that show that induced *Irgm1* KO lymphocytes and hematopoietic stem cells (HSCs) have increased number of autophagosomes (Feng et al., 2008b) (Feng et al., 2008a) (King et al., 2011). When *Irgm1* KO mice were exposed to dextran sulphate sulphate to induce intestinal inflammation, the number of LC3-positive autophagic structures was increased in their Paneth cells (Liu et al., 2013). Induced *Irgm1* KO lymphocytes also undergo cell death, which can be avoided by silencing of a protein of the autophagic cascade named Beclin-1 (Feng et al., 2008b). However, the possibility that the autophagy in *Irgm1* KO cells is the last attempt to rescue the cell before it dies has also been proposed (Deretic, 2011).

It is important to note that these opposing models are based on experiments performed in very different cells under different conditions: on the one hand on the non-IFNγ-induced, slow-dividing macrophages transfected with GFP-Irgm1 and, on the other hand, in the fast-dividing induced *Irgm1* KO lymphocytes, HSC and intestine cells that are sensitive to stress and cell death (Feng et al., 2009).

c) Irgm1 as a negative regulator of other IRG proteins

Instead of a role of Irgm1 as a direct effector involved in pathogen resistance, it has been proposed that the effects of losing this protein could be an indirect consequence of its function as a negative regulator of GKS IRG proteins. This model originates from the experiments that show that GMS proteins play a role as a negative regulators of GKS protein activation and aggregation (Hunn et al., 2008) (Papic et al., 2008) (Hunn and Howard, 2010). As previously explained (chapter 1.4.4.), GMS proteins keep GKS proteins in the GDP-bound state and when even one GMS protein is missing, GKS protein form non-functional aggregates (Hunn et al., 2008). Moreover, it has been shown that susceptibility of *GMS* KO mice to *T. gondii* is caused by the inability of aggregated GKS proteins to relocalize to the PVM (Hunn et al., 2008). However, many other pathogens, like *L. monocytogenes* and *M.*

avium (chapter 1.6.1.), are still able to kill the *Irgm1* KO mice, but not *Irgm3* KO or *Irgm1/Irgm3* KO mice. Thus, it has been proposed, that GKS aggregate-like structures in *Irgm1* KO, *Irgm3* KO or *Irgm1/Irgm3* KO cells have different localization that influences their toxicity (Hunn and Howard, 2010) (Howard et al., 2011).

Considering that GMS proteins are localized to different endocellular membranes, it has been proposed that each GMS protein protect the particular cellular membranes from accumulation of GKS proteins in aggregate-like structures by preventing their activation and maintaining the GDP-bound state (Hunn and Howard, 2010) (Howard et al., 2011). Irgm1 is the only GMS protein that localizes to the lysosomes and it is hypothesised that in the absence of Irgm1 activated GKS proteins can localize to the lysosomes. Likewise, the endoplasmic reticulum to which Irgm3 localizes, would accumulate activated GKS proteins in *Irgm3* KO cells. Localization of activated aggregated GKS proteins to different endocellular membranes could have different consequences for the cell: GKS proteins on the lysosomes in *Irgm1* KO cells might cause cytopathic defects in the cells thorough dysfunction or damage to lysosomes, while GKS proteins on the ER in *Irgm3* KO cells might not cause so severe phenotype (Howard et al., 2011). Recently it has been also been reported that in *Irgm1/Irgm3* KO cells, GKS proteins relocalize to the lipid droplets, a compartment carrying both Irgm1 and Irgm3, indicating that GMS proteins indeed could regulate sub-cellular localization of the GKS proteins (Haldar et al., 2013).

It has been proposed that the role of GMS proteins is to help GKS proteins to recognize membrane-bounded vacuoles containing pathogens by "missing self" principle (Martens, 2004) (Hunn and Howard, 2010) (Haldar et al., 2013) (Coers, 2013) (da Fonseca Ferreira-da-Silva et al., 2014). Pathogens like *T. gondii*, *C. trachomatis* and *E. cuniculi* enter the cell by unusual mechanisms, retaining, but modifying the plasma membrane (Chapther 1.5.1.). This modified vacuolar membrane, derived from plasma membrane, is not protected by GMS proteins, while all the endogenous intracellular membranes are probably coated with GMS proteins. Therefore, it has been proposed that the vacuolar membranes of these organisms, carrying no self GMS proteins, are unable to suppress the local activation of GKS proteins. Pathogens like *Mycobacterium*, that enter the cell via phagocytosis and are still protected by an unknown factor or effect that inhibits GKS activation at the unmodified plasma membrane are not attacked by GKS proteins (da Fonseca Ferreira-da-Silva et al., 2014). IFNγ induction, which occurs in *Mycobacteria* and other infections, is sufficient to induce IRG protein expression. Therefore, in IFNγ-induced *Irgm1* KO cells and infected *Irgm1* KO mice, unregulated GKS proteins could relocalize to the lysosomes and impact the proper function of these organelles. However, in induced *Irgm3* KO cells, activated GKS

proteins would preferentially occur on ER membranes with less severe consequences for the cell and for the mouse (Howard et al., 2011) (da Fonseca Ferreira-da-Silva et al., 2014).

1.7. The aim of study

A GMS protein Irgm1 was proposed to play very different roles: from a pan-defensive protein involved in resistance to a wide spectrum of pathogens, over important anti-inflammatory regulator involved in a variety of intestinal and neurological diseases to the positive/negative regulator of autophagy. Nevertheless, it has been shown that, after infection with a variety of pathogens, *Irgm1* deficient mice become strikingly leukopenic and die. However, *Irgm3* deficient mice can fully recover from infection with the most of pathogens that kill *Irgm1* KO mice.

The aim of this study is to better understand the mechanism of Irgm1 action and the difference between Irgm1 and other GMS proteins involved in IRG protein regulation. Therefore, it has been proposed that GMS proteins, except for keeping GKS proteins in the the inactive GDP-bound state, also protect endocellular membranes from GKS proteins. Since Irgm1 is the only GMS protein reported at the lysosomes, it has been hypothesized that GKS proteins localize to the lysosomes in its absence. In accordance to that, since Irgm3 is the only GMS protein at the endoplasmic reticulum, it has been suggested that GKS would localize to this organelle in its absence.

Thus, the first part of this study is dedicated to the analysis of GKS protein localization in the absence of GMS proteins. Moreover, the hierarchy of different GKS proteins during loading to cellular organelles and the importance of this hierarchy in mouse model have been investigated.

In the second part of this study, the intracellular mechanism of Irgm1 action has been investigated. After describing accumulation of GKS aggregate-like structures to lysosomes in *Irgm1* KO cells, the possible consequences of this accumulation, namely autophagic flux impairment, lysosomal acidity and lysosomal membrane permeablilization have been studied.

In the third part, death of *Irgm1* KO MEF and BMDM cells was analyzed, and finally, in the fourth part, solubility of the GKS aggregate-like structures was assessed.

2. MATERIALS AND METHODS

2.1. Materials

2.1.1. Instruments

Microscopes and special devices	Producer
Zeiss Axioplan II fluorescence microscope	Zeiss, Jena, Germany
AxioCam MRm camera	Zeiss, Jena, Germany
Zeiss Axiovert 200 M motorized microscope	Zeiss, Jena, Germany
Wrap-around temperature-controlled chamber	Zeiss, Jena, Germany
AxioCam MRm camera	Zeiss, Jena, Germany
UltraVIEW VoX confocal microscope	Nikon, Tokyo, Japan
Spinning disc CSU-X1	Yokogawa Corporation of America, Newnan, GA
EMCCD C9100-50 CamLink camera	CamLink, UK
Minifold I 96 well Dot-Blot system	Whatman, Dassel, Germany
Optima^{TM} TLX Ultracentrifuge	Beckman Coulter, Krefeld, Germany

2.1.2. Chemicals and supplies

Chemicals and supplies	Producer
4',6-Diamidino-2-phenylindol (DAPI)	Roche Diagnostics, Mannheim, Germany
Albumin fraction V (BSA)	Carl Roth, Karlsruhe, Germany
Bafilomycin	Sigma-Aldrich, St Louis, MO
Bradford reagent	Bio-rad, Hercules, CA
Coverslips and microscopy slides	Paul Marienfeld, Lauda, Germany
Gene ruler DNA ladder mix	Thermo Scientific, Waltham, MA
Guanosine-triphosphate (GTP)	Sigma-Aldrich, St Louis, MO
FuGene 6 DNA Transfection reagent	Basel, Switzerland
H-Leu-Leu-OMe HBr	Bachem, Bubendorf, Switzerland
Hoechst 33342 (Bisbenzimide)	Sigma-Aldrich, St Louis, MO
Lipopolysaccharide (LPS)	Sigma-Aldrich, St Louis, MO
Lysotracker Red DND-99	Life Technologies, Carlsbad, CA
µ-Slide I chambers	Ibidi, Martisried, Germany
Mifepristone	Sigma-Aldrich, St Louis, MO

Mouse Interferon gamma	Peprotech, Rocky Hill, NJ
my-Budget 5x PCR-Master mix	Biozym, Oldendorf, Germany
Page ruler prestained protein ladder	Thermo Scientific, Waltham, MA
Pierce BCA protein assay	Thermo Scientific, Waltham, MA
Pierce ECL western blotting substrate	Thermo Scientific, Waltham, MA
ProLong Gold anti-fade reagent	Life Technologies, Carlsbad, CA
Propidium-Iodide	Life Technologies, Carlsbad, CA
Rapamycin	Sigma-Aldrich, St Louis, MO
Saponin	Sigma-Aldrich, St Louis, MO
Super RX films	Fujifilm, Tokyo, Japan
X-treme GENE 9 DNA Transfection reagent	Roche, Basel, Switzerland

2.1.3. Antibodies

Primary antibodies	Antigen recognized	Type	Dilution	Source
165/3	Recombinant mouse Irga6	rabbit polyclonal	IF 1:8000	(Uthaiah et al., 2003) (Martens et al., 2004)
10E7	Recombinant mouse Irga6	Mouse monoclonal	IF 1:1000	(Zerrahn et al., 2002) (Martens et al., 2004) (Papic et al., 2008)
10D7	Recombinant mouse Irga6	Mouse monoclonal	IF 1:1000	(Zerrahn et al., 2002) (Martens et al., 2004) (Papic et al., 2008)
141/3	Mouse Irgb6	rabbit polyclonal	IF 1:5000	(Khaminets et al., 2010)
81/3	Mouse Irgd	rabbit polyclonal	IF 1:8000	AG Howard collection
1D4B	LAMP1	Rat monoclonal	IF 1:1000	1.Developmental Studies Hybridoma Bank, University of Iowa 2.AbCam ab25245
GM130	GM130	Mouse monoclonal	IF 1:1000	BD Bioscience, Heidelberg, Germany
L7543	LC3B	Rabit polyclonal	WB 1:5000	Sigma-Aldrich
A2228	B-Actin	Mouse	WB	Sigma-Aldrich

		monoclonal	1:5000	
AF965	Cathepsin B	Goat polyclonal	IF 1:1000	R&D systems
FK2	Ubiquitin conjugates	Mouse monoclonal	WB 1:1000	Biotrend

Secondary antibodies	Dilution	Source
Alexa Fluor 488/555/647: • donkey anti-mouse, • donkey anti-rabbit, • donkey anti-rat • donkey anti-goat	IF 1:1000	Life Technologies, Carlsbad, CA
HRP-conjugated: • goat anti-mouse • donkey anti-rabbit • goat anti-mouse	WB 1:5000	Sigma-Aldrich, St Louis, MO Sigma-Aldrich, St Louis, MO Pierce, Rockford, IL

2.1.4. Buffers and media

Buffer	Recipe
Phosphate buffer saline (PBS)	137 mM NaCl, 2.7 mM KCl, 10 mM Na_2HPO_4, 1.8 mM KH_2PO_4 in H_2O pH 7.4
RIPA buffer	25 mM Tris pH 8 150 mM NaCl 0.1% sodium dodecyl sulfate 0.5% sodium deoxycholat 1% Nonidet P-40 10% Glycerol 2 mM EDTA
Modified RIPA buffer	150 mM sodium chloride 1.0% SDS 0.5% sodium deoxycholate 0.1% Triton X

	50 mM Tris, pH 7.4
IF fixation buffer	3% Paraformaldehyde (PFA) (w/v) in PBS
IF washing buffer	0.1% Saponin (w/v) in PBS
IF blocking buffer	3% bovine serum albumin (BSA) (w/v) 0.1% Saponin (w/v) in PBS
NP-40 cell lysis buffer	0,1% NP-40 (w/v) in PBS
Laemmli buffer (10x SDS sample loading buffer)	0.5 M Tris-HCl, pH 6.8 50% Glycerol (v/v) 10% SDS (w/v) 0.025% Bromphenol blue (w/v) 7% β-Mercaptoethanol (v/v)-right before use
SDS running buffer	250 mM Tris 1.92 M glycine 34.67 mM SDS
WB transfer buffer	250 mM Tris 1.92 M glycine
WB washing buffer	0,1% Tween 20 (w/v) in PBS
WB blocking buffer	5% milk powder (w/v) 0,1% Tween 20 (w/v) in PBS
Triton X lysis buffer	0,1 % Triton X (w/v) in PBS
TBST	50 mM Tris 150 mM NaCl 0.05% Tween 20 pH 7.6
Detection solution 1	88.5 ml H2O 10 ml 1M Tris-HCl, pH 8.5 1 ml 250 mM Luminol (3-Aminophthalhydrazide) in DMSO 0.44 ml 90 mM p-Coumaric acid in DMSO
Detection solution 2	90 ml H_2O 10 ml 1 M Tris-HCl pH 8.5 60 µl 30% H_2O

Cell culture reagents	Recipe
Medium for: • Mouse embryonic fibroblasts (MEFs) • A31 3T3 fibroblasts • GS 3T3 fibroblasts • Diaphragm-derived cells • RAW309 macrophages	• Dulbecco's modified Eagle's medium (DMEM) high glucose (2010-2012: PAA, Pasching, Austria; 2013-2014 Life Technologies) • 10% fetal calf serum (FCS),(2010-2012: PAA, 2013-2014 Biochrom, Berlin, Germany) • 2 mM L-glutamine (PAA), • 1 mM sodium pyruvate (PAA, Life Technologies), • 1x MEM non-essential amino acids (PAA, Life Technologies), • 100 U/ml penicillin and 100 µg/ml streptomycin (PAA, Life Technologies), • For GS 3T3 fibroblasts also: 50µg/ml Hygromycin and 200 µg/ml Zeocin (Life Tech)
Bone-marrow derived macrophages (BMDMs) medium	• Roswell Park Memorial Institute medium(RPMI) (2010-2012: PAA, Pasching, Austria; 2013-2014 Life Technologies) • 25% fetal calf serum (FCS), 2010-2012: PAA, 2013-2014 Biochrom, Berlin, Germany) • 10% L929 P2 cell-conditioned medium • 2 mM L-glutamine (PAA), • 1 mM sodium pyruvate (PAA, Life Technologies), • 1x MEM non-essential amino acids (PAA, Life Technologies), • 100 U/ml penicillin and 100 µg/ml streptomycin (PAA, Life Technologies)
Medium for cell freezing (Freeze mix)	• 10% Dimethyl-sulfoxide (DMSO) (v/v) • 90% FCS
Trypsin	• 5% Trypsin (1:250) (w/v) (Life technologies) • 17 mM EDTA • 145 mM NaCl

2.1.5. Constructs

The following expression constructs were used:

Construct	Source
pGW1H-Irgm1	(Martens et al., 2004)
pGW1H-Irgm2	(Martens et al., 2004)
pGW1H-Irgm3	(Martens et al., 2004)
pmCherry-N3	(Zhao et al., 2010)
pEGFP-Irga6-ctag1	(Zhao et al., 2010)
pEYFP-Calreticulin	Kindly provided by Astrid Schauss, CECAD Imaging Facility
pEGFP-LC3	Howard lab collection, Yang Zhao

2.1.6. Mice

All mice were bred at the Institute for Genetics, University of Cologne (Cologne, Germany). The mice were kept on a 12/12 h light/dark cycle. Pelleted food (Altromin, Lage, Germany) and water were available *ad libitum*. A maximum of four animals were caged together.

Irgm1 KO mice were generated as previously described (Collazo et al., 2001) and kindly donated by Dr. Gregory Taylor (Duke University, Durham, NC). *Irga6* KO mice were generated as previously described (Liesenfeld et al., 2011) and bred at the Institute for Genetics.

$Irgm1^{-/-}/Irga6^{-/-}$ mice were generated by crossing $Irgm1^{-/-}/Irga6^{+/+}$ mice with $Irgm1^{+/+}/Irga6^{-/-}$ to form heterozygous $Irgm1^{+/-}/Irga6^{+/-}$ offspring. The heterozygous $Irgm1^{+/-}/Irga6^{+/-}$ mice were intercrossed and their offspring was weighted and genotyped 3 weeks after birth. 4-8 weeks old $Irgm1^{-/-}/Irga6^{-/-}$, $Irgm1^{+/+}/Irga6^{-/-}$, $Irgm1^{-/-}/Irga6^{+/+}$ and $Irgm1^{+/+}/Irga6^{+/+}$ mice were used for infection experiments with *Listeria monocytogenes*.

2.1.7. Cells

Mouse embryonic fibroblasts (MEFs)

MEFs were prepared from C57BL/6 mice at day 14 post coitum and propagated in supplemented DMEM medium maximal 15 passages.

Immortalized MEFs

Irgm1$^{-/-}$, Irgm3$^{-/-}$, Irgm1/Irgm3$^{-/-}$ (kindly provided by Dr Gregory Taylor) and WT MEFs or were immortalised by the simian virus 40 large T antigen, which alters the effect of the tumour suppressor proteins pRb and p53. Because the knock-out cells were already neomycin resistant an additional plasmid carrying a puromycin resistance gene was transfected. Therefore, 5 μg pSV3-neo plasmid and 0.5 μg pPur were mixed and co-transfected. After 24 h, cells were put under selection with 3 μg/ml puromycin (Springer-Frauenhoff, 2014).

A31 3T3 cells

A31 3T3 BALB/C mouse fibroblasts were purchased from ATCC (stored in Howard lab collection) and propagated in supplemented DMEM medium.

Gene Switch (GS) 3T3 fibroblasts

Gene switch (GS) 3T3 cells contain hormone-inducible mamilian expression system that induces Irga6 production upon Mifepristone induction (Hunn, 2008). These cells were cultured in previously described medium with addition of 200 μg/ml Zeocin (Invivogen, San Diego, CA) and 50 μg/ml Hygromycin (Invivogen). Irga6 expression was induced with 1 nM Mifepristone (Life Technologies).

Bone marrow derived macrophages (BMDMs)

Primary bone marrow derived macrophages (BMDM) were isolated from tibia and femurs of 4- to 5-weeks old C57BL/6 mice and *Irgm1* KO mice as previously described (Henry et al., 2007) and differentiated in 10 cm cell culture dishes in previously described medium for 7 days, with regular medium exchange. Differentiated cells were frozen.

Diaphragm –derived cells (DDCs)

Diaphragm-derived cells (DDCs) were prepared from diaphragm tissue (Antony et al., 1989). Shortly, the diaphragm was removed under sterile conditions, washed thoroughly with PBS, homogenized, incubated with collagenase/dispase (1 mg/ml, Roche, Mannheim, Germany) for 1 h at 37°C and then centrifuged for 15 sec at 100 ×*g*. The supernatant was

collected, centrifuged for 5 min at 500 ×*g* and the pellet plated in DMEM. The remaining cell debris after collagenase/dispase-incubation were further incubated in 1× trypsin for 1 h at 37°C, and then centrifuged for 15 sec at 100 ×*g*. The supernatant was collected, centrifuged for 5 min at 500 ×*g* and the pellet was plated. DDCs were grown until they had reached about 80 percent confluence and were then immortalized by transfection with 1 µg of psv3-neo plasmid. Cells were grown and passaged for 5 weeks until immortalised clones had overgrown the culture.

RAW309 macrophages

RAW309 macrophages were purchased from ATCC and propagated in previously described medium.

2.1.8. Software

The images from Zeiss microscopes were processed with Axiovision 7.4. software. The images from spinning disc microscope were processed with Velocity 6.3 software (Zeiss, Jena, Germany). Cell death assay images were quantified with Velocity 6.3 software (PerkinElmer, Waltham, MA) using nuclei recognition selection filter.

The intensities of the antibody-stained bands after SDS-PAGE/Western-Blot analysis were quantified with Quantity One software (Biorad, Hercules, CA).

2.2. Methods

2.2.1. Freezing and thawing the of the mammalian cells

Mammalian cells were harvested by trypsinization (except for BMDMs), pelleted by spinning at 400 g for 5 min, and resuspended ($4*10^6$ cells/ml) in ice-cold sterile FCS with 10% DMSO (v/v) and frozen at -80°C. Frozen cells were stored in liquid nitrogen for long-term storage. BMDMs and RAW309 macrophages were not trypsinized, but detached by 5 minute incubation on ice, and pelleted at 300g for 5 minutes.

Cells were thawed at 37°C, immediately transferred into 10 ml of medium, pelleted and plated in fresh medium in a T75 flask.

2.2.2. Passaging and seeding of the cells

For passaging, cells were first washed once with sterile PBS and then detached by 2 minute incubation with 5 ml trypsin solution at 37°C. After addition of 5 ml medium, cells were pelleted by centrifugation, resuspended in fresh medium and plated.

Following amounts of cells were used for the following experiments:

- Immunofluorescence microscopy on fixed cells: 150 000 Immortalized MEFs, A31 cells or GS 3T3 cells; 500 000 BMDMs per well of the 6 well plate
- Live cell fluorescence microscopy: 60000 immortalized MEFs in μ-Slide I chambers
- Cell death assay: 300 000 immortalized MEFs or 400 000 BMDMs in 6 cm cell culture dish.
- LC3 turnover WB analysis: 300 000 immortalized MEFs per well of the 6 well plate
- Filter trap assay and ultracenrifugation aggregate solubility assay: 300 000 GS 3T3 cells per well of the 6 well plate

2.2.3. Transfection

Transient transfection of cells was conducted with 1:3 mixture of DNA (1-2 μg) and transfection reagents FuGene 6 or X-tremeGene 9. The DNA was mixed with 100μl of the serum-free DMEM or RPMI medium and transfection reagent was carefully added into the solution. After 15 minutes of incubation, mixture was spread over the cells in 6 well cell culture plates in a dropwise manner. Samples were analysed 24 h later.

For the live cell imaging experiments, the 100μl transfection mixture containing maximum 0,5μg of DNA was added into the cell-filled channel of the of μ-Slide I chambers. The reservoirs of the chamber were also supplied with FCS-free medium. The total medium was replaced with FCS-containing medium 8 hours post transfection.

2.2.4. Indirect immunofluorescence microscopy

For immunocytochemistry, cells were grown on previously flamed cover slips in 6-well plates. After treatments, cells were carefully rinsed once with PBS to remove the medium, fixed in 3% paraformaldehyde for 10 minutes at the room temperature and then triple washed

with PBS. The cells were permeabilized with washing buffer for 15 minutes and treated with blocking buffer for 1 hour at the room temperature. Staining with primary or secondary antibodies, which were diluted in blocking buffer, was performed at the room temperature in the wet chamber for 1 hour or 30 minutes respectively. Between the staining steps cells were triple washed for 5 minutes per wash with IF washing buffer (0.1% saponin in PBS). Washed cover slips with stained samples were mounted on glass microscopic slides in ProLong Gold anti-fade reagent.

The images were taken with an Axioplan II fluorescence microscope and AxioCam MRm camera at 630x magnification and processed by Axiovision 4.7 software. Alternatively, confocal images were taken with UltraVIEW VoX spinning disc (CSU-X1; Yokogawa Corporation of America) confocal microscope (Nikon, Tokyo, Japan) with EMCCD C9100-50 CamLink camera at 630x magnification. Confocal images were processed with Volocity 6.3 software (Perkin Elmer, Waltham, MA).

2.2.5. Blind co-localization analysis

Blind analysis of the samples was applied in all experiments in which it was possible. To analyze the co-localization of GKS proteins with endocellular membranes, prepared and labelled microscopic slides were blinded with tape before imaging. After imaging, the pictures of the samples were screened and the appropriate minimal size of the GKS-structure, which should be counted, was determined. GKS structures bigger than the given size were manually counted and for every structure was manually estimated whether it co-localizes with the marker of interest, for example with LAMP1 structures. The identity of the samples was revealed only upon full quantification and plotting of the data.

2.2.6. Live cell imaging

Live cell imaging was performed in μ-Slide I chambers (Ibidi, Martinsried, Germany). 60 000 cells were seeded in each chamber. After 24 hours, cells were transfected with 0,5 μg DNA and 1,5 μl X-tremeGENE 9 transfection reagent as previously described and incubated for 24 hours. Directly before imaging, medium was exchanged with fresh phenol red free medium containing 50mM of Lysotracker Red. Imaging was performed by Axiovert 200 M microscope with AxioCam MRM camera (Zeiss) at 630x magnification, which was fitted with a wrap-around temperature-controlled chamber at 37°C. The images were processed with Axiovision 4.7. software.

2.2.7. Cell death assay

200 000 of immortalized MEFs or 300 000 BMDM cells were seeded on 6 cm cell culture dish in 2 ml of medium. Samples were induced with 200 U/ml IFNγ, 10 mM LeuLeuOMe, 500 ng/ml Lipopolysaccharide or left un-treated for 24, 48 or 72 hours. Before analysis, 500 μl of medium containing 2,5 μg/ml of Propidium Iodide and 2,5 μg/ml Hoechst 33342 dye was added directly the cells without removal old medium and incubated for 15 minutes at 37°C.

10 images of each sample, each containing 500-1000 cells, were taken with the fluorescent Axiovert 200 microscope at 100x magnification. Number of Hoechst positive nuclei (blue) and PI positive (red) punctae was quantified with Volocity 6.3 software.

2.2.8. SDS-PAGE/ Western Blot analysis

Sodium dodecyl sulphate polyacrylamide gel electrophoresis (SDS-PAGE) was used to separate proteins of cell lysates. A discontinuous gel-system concentrates polypeptides on the intersection of two gel phases before they get separated according to their molecular weight in the resolving gel. Upper ¼ of the gel consists of the stacking gel, with has 4% of acrylamid and pH 6.8 and bottom ¾ of the gel consists of the separating gel, which has 10% acrylamid and pH 8.8. Gels were casted in between two glass plates, which are separated by plastic spacers. Equal amounts of the protein samples and PageRuler™ Prestained Protein Ladder were loaded onto gels. The SDS-PAGE was run in electrophoresis buffer at a current 20 mA for several hours.

For immunodetection the separated proteins were transferred from the polyacrylamide gel onto nitrocellulose membrane by wet Western Blotting. Therefore, the gel was carefully placed on top of the membrane, sandwiched between eight sheets of Whatman paper and two electrodes and placed in a blotting chamber. The chamber was filled with 1x Electrophoresis Transfer buffer and 0.5 Volts were applied, so that the negatively charged proteins were migrating towards the anode onto the membrane. After 1 h at RT the successful transfer was confirmed by unselective staining of proteins on the membrane with Ponceau S solution.

First the unspecific binding sites on the membrane were blocked with 5% milk powder in WB washing buffer for about 1h at room temperature. The primary antibody was diluted in 1% FCS in PBS an incubated with the membranes over night at 4°C. The next day, the

membranes were washed three times with WB washing buffer for 10 min and subsequently incubated for 30 minutes with HRP-conjugated secondary reagents diluted in 1% FCS in PBS. The membranes were triple washed. Detection buffer 1 and 2 were mixed in a ratio 1:1 and incubated with the membranes for 60 seconds. Membranes were dried and chemiluminescence was visualised by exposure of Super RX films (usually 5s, 30s, 1min to 5min) and film development.

2.2.9. LC3 turnover monitoring

100 000 MEFs/well were seeded in 12 well cell culture plate. Samples were induced with 200 U/ml IFNγ for 24 hours, with 40 µg/ml Rapamycin or with 200nM Bafilomycin for 2 hours, or left untreated. Samples were lysed with 80 µl modified RIPA buffer (0,1% NP-40 and 1% SDS) by 5 minutes of shaking and 5 minutes of 95°C incubation. The amount of protein was quantified with BCA assay and 20 µg of samples were subjected to 10% SDS-PAGE and Western blot analysis. Membranes were blocked in 5% non-fat dry milk in TBST buffer and probed for the proteins of interest with anti-LC3B and anti-β-Actin antibody and corresponding secondary antibodies. Membranes were triple washed with TBST buffer after primary and secondary antibody incubation. For the secondary antibody signal detection, membranes were incubated with Pierce ECL solution for 60 seconds. The intensity of the Western Blot LC3 and β-actin bands was quantified with Quantity One software (Biorad, Hercules, CA).

This experiment was performed in co-operation with Dr Susanne Bohlen at the Institute for Medical microbiology, immunology and hygiene, University of Cologne.

2.2.10. Filter trap assay and ultracentrifugation solubility analysis

1 000 000 RAW309 macrophages were seeded at 10 cm bacterial dishes, incubated for 24 hours and induced with 500 ng/ml LPS. After 12 hours cells were harvested and lyzed with the modified RIPA buffer. The protein content of the lysates was quantified with the Braford assay.

300 000 GS 3T3 Irga6 cells were seeded in each well of 6 well cell culture plate, incubated for 24 hours and treated with 1nM Mifepristone or 200 U/ml IFNγ prior for 24 hours. When stated, FCS-free medium containing 300µM $AlCl_3$, 10µM NaF and/or 0,5 mM GTP was added to the cells prior to the lysis. Cells were harvested, counted and lyzed in 0,5% Thesit in PBS, with $AlCl_3$, NaF or GTP added when stated.

For filter trap assay the nitrocellulose membrane was placed in the dot blotter and incubated with the WB washing buffer for 15 minutes. 50 µg cell lysate for RAW309 macrophages or labeled number of GS 3T3 cells was applied to each dot on the nitrocellulose membrane and filtered through the membrane. The filtration was followed by two washing steps with WB washing buffer. Membranes were treated similarly as in Western Blot analysis: blocked with WB blocking buffer, probed with particular antibodies, washed with WB washing buffer and detected with the detection solution. These experiments were preformed in collaboration with Dr Nadja Kettern at the Institute for Cell Biology, University of Bonn.

For the solubility ultracentrifugation analysis, the lysates of 30 000 GS 3T3 Irga6 cells were ultracentrifuged at 13000 rpm, pellet and supernatant were separated and analyzed with SDS-PAGE/Western Blot, as described in chapter 2.2.7.

2.2.11. Mouse genotyping

For mouse genotyping, tail samples were taken with flamed scalpel from anesthesized mice. DNA was extracted from mouse tail tip with 100µl 50mM NaOH at 95°C for 30 minutes. The samples were neutralized with 30µl 1M TRIS buffer of pH7.

The PCR mixture contained: 5µl of my-Budget 5x PCR-Master mix, 0,5µl of each primer, 17,5µl of water and 1µl of the isolated DNA. The following primers were used for Irgm1 and Irga6 genotyping:

Primer name	5'-3' sequence	Application
LRG1	GGAGAAAGTGAAGTACCC	Irgm1 genotyping
LRG3	CTCTGACACCGAGAGAAT	Irgm1 genotyping
NeoPr1	CATTTGTCACGTCCTGCA	Irgm1 genotyping
5 DEL (810)	TTGTTATTCAGGGAAGCTAAG	Irga6 genotyping
3 DEL (811)	TGTCTGGTGAATCTCATTAGC	Irga6 genotyping
5EX2 (812)	CTCAGGTTATCTAACATTCTG	Irga6 genotyping

PCR analysis was performed as stated in the table:

Irgm1 typing			*Irga6* typing		
95°C	5 min		94°C	2 min	
95°C	30 sec	|	94°C	30 sec	|
51°C	30 sec	|	58°C	30 sec	|
72°C	30 sec	|	72°C	45 sec	|
72°C	5 min		72°C	10 min	
4°C	~		4°C	~	
| 34 cycles			| 35 cycles		

The amplified fragments were separated at 2% Agarose gel. The 400 bp band (for *Irgm1*) and 450 bp band (for *Irga6*) represent the KO genotype. The 200 bp band represents the WT genotype.

2.2.11. Mouse infection with *L. monocytogenes*

Listeria monocytogenes were grown overnight in brain-heard infusion (BHI) medium, resuspended in fresh BHI medium and harvested during mid-log phase.

Four to eight week old *WT*, *Irga6*$^{-/-}$, *Irgm1*$^{-/-}$ and *Irgm1*$^{-/-}$/*Irga6*$^{-/-}$ mice (all offspring of *Irgm1*$^{+/-}$/*Irga6*$^{+/-}$ mice) were intraperitoneally infected with 2400 *L. monocytogenes,* which was resuspended in 200µl PBS, and their survival was monitored for two weeks.

The experiment was performed in cooperation with Dr Michael Schramm at the Institute for Medical microbiology, immunology and hygiene, University of Cologne.

3. RESULTS

3.1. Localization of GKS proteins is regulated by GMS proteins

3.1.1. Irga6 forms aggregates in the absence of GMS proteins

It has been well established that GMS proteins regulate nucleotide binding and aggregation of GKS proteins (Chapter 1.4.4.) (Papic et al., 2008) (Hunn et al., 2008). After IFNγ induction of mouse cells, endogenous GKS and GMS proteins are both expressed and immunostaining of these cells reveals that GKS proteins have a smooth, non-aggregated pattern (Martens et al., 2004) (Boehm et al., 1997) (Papic et al., 2008). However, immunostaining after expression of GKS proteins in the absence of GMS proteins results in formation of GKS aggregate-like structures (Martens et al., 2004) (Hunn et al., 2008) (Papic et al., 2008). When all three GMS proteins are co-transfected into these cells, the GKS proteins reconstitute a smooth non-aggregated pattern and re-gain the ability to load to the PVM of *T. gondii* (Hunn et al., 2008).

To reproduce recent reports about GMS regulation of GKS proteins, experiments analyzing the aggregation of Irga6 in the absence of different GMS proteins were conducted (Hunn et al., 2008) (Figure 6). For this purpose, four samples were prepared in parallel. In the first sample, A31 3T3 fibroblasts were left untreated and therefore did not express any GMS or GKS proteins (Figure 6A). In the second sample, A31 3T3 fibroblasts were induced with IFNγ to express the full set of GMS and GKS proteins (Figure 6B). In the third sample, cells were transfected with pGW1H-Irga6 to express only the GKS protein Irga6 in the absence of all GMS proteins (Figure 6C). In the fourth sample, *Irgm1* knock-out (KO) mouse embryonic fibroblasts (MEFs) were induced with IFNγ to express all GKS proteins and only two GMS proteins: Irgm2 and Irgm3 (Figure 6D). Cells were fixed, immunostained with the monoclonal antibody 10E7, which detects Irga6, and immunofluorescence microscopy images were taken.

In accordance with previous reports (Martens et al., 2004) (Hunn et al., 2008), immunofluorescence analysis of these samples revealed that Irga6 was not expressed in non-treated cells (Figure 6A), but showed smooth cytosolic/ER localization in IFNγ-induced A31 3T3 fibroblasts (Figure 6B). In the absence of GMS proteins, transfected Irga6 formed aggregate-like structures in A31 3T3 cells (Figure 6C). Irga6 also formed aggregate-like structures in IFNγ-induced *Irgm1* KO MEFs (Figure 6D), but of different appearance from those in Figure 6C, where all GMS proteins were absent. The transfected Irga6 in A31 3T3 cells, where all three GMS proteins are absent, formed fiber-like structures. However, in

IFNγ-induced *Irgm1* KO MEFs Irga6 aggregate-like structures had a ring-like shape. Clearly, Irga6 aggregates have different localizations depending on the presence of some or no GMS proteins.
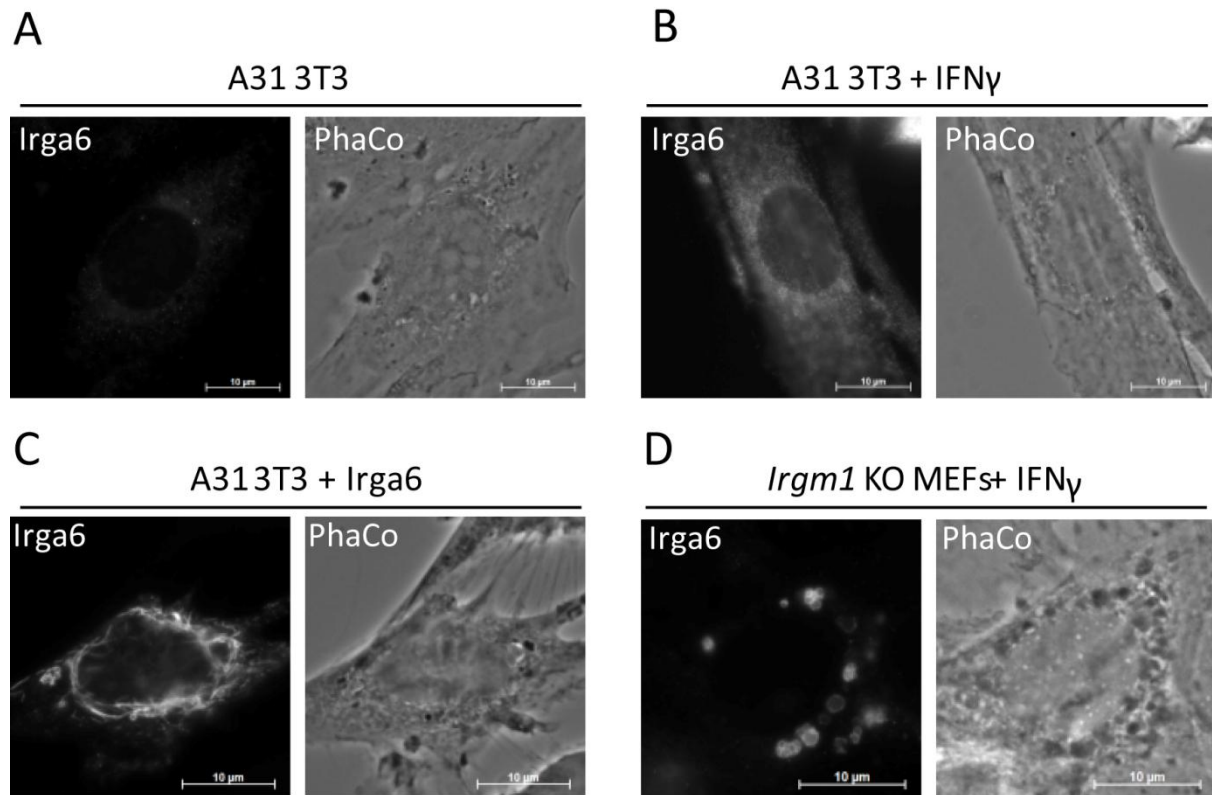

Figure 6. Irga6 forms aggregates in the absence of GMS proteins A31 3T3 fibroblasts were **A)** left untreated, **B)** induced with 200 U/ml IFNγ for 24 hours, **C)** transfected with pGW1H-Irga6, **D)** *Irgm1* KO MEFs were induced with 200 U/ml IFNγ for 24 hours. Cells were fixed and stained with an antibody against Irga6 (10E7). Representative images of Irga6 staining and Phase contrast (PhaCo) are shown.

3.1.2. Irga6 localizes to lysosomes in the absence of Irgm1

It has been reported that certain GMS proteins localize to certain endomembranes (Chapter 1.4.3.) and keep the GKS proteins in a GDP-bound inactive state (Hunn et al., 2008). Therefore, it has been proposed that particular GMS proteins protect particular endomembranes from the GKS protein accumulation and off-target activation and that in the absence of these GMS proteins, GKS proteins can accumulate at these membranes (Hunn and Howard, 2010).

Up to now, Irgm1 is the only GMS protein reported to localize to the lysosomes (Zhao et al., 2010). Thus, in this study we examined the possibility that in the absence of Irgm1, GKS proteins could accumulate at the lysosomes in IFNγ-induced *Irgm1* KO cells. Similarly, the absence of Irgm3 should give a different result with activated Irga6 expected at Endoplasmic reticulum (ER) membranes and not at lysosomes.

a) Endogenous Irga6 co-localizes with lysosomes specifically in *Irgm1* KO MEFs

To test whether Irga6 localizes to the lysosomes in the absence of Irgm1, immortalized wild-type (WT) MEFs, *Irgm1* KO MEFs, *Irgm3* KO MEFs and *Irgm1/Irgm3* KO MEFs were induced with IFNγ for 24 hours, immunostained for Irga6 (165/3 antiserum) and Lysosomal-Associated Membrane Protein 1 (LAMP1) (1D4B antibody) as late endosome/lysosome marker and subsequently analyzed by immunofluorescence microscopy (Figure 7A). Co-localization of Irga6 ring-like structures with LAMP1 was quantified by blind manual counting (materials and methods, chapter 2.2.5.) (Figure 7B).

In *Irgm1* KO cells, Irga6 formed clear ring-like structures of which over 95 percent co-localized with LAMP1. In contrast, in *Irgm3* KO cells less than 3 percent of Irga6 aggregate-like structures co-localized with LAMP1. In *Irgm1/Irgm3* double KO cells Irga6 structures did not co-localize with lysosomes, even though their surfaces are probably GMS-free.

Lysosomes in IFNγ-induced *Irgm1* KO cells appeared to be enlarged. The ring-like appearance of Irga6 at the lysosomes resembled the GKS protein rings that localize to the PVM of *T. gondii.* Hence, it might be that Irga6 ring-like structures do not represent conventional aggregates of non-functional missfolded proteins, but rather active GKS proteins that could be similar to GKS proteins at the PVM.
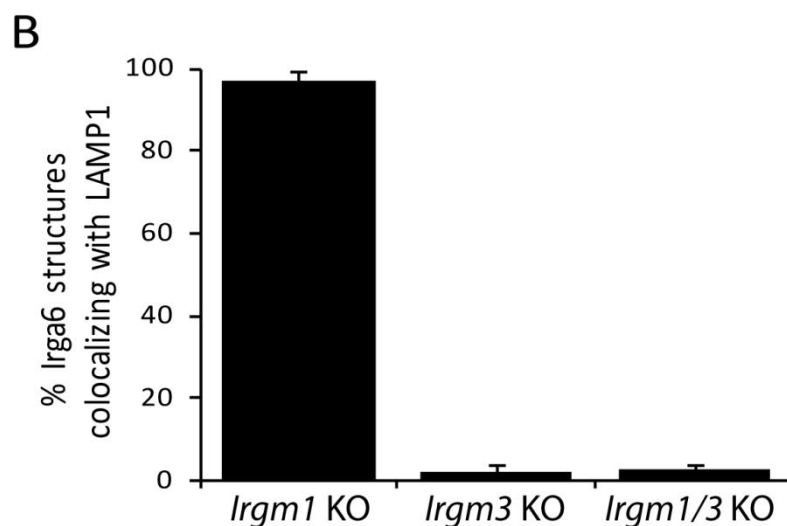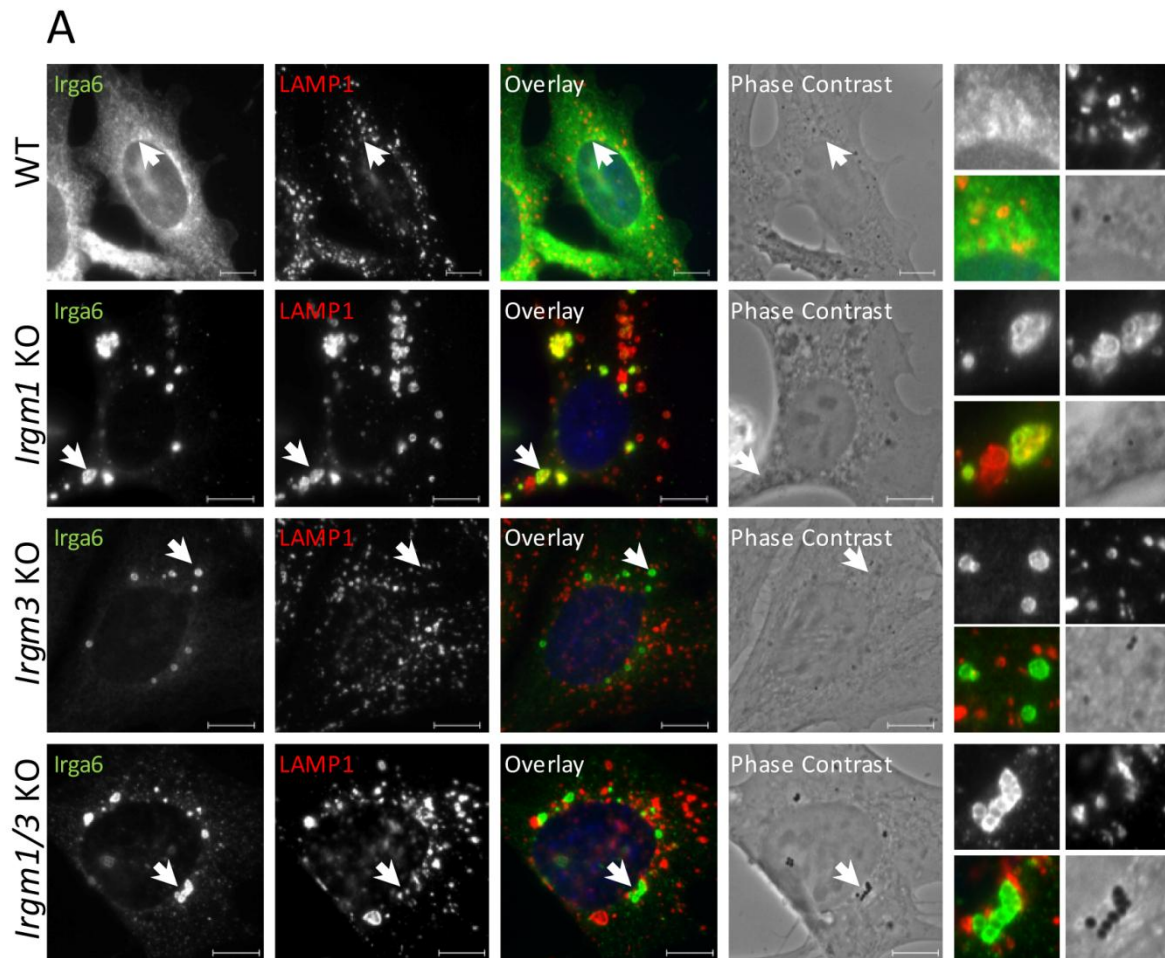
Figure 7. Irga6 co-localizes with LAMP1 in *Irgm1* KO MEFs A) WT, *Irgm1* KO, *Irgm3* KO and *Irgm1/Irgm3* KO MEFs were induced with 200 U/ml IFNγ for 24 hours. Cells were fixed and stained with immunoreagents against Irga6 (165/3) and LAMP1. Representative microscopic images of Irga6 and LAMP1 are shown. Arrows point at the Irga6 structures that are magnified at the end of each panel (zoom in the following order: upper left: Irga6, upper right: LAMP1, lower left: overlay, lower right: phase contrast). Scale bars represent 10 μM. **B)** Quantification of 7A, showing percent of Irga6 structures that co-localize with LAMP1. 100 cells per sample were counted and the means of three independent experiments +/- standard deviation are given.

To test whether Irga6 accumulations at the lysosomes are also in the GTP-bound state, similarly to previously described aggregates of transfected Irga6 (Martens et al., 2004) (Papic et al., 2008) and GKS accumulations on *T. gondii* PVM (Papic et al., 2008), IFNγ-induced *Irgm1* KO MEFs were stained for LAMP1 and with the 10D7 antibody, which exclusively detects the GTP-bound form of Irga6. The results of this experiment indicate that Irga6 accumulations at the lysosomes are indeed in the GTP-bound form (Figure S1). To exclude cross-reactivity during secondary staining of 10D7, which is a mouse antibody, and of 1D4B, which is a rat antibody, the control staining with each of the primary and secondary antibodies being omitted was performed (Figure S2).

b) Transfected EGFP-Irga6 co-localizes with lysosomes in *Irgm1* KO MEFs

Further, it was investigated whether transiently transfected EGFP-tagged Irga6 also accumulates to LAMP1 structures in the same manner as endogenous Irga6. Therefore, *Irgm1* KO MEFs were induced with IFNγ and simultaneously transfected with pEGFP-Irga6-ctag1 construct. Cells were fixed, stained for LAMP1 and analyzed by immunofluorescence microscopy.

Indeed, EGFP-Irga6 formed ring-shaped structures that co-localized with LAMP1 in the same manner as endogenous Irga6 (Figure 8). Therefore, transfected EGFP-Irga6 is also suitable for co-localization analysis when using endogenous Irga6 is not possible.
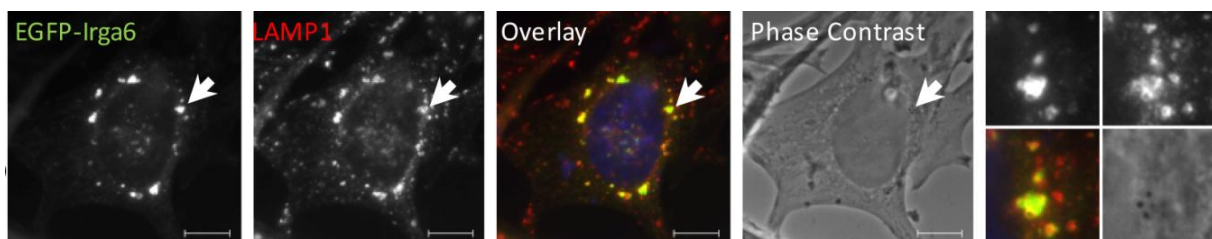
Figure 8. Transiently transfected EGFP-Irga6 co-localizes with LAMP1 in *Irgm1* KO MEFs *Irgm1* KO MEFs were induced with 200 U/ml IFNγ for 24 hours and simultaneously transiently transfected with pEGFP-Irga6-ctag. Cells were fixed and immunostained for LAMP1. Representative microscopic images of Irga6 and LAMP1 are shown. Arrows point at the Irga6 structures which are magnified at the end of each panel (zoom in the following order: upper left: Irga6, upper right: LAMP1, lower left: overlay, lower right: phase contrast).Scale bars represent 10 µM.

c) Irga6 co-localizes with lysosomes in Irgm2 and Irgm3-transfected cells

It was reported earlier that co-transfection of all three GMS proteins is necessary to reconstitute smooth non-aggregated structure of the tramsfected GKS proteins (Hunn et al., 2008) (Chapter 1.4.4). To understand better how different GMS proteins affect GKS aggregation and accumulation at different sub-cellular compartments, combinations of different GMS constructs were transfected into cells that contained only Irga6.

To validate this approach, cells were initially co-transfected with different combinations of GMS constructs and stained with Irgm1, Irgm2 and Irgm3 antibodies, showing that all GMS proteins from a transfection mixture were expressed in the same cell (data not shown). To avoid staining for every individual GMS protein in the final experiment, cytosolic pmCherry was co-transfected with GMS constructs to identify transfected cells (data not shown).

To test the localization of Irga6 in the presence of combinations of different GMS proteins, Gene Switch (GS) 3T3 cells, that stably express Irga6 under control of Mifepristone (MIF), were treated with MIF and transiently transfected with combinations of pGW1H-Irgm1, pGW1H-Irgm2, pGW1H-Irgm3 and mCherry. These cells were not treated with IFNγ, and thus did not express endogenous IRG proteins, but only Irga6 and transfected GMS proteins (Figure 9A). The cells were co-stained for Irga6 and LAMP1 and due to the round shape of the GS 3T3 Igra6 cells after induction and multiple transfections, analyzed by confocal microscope, which yielded slightly different look of lysosomes and Irga6 structures in comparison to other experiments. The co-localization of Irga6 structures and LAMP1 was quantified in mCherry positive cells, which are presumably GMS-transfected (Figure 9B).

When Irgm1 was transfected into the MIF-induced GS 3T3 Irga6 cells, less than 10 percent of the Irga6 structures co-localized with the lysosomes, which is in accordance with the hypothesis that Irgm1 protects the lysosomes from GKS protein accumulation. Similarly, in Irgm1 and Irgm2 or Irgm1 and Irgm3 co-transfected MIF-induced GS 3T3 Irga6 cells, less than 20 percent of Irga6 co-localized with LAMP1, which also corresponds to the hypothesis that Irgm1 might protect the lysosomes from GKS accumulation.

Opposingly, when Irgm2 and Irgm3 were co-transfected into these cells, more than 70 percent of Irga6 structures co-localized with the lysosomes, which corresponds to the GKS co-localization with the lysosomes in *Irgm1* KO cells. When Irgm3 alone was transfected into these cells, about 35 to 40 percent of the Irga6 structures co-localized with LAMP1, indicating that the Irga6 could be distributed between the lysosomes and the other structures which are not GMS coated, like for example Golgi.

However, further results of this experiment indicate that simplistic model, by which GKS proteins would localize to any membrane that is not GMS-protected, is probably not correct. Firstly, in non-transfected, MIF-induced GS 3T3 Irga6 cells, in which all endocellular membranes are GMS free, less than 10 percent of Irga6 co-localized with LAMP1. Secondly, in Irgm2 transfected MIF-induced GS 3T3 Irga6 cells, in which Golgi should be protected from GKS accumulation and other membranes should be GMS-free, less than 20 percent of Irga6 co-localized with LAMP1.
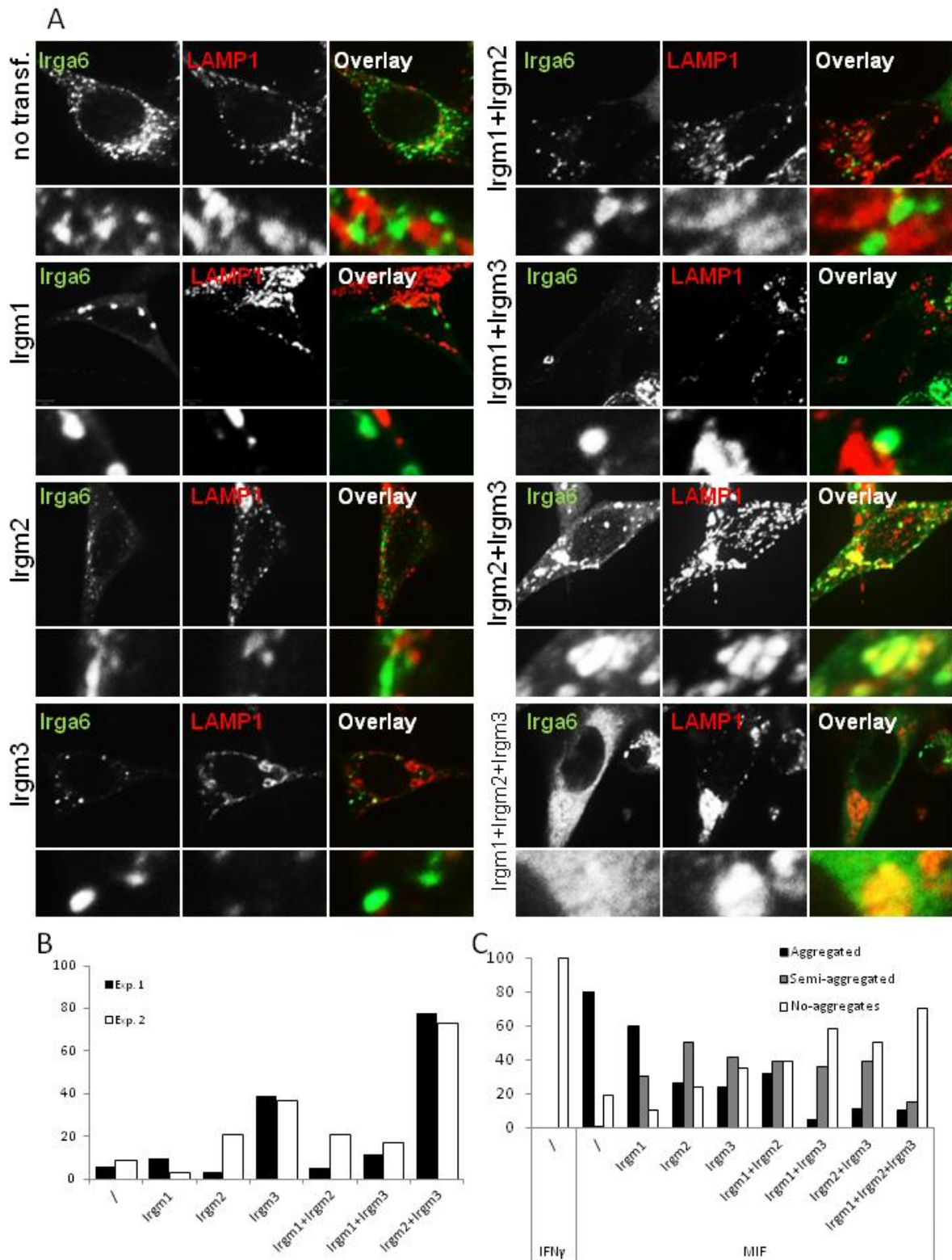
Figure 9. Irga6 co-localization with LAMP1 in cells transiently transfected with GMS protein A) Gene Switch (GS) 3T3 cells stably transfected with inducible Irga6 were stimulated with Mifepristone and simultaneously transiently transfected with pGW1H-Irgm1, pGW1H-Irgm2 and pGW1H-Irgm3 and pmCherry for 24 hours. Cells were fixed and stained with anti-Irga6 antiserum 165/3 and with anti-LAMP1 antibody. Pictures were taken with a confocal microscope. Representative microscopic images of Irga6 and LAMP1 are shown. Arrows point at the Irga6 structures which are magnified below each panel. **B)** Quantification of 9A, showing percent of Irga6 structures that co-localize with LAMP1. 50 cells per sample were quantified and counts of two independent experiments are shown. **C)** Quantification of 9A, showing percent of cells with aggregated, semi-aggregated and non-aggregated Irga6 structures. 100 cells per sample were quantified.

Previously, it has been shown that the co-transfection of all three GMS proteins is able reconstruct the smooth non-aggregated Irga6 pattern in MEF-induced GS 3T3 Irga6 cells (Hunn, 2008). The transfection of single GMS proteins also reconstructed the smooth Irga6 pattern in 20-50 percent of these cells (Hunn, 2008). To reproduce and better understand these results, the percentage of GMS-transfected MIF-induced GS 3T3 cells with aggregated, semi-aggregated and non-aggregated Irga6 was blind counted (Figure 9C). As previously shown, almost 100 percent of IFNγ-induced cells had a smooth Irga6 pattern and, in contrast, over 80 percent of MIF-induced cells, which were not GMS-transfected, had Irga6 aggregates (Hunn, 2008). In the cells that were transfected with only one of the GMS proteins, 65 to 90 percent of them revealed aggregates. When these cells were transfected with two GMS proteins, 40 to 60 percent of them showed aggregates. However, when all three GMS proteins were co-transfected in GS 3T3 Irga6 cells, 70 percent of the cells reconstructed relatively smooth pattern of Irga6.

d) Irga6 also co-localizes with lysosomes in Irgm1 KO DDCs and BMDMs

To test whether co-localization of Irga6 with lysosomes is characteristic only for IFNγ-induced *Irgm1* KO mouse embryonic fibroblasts (MEFs) or also for other cell types, *Irgm1* KO Diaphragm-Derived Cells (DDCs) and Bone Marrow Derived Macrophages (BMDMs) were subjected to analysis.

DDCs were prepared from the diaphragm tissue of *Irgm1* KO mouse, induced with 200 U/ml IFNγ for 24 hours, fixed and stained with the immunoreagents against Irga6 (165/3) and LAMP1. Immunofluorescence microscopy images of stained cells were taken and co-localization of Irga6 structures with LAMP1 was analyzed (Figure 10A). As in *Irgm1* KO MEFs, almost all Irga6 aggregate-like structures were observed to co-localize with LAMP1.

BMDMs were derived from the bone marrow of *Irgm1* KO mice and induced with 400 U/ml of IFNγ for 24 hours. Cells were fixed and stained for Irga6 and LAMP1. Confocal microscopy images of BMDMs were taken and co-localization of Irga6 with LAMP1 was analyzed (Figure 10B). In *Irgm1* KO BMDMs, almost all Irga6 structures co-localized with the lysosomes.

Taken together, Irga6 localizes to the endolysosomal compartment in the absence of Irgm1, but not when Irgm2 or Irgm3 are also missing from the GMS pool. The localization of Irga6 onto lysosomes in the absence of Irgm1 tested here in four different experimental setups suggests that Irgm1 functions as the lysosomal protector, preventing accumulation of GKS protein Irga6 on the lysosomes.
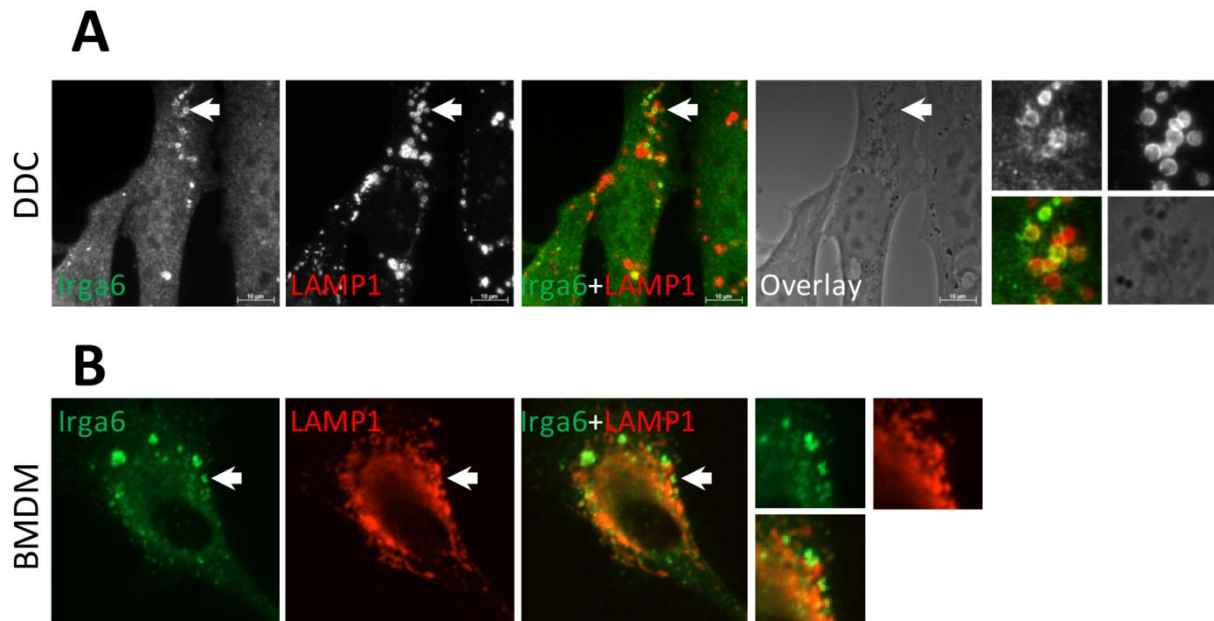
Figure 10. Irga6 co-localizes with LAMP1 in *Irgm1* KO DDCs and BMDMs A) *Irgm1* KO DDCs were induced with 200 U/ml IFNγ for 24 hours. Cells were fixed and stained with immunoreagents against Irga6 (165/3) and LAMP1. Representative microscopic images of Irga6 and LAMP1 are shown. Arrows point at the Irga6 structures, which are magnified at the end of each panel (zoom in the following order: upper left: Irga6, upper right: LAMP1, lower left: overlay, lower right: phase contrast). Scale bars represent 10 μM. **B)** *Irgm1* KO BMDMs were induced with 400 U/ml IFNγ for 24 hours. Cells were fixed and stained with antibodies against Irga6 (10D7) and LAMP1. Representative confocal microscopy images of Irga6 and LAMP1 are shown. Arrows point at the Irga6 structures which are magnified at the end of each panel (zoom in the following order: upper left: Irga6, upper right: LAMP1, lower left: overlay).

3.1.3. Irga6 localizes to the endoplasmic reticulum in *Irgm3* KO cells

Irgm3 is so far the only identified GMS protein that localizes to the endoplasmic reticulum (ER) (Taylor et al., 1997). Therefore, it was questioned whether in absence of Irgm3, Irga6 can accumulate at the ER. Previously, immuno-electron microscopy images had shown that transfected Irga6 can associate to the ER membranes in NIH fibroblasts in the absence of all GMS proteins and contribute to their enlargement (Kaiser, 2005) (Hunn et al., 2008). However, the co-localization of Irga6 aggregates and ER was not analyzed in IFNγ-induced *Irgm3* KO cells.

To examine this, *Irgm1* KO, *Irgm3* KO and *Irgm1/Irgm3* KO MEFs were induced with IFNγ and simultaneously transfected with the ER marker pEYFP-Calreticulin. The cells were fixed, stained for Irga6 with 10D7 antibody, which specifically recognizes Irga6 in GTP-bound form, and microscopic pictures were taken (Figure 11A). The percentage of Irga6 structures that co-localize with Calreticulin was quantified (Figure 11B). In *Irgm3* KO cells, more than 85 percent of Irga6 structures apparently co-localized with Calreticulin. In contrast, less than 5 percent of Irga6 structures co-localized with Calreticulin in *Irgm1* KO and *Irgm1/Irgm3* KO

MEFs and it even appeared that Irga6 structures excluded the ER network in these cells. Taken together, these results suggest that Irgm3 protects ER from the accumulation of Irga6.
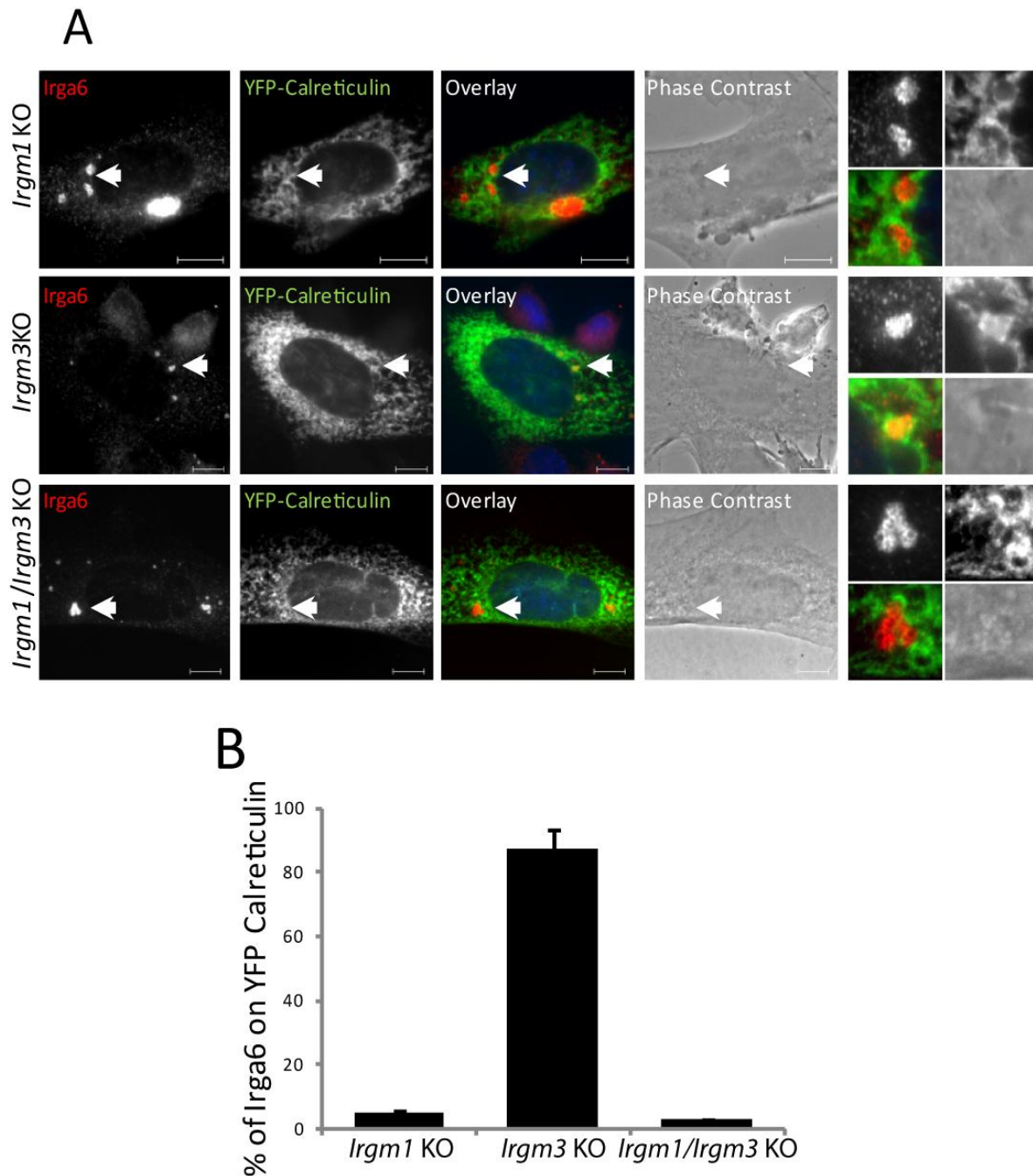

Figure 11. Irga6 co-localizes with calreticulin in *Irgm3* KO cells A) *Irgm1* KO, *Irgm3* KO and *Irgm1/Irgm3* KO MEFs were induced with 200 U/ml IFNγ and transfected with ER marker pEYFP-Calreticulin for 24 hours. Cells were fixed and immunostained for Irga6 with monoclonal 10D7 antibody. Representative microscopic images of Irga6 and Calreticulin are shown. Arrows point at the Irga6 structures which are magnified at the end of each panel (zoom in the following order: upper left: Irga6, upper right: Calreticulin, lower left: overlay, lower right: phase contrast). Scale bars represent 10 µM. **B)** Quantification of 11A, that shows percent of Irga6 structures co-localizing with Calreticulin. 50 cells per sample were quantified and the means of three independent experiments +/- standard deviation are shown.

3.1.4. Irga6 does not co-localize with the Golgi apparatus in the absence of GMS proteins

Upon IFNγ induction, the Golgi apparatus is coated with two GMS proteins Irgm1 and Irgm2 (Martens et al., 2004) (Martens and Howard, 2006). To test whether Irga6 co-localizes to the Golgi in the absence of GMS proteins, WT, *Irgm1* KO, *Irgm3* KO and *Irgm1/Irgm3* KO MEFs were induced with IFNγ, fixed and stained against Irga6 (165/3) and against the Golgi protein GM130. Immunofluorescence microscopy images were taken (Figure 12A) and frequency of Irga6 structures that co-localize with GM130 was quantified (Figure 12B). Less than 3 percent of the Irga6 aggregate-like structures co-localized with GM130 in all samples tested.

However, in all these cases Irgm2 is expressed, which is accurately localized to the Golgi and therefore it was possible that Irgm2 prevents the accumulation of GKS proteins at the Golgi. This possibility was tested by the transfection experiment described in chapter 3.1.2.c. GS 3T3 Irga6 cells were stimulated with MIF and simultaneously transiently transfected with combinations of pGW1H-Irgm1, pGW1H-Irgm2, pGW1H-Irgm3 and in each case with pmCherry as a transfection marker. The cells were fixed and stained for Irga6 and GM130. Co-localization of these two proteins was quantified in mCherry positive cells (Figure 13, Figure 14). No apparent co-localization of Irga6 and GM130 could be observed in any samples. Even in cells transfected with Irgm3 alone, in which Golgi structures should presumably not be GMS protected and ER should be GMS coated, Irga6 did not co-localize with Golgi. No abnormalities were observed in Golgi structure, at least at the light microscopical level, in these cells.

Taken together, Irga6 aggregate-like structures do not co-localize with Golgi even when no Golgi-localising GMS protein is present. Thus, it seems that the Golgi apparatus is not endangered by GKS aggregate-like structures and that this result also challenges the generality of the "missing self" model.
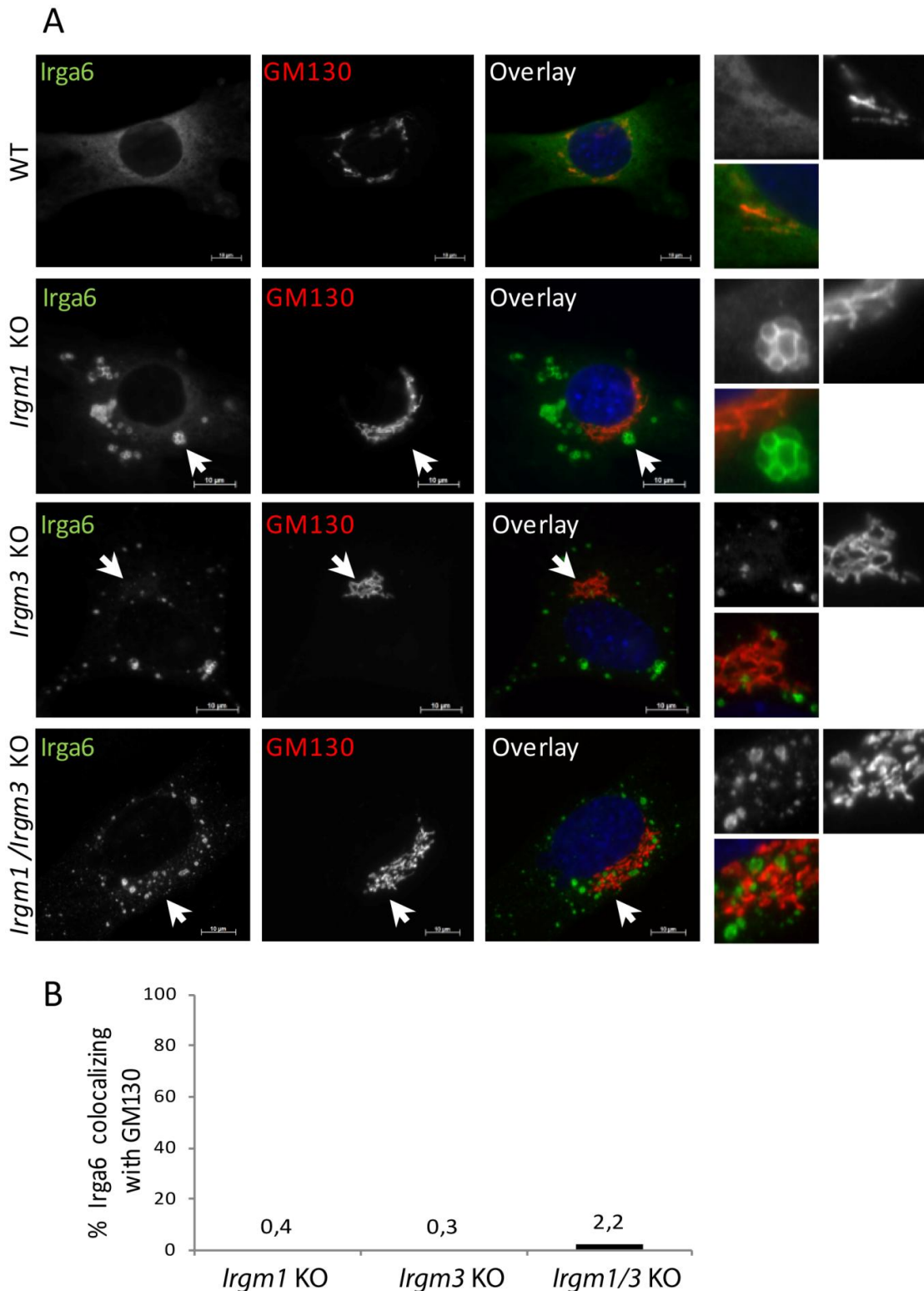
Figure 12. Irga6 does not co-localize with GM130 in GMS KO MEFs A) WT, *Irgm1* KO, *Irgm3* KO and *Irgm1/Irgm3* KO MEFs were induced with 200 U/ml IFNγ for 24 hours. Cells were fixed and stained against Irga6 (165/3) and against the Golgi protein GM130. Representative microscopic images of Irga6 and GM130 are shown. Arrows point at the Irga6 structures which are magnified at the end of each panel (zoom in the following order: upper left: Irga6, upper right: GM 130, lower left: overlay). Scale bars represent 10µm. **B)** Quantification of 12A, showing percent of Irga6 structures that co-localize with GM130. 100 cells per sample were blind-counted.
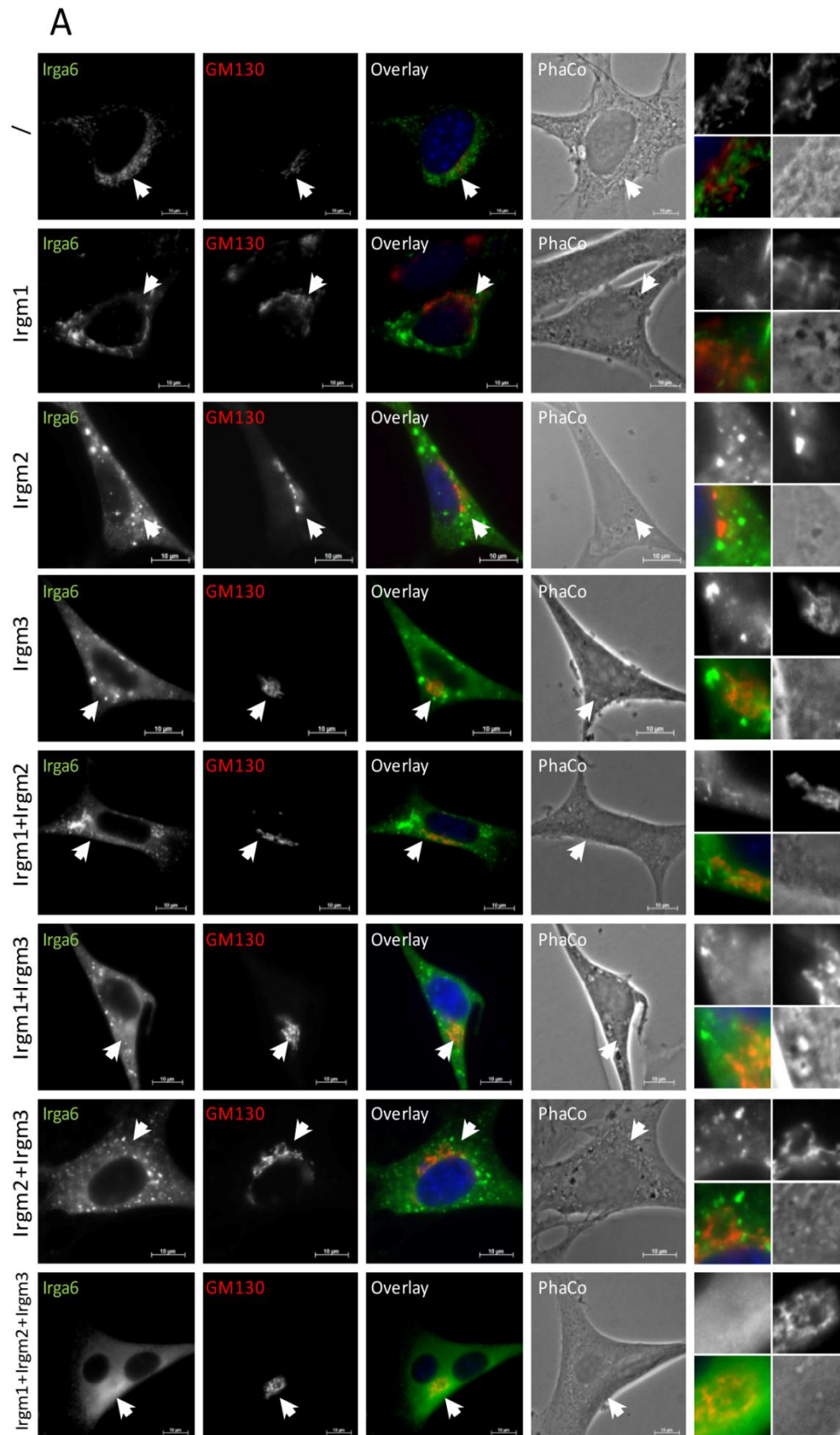
Figure 13. Irga6 does not co-localize with Golgi in GMS transfected cells. Irga6-inducible Gene Switch 3T3 cells were stimulated with Mifepristone and simultaneously transiently transfected with pGW1H-Irgm1, pGW1H-Irgm2 and pGW1H-Irgm3 for 24 hours. Cells were fixed and stained with antiserum against Irga6 (165/3) and the antibody against the Golgi protein GM130. Representative microscopic images of Irga6 and GM130 are shown. Arrows point at the Irga6 structures which are magnified at the end of each panel (zoom in the following order: upper left: Irga6, upper right: GM130, lower left: overlay, lower right: phase contrast). Scale bars represent 10µm. 57
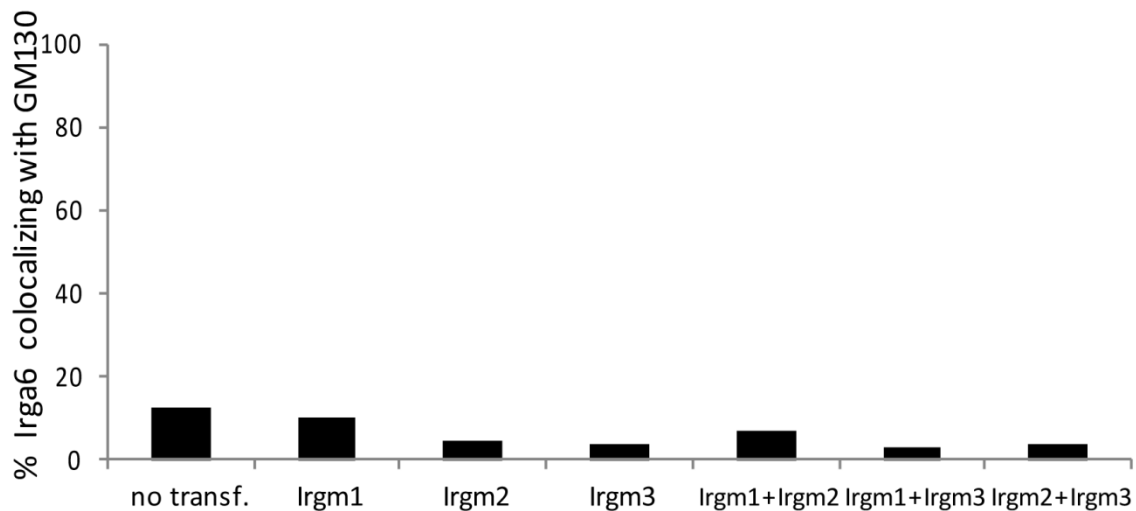
Figure 14. Irga6 does not co-localize with GM130 in GMS transiently transfected cells. Quantification of Figure 13, showing percent of Irga6 structures that co-localize with Golgi protein GM130 in GMS transfected MIF-induced GS 3T3 Irga6 cells. 50 cells per sample were quantified.

3.1.5. Irga6 co-localizes with lipid droplets in *Irgm1/Irgm3* KO cells

A recent publication from the laboratory of Joern Coers (Haldar et al., 2013) also approached the "missing self" model from a standpoint similar to our own. In that study they showed that GKS proteins, Irgb10 and Irga6, both co-localize to lipid droplets (LDs) in IFNγ-induced *Irgm1/Irgm3* double KO cells. In addition, Irgb10 structures were shown to partially co-localize with LDs in *Irgm3* KO cells and there was no Irgb10 co-localization with the LDs in *Irgm1* KO MEFs (Haldar et al., 2013). The co-localization of Irga6 and LDs was never investigated in *Irgm1* KO and *Irgm3* KO MEFs. Since Irgm1 and Irgm3 were shown to localize to LDs in WT cells (Bougneres et al., 2009) (Haldar et al., 2013), this compartment should be GMS-free in *Irgm1/Irgm3* KO cells, and therefore GKS localization to the LDs contributes to the idea that these proteins target the membranes by the "missing self" principle.

In the present study it was observed that in IFNγ-induced *Irgm1/Irgm3* KO MEFs Irga6 structures accumulate at the optically dense structures visible in phase contrast, which, in accordance to the data from the Coers lab, probably represent lipid droplets. To partially reproduce the data from that publication, *Irgm1/Irgm3* KO MEFs, but also *Irgm1* KO and *Irgm3* KO MEFs, were induced with IFNγ and stained for Irga6. Unfortunately, the staining with Bodipy lipid dye, which was performed by the protocol described in the publication (Haldar et al., 2013) was not successful after multiple attempts and therefore co-localization of Irga6 and optically dense lipid droplet-like structures was quantified. In accordance to

Haldar's data, 63 percents of Irga6 co-localized with the LD-like structures in *Irgm1/Irgm3* KO cells, 15 percent did so in *Irgm3* KO cells and only 4 percent of Irga6 co-localized with the LD-like structures in *Irgm1* KO cells (Figure 15).
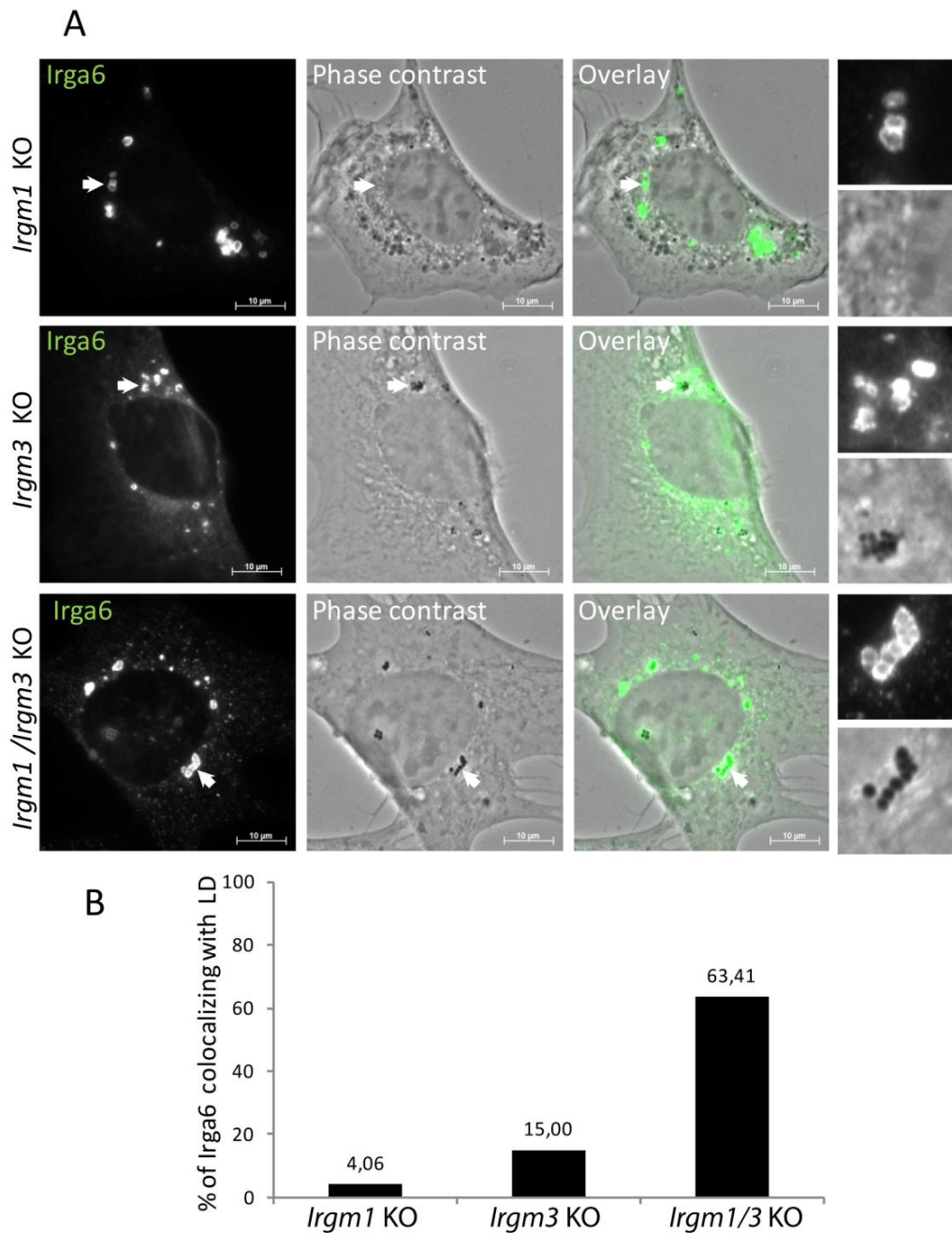

Figure 15. Irga6 co-localizes with lipid droplet-like structures in *Irgm1/Irgm3* KO MEFs A) *Irgm1* KO, *Irgm3* KO and *Irgm1/Irgm3* KO MEFs were induced with 200 U/ml IFNγ for 24 hours, fixed and stained with an antibody against Irga6 (10E7). Representative microscopic images of Irga6 and LD-like structures are shown. Arrows point at the Irga6 structures which are magnified at the end of each panel (zoom in the following order: upper: Irga6, lower: phase contrast). Scale bars represent 10 µM. **B)** Quantification of 15A, showing percent of Irga6 structures co-localizing with LD-like structures. 50 cells per sample were quantified.

To investigate the localization of Irgb6 structures in GMS KO cells, *Irgm1* KO, *Irgm3* KO and *Irgm1/Irgm3* KO MEFs were induced with IFNγ and stained for Irgb6. The co-localization of Irgb6 and optically dense structures was quantified. More than 90 percent of Irgb6 co-localized with the LD-like structures in *Irgm1/Irgm3* KO MEFs, 19 percent in *Irgm1* KO and 6 percent *Irgm3* KO MEFs does so (Figure 16).
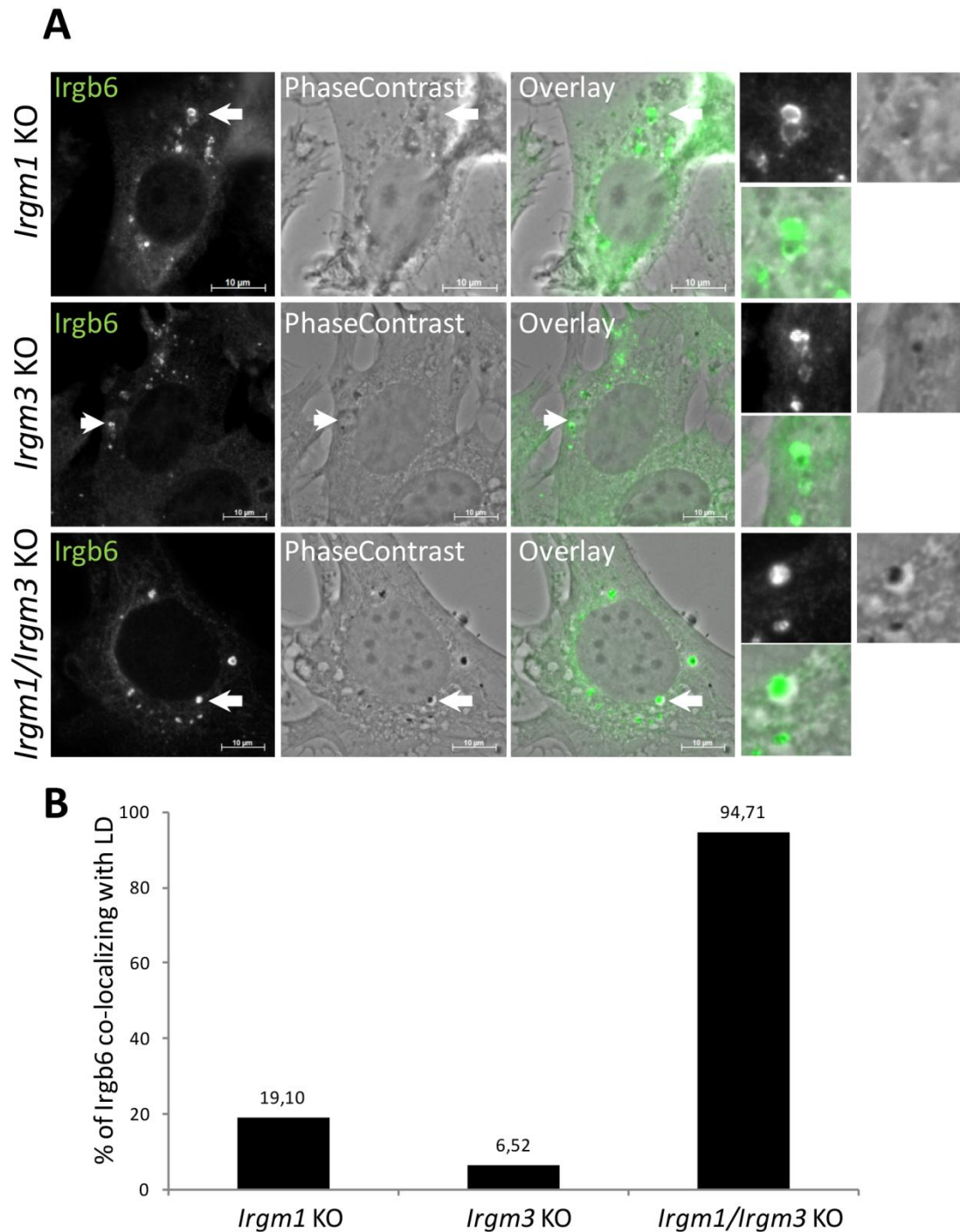

Figure 16. Irgb6 co-localize with lipid droplet-like structures in *Irgm1/Irgm3* KO MEFs A) *Irgm1* KO, *Irgm3* KO and *Irgm1/Irgm3* KO MEFs were induced with 200 U/ml IFNγ for 24 hours, fixed and immunostained for Irgb6 (141/3). Representative microscopic images of Irgb6 and LD-like structures are shown. Arrows point at the Irga6 structures which are magnified at the end of each panel (zoom in the following order: upper left: Irgb6, upper right: phase contrast, lower left: overlay). Scale bars represent 10 μM. **B)** Quantification of 16A, showing percent of Irgb6 structures that co-localize with LD-like structures. 50 cells per sample were quantified.

Taken together, in addition to previously described co-localization of Irgb10 and Irga6 with the LDs in IFNγ-induced *Irgm1/Irgm3* KO cells (Haldar et al., 2013), in this study it was reproduced that Irga6 co-localizes with optically dense LD-like structures and shown that Irgb6 also follows the pattern of LD localization in IFNγ-induced *Irgm1/Irm3* KO cells. It was also first time shown that Irga6 does not co-localize with LD-like structures in *Irgm1* KO cells and partially co-localize with LD-like structures in *Irgm3* KO MEFs.

3.1.6. Other GKS proteins also localize to lysosomes in *Irgm1* KO cells

It was further questioned whether GKS proteins generally accumulate at lysosomes in the absence of Irgm1, or whether this co-localization is specific for Irga6. To answer this question, WT, *Irgm1* KO, *Irgm3* KO and *Irgm1/Irgm3* KO MEFs were induced with IFNγ and stained for different GKS proteins: Irgb6, Irgb10 or Irgd and for LAMP1 (Figure 17A) (images shown for *Irgm1* KO cells). The amount of different GKS structures that co-localize with LAMP1 was quantified. Indeed, over 90 percent of all tested GKS aggregate-like structures co-localized with LAMP1 in *Irgm1 KO* MEFs and almost none did so in *Irgm3* KO and *Irgm1/Irgm3* KO MEFs (Figure 17B, C, D).
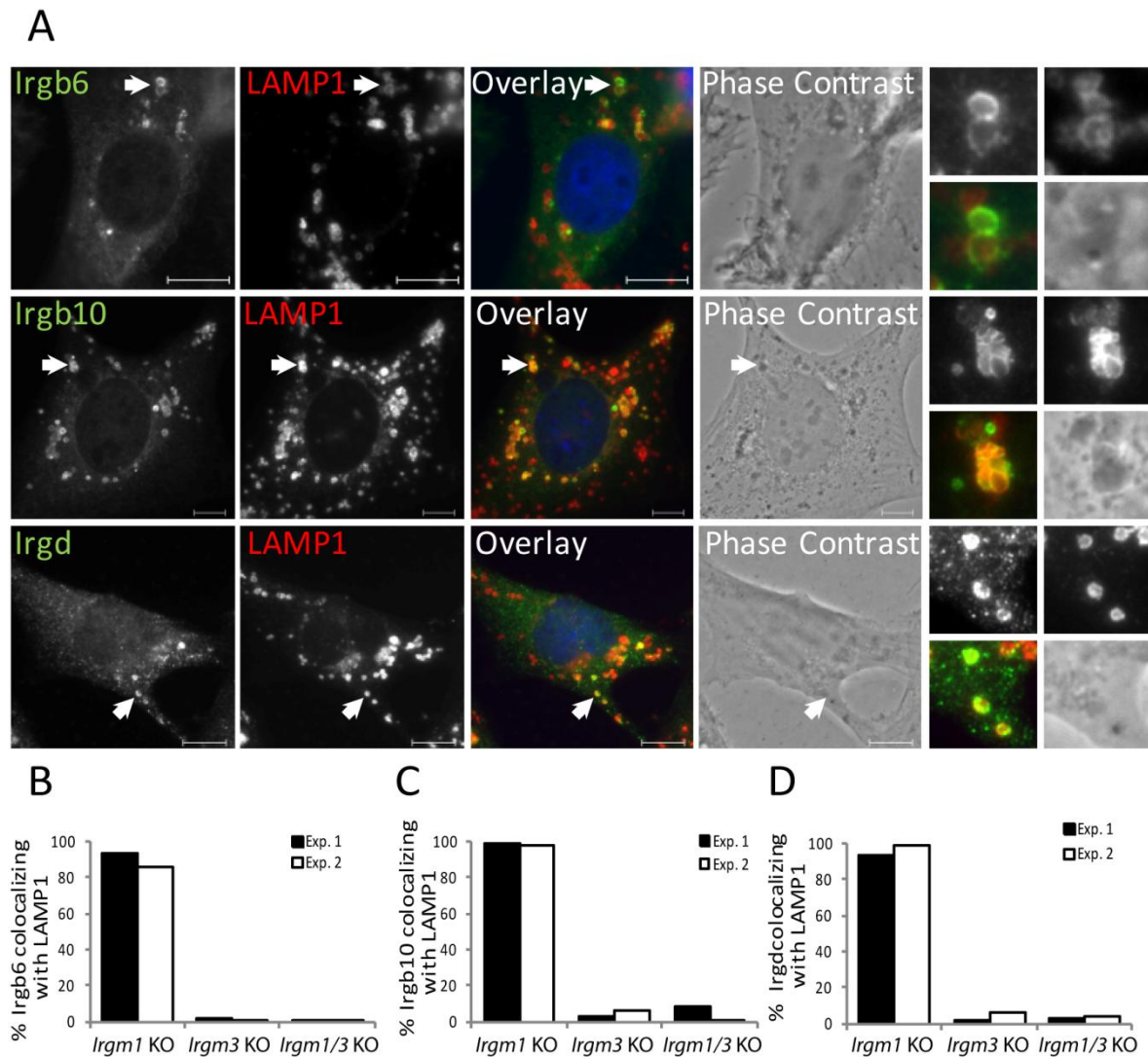
A

B   C   D

Figure 17. GKS proteins co-localize with LAMP1 in *Irgm1* KO cells A) *Irgm1* KO, *Irgm3* KO and *Irgm1/Irgm3* KO MEFs were induced with 200 U/ml IFNγ for 24 hours. Cells were fixed and stained with antisera against Irgb6 (141/3), Irgb10 (940/6) or Irgd (81/4) and an antibody against LAMP1. Representative microscopic images of GKS and LAMP1 in *Irgm1* KO cells are shown. Arrows point at the GKS structures which are magnified at the end of each panel (zoom in the following order: upper left: GKS, upper right: LAMP1, lower left: overlay, lower right: phase contrast). Scale bars represent 10 µM. **B) C) D)** Quantification of 17A that shows percent of GKS structures that co-localize with LAMP1. 50 cells per sample were quantified and results of two independent experiments are shown.

3.1.7. Different GKS proteins load to the same lysosomes in *Irgm1* KO cells

Different GKS proteins load onto the same *T. gondii* PVMs in a cooperative and hierarchical manner (Khaminets et al., 2010). The finding that different GKS proteins accumulate to LAMP1 structures in *Irgm1* KO cells opened the question of whether these different GKS proteins localize to the same lysosomes. Moreover, it was questioned whether they also do so in a cooperative and hierarchical manner, like GKS proteins on the PVM of *T. gondii*. To answer these questions, IFNγ-induced *Irgm1* KO MEFs were fixed, stained for LAMP1 and for several combinations of GKS proteins (Figure 18A). The percentage of GKS aggregate-like structures that together or alone co-localize with the lysosomes was quantified (Figure 18B).

Co-staining of Irga6 and Irgb6 revealed that these proteins can be found at the same lysosomes. Irga6 was also often observed on lysosomes without Irgb6. However, Irgb6 was present at the lysosome almost always together with Irga6 and rarely alone. Similarly, co staining of Irgd and Irga6 revealed that Irgd could be also found on the lysosomes together with Irga6. Irga6 was also observed on the lysosomes without Irgd. As for Irgb6, Irgd was almost never observed on the lysosomes in the absence of Irga6.

However, co-staining of Irga6 and Irgb10 showed that these proteins can be on the lysosomes together or alone. Similarly, co-staining of Irgb6 and Irgd had shown that these proteins could be observed on the lysosomes together, or both of them could be detected independently.

The co-staining of Irgb6 and Irgb10 revealed that these proteins can localize to the lysosomes together. Irgb10 was also often observed on the lysosome without Irgb6, but Irgb6 could almost never be found on the lysosome without Irgb10.

Taken together, Irga6 and Irgb10 represent leading GKS proteins that accumulate at the lysosomes in IFNγ-induced *Irgm1* KO MEFs. Irgb6 and Irgd were observed only on the lysosomes that are already Irga6 and/or Irgb10 coated. It is also important to note that, like IRG protein loading on the PVM of *T. gondii,* some lysosomes are not coated with any of the GKS protein couples tested.
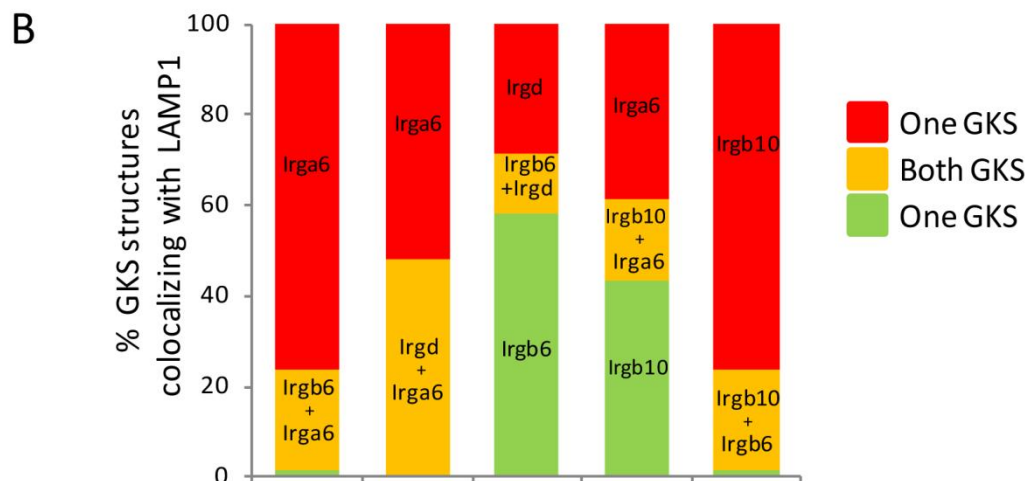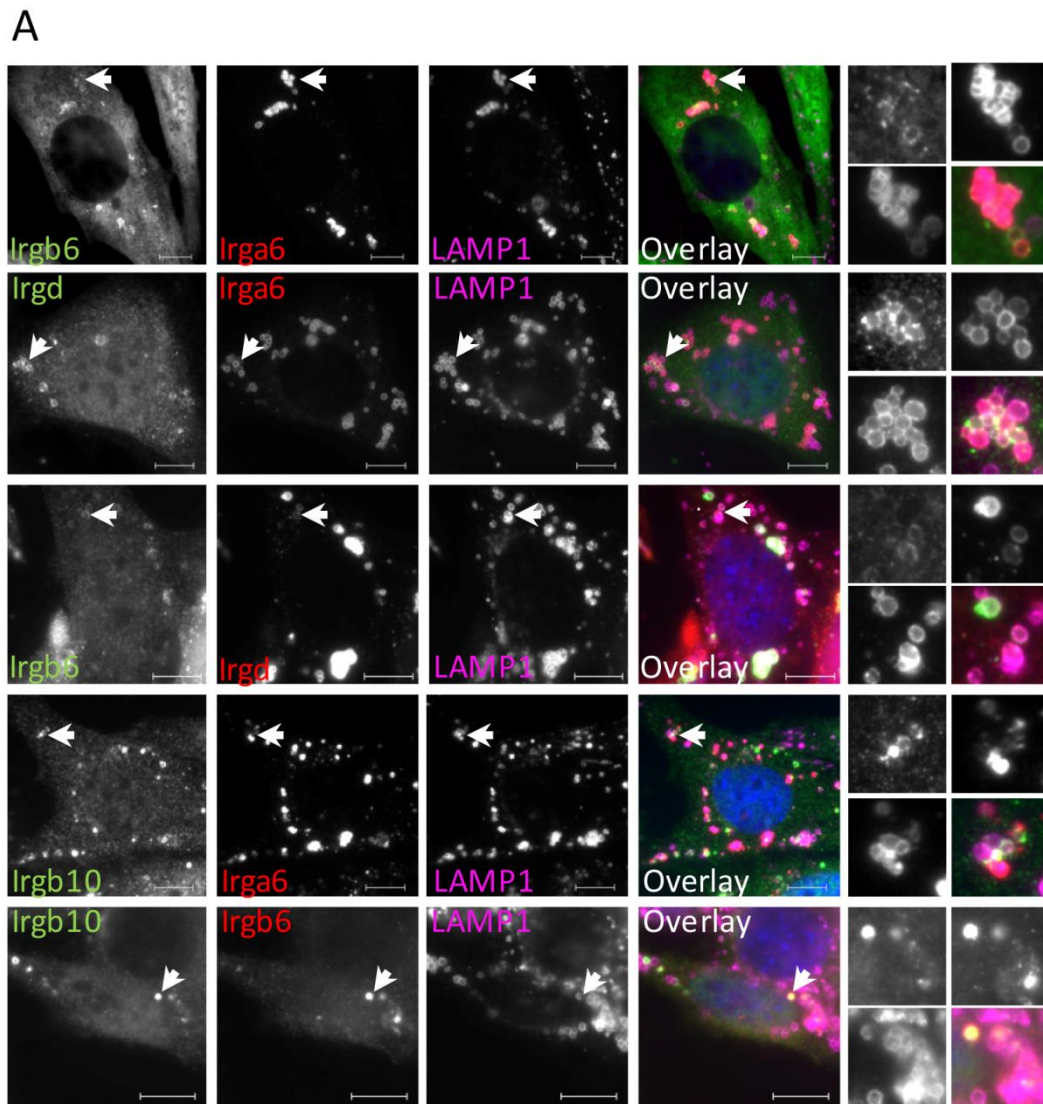
Figure 18. Different GKS proteins co-localize to the same or different lysosomes in *Irgm1* KO cells.
A) *Irgm1* KO MEFs were induced with 200 U/ml IFNγ for 24 hours, fixed and stained for Irga6, Irgb6 and LAMP1; Irgd, Irga6 and LAMP1; Irgb6, Irgd and LAMP1; Irga6, Irgb10 and LAMP1; or Irgb6, Irgb10 and LAMP1. Representative microscopic images of GKS structures and LAMP1 are shown. Arrows point at the GKS structures which are magnified at the end of each panel (zoom in the following order: upper left: first GKS protein, upper right: second GKS protein, lower left: LAMP1, lower right: overlay). Scale bar represents 10µM. **B)** Quantification of 18A, showing the percent of GKS protein structure co-localization. 50 cells per sample were quantified.

3.2. Removal of Irga6 does not affect the *Irgm1* KO mouse phenotype

3.2.1. *Irgm1/Irga6* double KO mice are susceptible to *Listeria monocytogenes*

It has been well established that *Irgm1* KO mice succumb to a variety of infections that do not affect the survival of *Irgm3* KO, *Irgm1/Irgm3* KO, *Irga6* KO or *Irgd* KO mice (chapter 1.6.1.). As demonstrated in chapter 3.1.2., *Irgm1* KO cells are the only *IRG* KO cells in which GKS aggregate-like structures localize to lysosomes. Even though the relationship between GKS proteins on the lysosomes in *Irgm1* KO cells and the susceptibility of *Irgm1* KO mice is not fully understood, there is a possibility that susceptibility of these mice is indeed caused by the GKS coating of the lysosomes.

In *Irgm1* KO cells, the GKS proteins that accumulate at lysosomes are predominantly Irga6 and Irgb10 (chapter 3.1.6.). Other GKS proteins, like Irgb6 and Irgd are found at the lysosomes only if Irga6 and/or Irgb10 are also present there, suggesting that loading of Irgb6 and Irgd requires initial loading of Irga6 and/or Irgb10.

This raised the question whether in *Irgm1/Irga6* double KO mice the absence of Irga6 would cause reduced loading of other GKS proteins on the lysosomes and possibly reduce post-infection lymphopenia and death.

Irgm1/Irga6 double KO mice were generated by crossing *Irgm1* KO mouse and *Irga6* KO mouse. Firstly, $Irgm1^{-/-}$ mice were crossed with $Irga6^{-/-}$ mice to generate $Irgm1^{+/-}/Irga6^{+/-}$ mice. Then, heterozygous $Irgm1^{+/-}/Irga6^{+/-}$ mice were crossed with the other $Irgm1^{+/-}/Irga6^{+/-}$ mice and their offspring was genotyped and further analyzed.

During $Irgm1^{+/-}$ mouse breeding under non-SPF conditions, it was observed that $Irgm1^{-/-}$ mice weight 20-30 percent less than their $Irgm1^{+/+}$ and $Irgm1^{+/-}$ littermates. The reason for this weight difference is probably the presence of mild intercurrent infections that induce IFNγ and consequent unthriftiness in $Irgm1^{-/-}$ mice. Hence, the weight of the *GMS* KO mice raised under non-sterile conditions is probably correlated to their resistance to the pathogens.

To have an insight into the resistance of *Irgm1/Irga6* double KO mice, the weight of the $Irgm1^{+/-}/Irga6^{+/-}$ offspring was measured 3 weeks after birth (Figure 19). The average weights of the mice with $Irgm1^{+/+}$ or $Irgm1^{+/-}$ genotype was between 9 and 11 grams. However, the average weight of the mice with $Irgm1^{-/-}/Irga6^{+/+}$ genotype was only 5,5 grams and the average weight of the mice with $Irgm1^{-/-}/Irga6^{-/-}$ was 7,2 grams. Thus, the weight of

Irgm1⁻ᐟ⁻/Irga6⁻ᐟ⁻ mice is slightly higher than the weight of the *Irgm1⁻ᐟ⁻/Irga6⁺ᐟ⁺* mice, but still much lower than the weight of the *Irgm1⁺ᐟ⁺* and *Irgm1⁺ᐟ⁻* mice, no matter their Irga6 genotype.
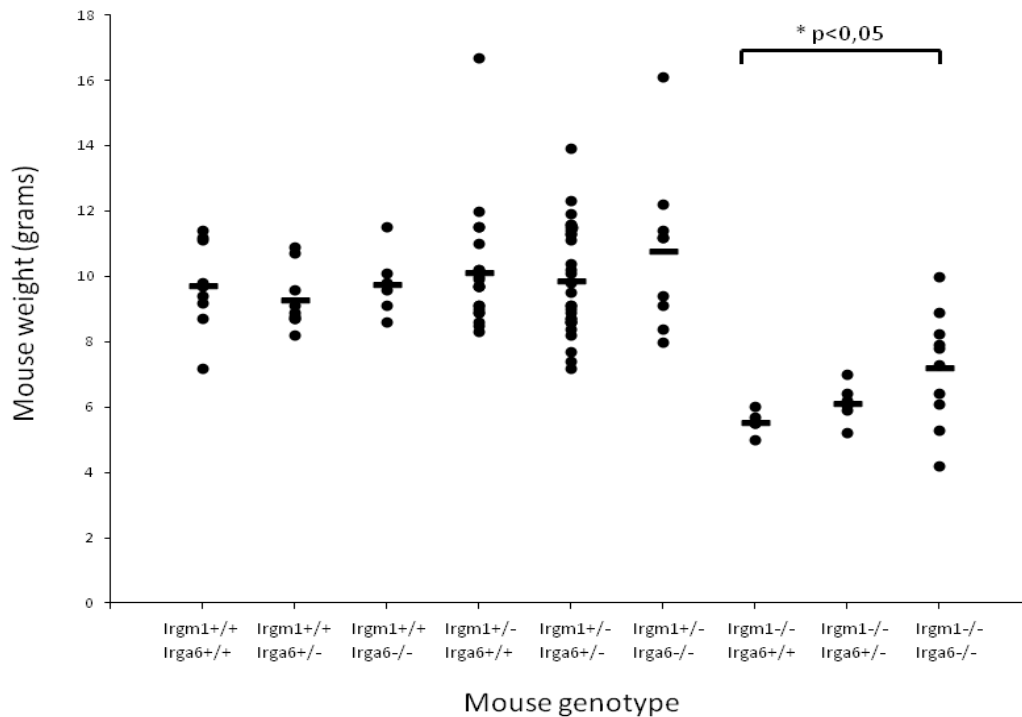

Figure 19. Weight of *Irgm1⁺ᐟ⁻/Irga6⁺ᐟ⁻* mouse offspring. The offspring of *Irgm1⁺ᐟ⁻/Irga6⁺ᐟ⁻* x *Irgm1⁺ᐟ⁻/Irga6⁺ᐟ⁻* mice was weighted and genotyped 3 weeks (+/- 1 day) after birth. Punctae represent the weights of individual mouse and mean values for every genotype group are depicted. Significant difference between *Irgm1⁻ᐟ⁻/Irga6⁺ᐟ⁺* and *Irgm1⁻ᐟ⁻/Irga6⁻ᐟ⁻* was calculated with a two tailed T-test. More than 100 mice in total were analyzed.

Previous studies had shown that *Irgm1⁻ᐟ⁻* mice die 4 to 5 days after infection with *Listeria monocytogenes* (Collazo et al., 2001). In collaboration with Dr. Michael Schramm (Institute for Medical microbiology, immunology and hygiene, University of Cologne), the resistance of *Irgm1⁻ᐟ⁻/Irga6⁻ᐟ⁻* mice to *L. monocytogenes* was tested. *WT*, *Irga6⁻ᐟ⁻*, *Irgm1⁻ᐟ⁻* and *Irgm1⁻ᐟ⁻/Irga6⁻ᐟ⁻* mice were intraperitoneally inoculated with 2400 *L. monocytogenes* per mouse (Figure 20). In accordance with published data, 100 percent of WT mice survived the infection and 80 percent of *Irgm1⁻ᐟ⁻* mice died within 4 days. Even though it was previously published that all *Irga6⁻ᐟ⁻* mice survive the infection with *L. monocytogenes*, two out of five *Irga6⁻ᐟ⁻* mice had died. Finally all four *Irgm1⁻ᐟ⁻/Irga6⁻ᐟ⁻* had also died within four days of infection.

Taken together, these data indicate that *Irgm1⁻ᐟ⁻/Irga6⁻ᐟ⁻* mice are equally, or even slightly more susceptible to *L. monocytogenes* infection than *Irgm1⁻ᐟ⁻* mice. Therefore, even though very small sample was analyzed, the removal of Irga6 certainly does not reduce the phenotype of *Irgm1⁻ᐟ⁻* mouse.

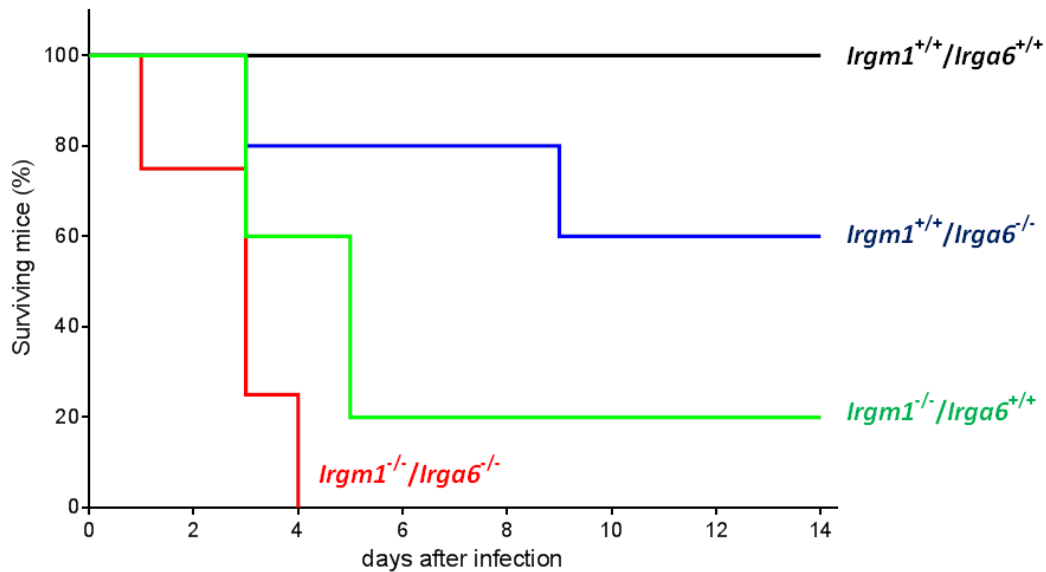**Figure 20. *Irgm1/Irga6* double KO mice are susceptible to *L. monocytogenes*.** 4-8 weeks old WT (n=6), *Irga6*$^{-/-}$ (n=5), *Irgm1*$^{-/-}$ (n=5) and *Irgm1*$^{-/-}$/*Irga6*$^{-/-}$ (n=4) mice were intraperitoneally inoculated with 2400 *L. monocytogenes*. The survival of the mice was monitored for 14 days.

3.2.2. Irgb6 can localize to the lysosomes independently of Irga6 and Irgb10

Next, it was questioned how does the removal of Irga6, which is suggested to act as one of the GKS-pioneers of lysosomal accumulation, influences the localization of other GKS proteins onto lysosomes in IFNγ-induced *Irgm1* KO cells.

As demonstrated in chapter 3.1.7., in *Irgm1* KO cells, Irgb6 accumulates only at the lysosomes that are already Irga6 or Irgb10 positive. Therefore it was questioned if in the IFNγ-induced *Irgm1/Irga6* KO cells, Irgb6 can accumulate only at the lysosomes that are already Irgb10 positive, or whether it can also load to the lysosomes that are not Irga6/Irgb10 coated.

To answer this question, diaphragm derived cells (DDCs) were generated from the *Irgm1* KO and *Irgm1/Irga6* KO mice. *Irgm1* KO DDCs and *Irgm1/Irga6* KO DDCs were induced with IFNγ for 24 hours, fixed and stained against Irgb6 (A20), Irgb10 (940/6) and LAMP1. Immunofluorescence images of the samples were taken (Figure 21A) and co-localization of Irgb6 structures with Irgb10 structures and LAMP1 structures was quantified (Figure 21B). In *Irgm1* KO DDCs, 60 percent of Irgb6 co-localizes with Irgb10. Considering the data from chapter 3.1.7., the other 40 percent of Irgb6 probably co-localizes with Irga6, which was not stained in these cells. In *Irgm1/Irga6* KO DDCs, only 59 percent of Irgb6 co-localized with Irgb10. Since Irga6 is absent from *Irgm1/Irga6* KO cells, these results indicate

that remaining 41 percent of Irgb6 can localize to the lysosomes that are not Irga6 or Irgb10 coated.

It has been also questioned if in the additional absence of Irga6, Irgb10 proteins can coat more lysosomes and form more aggregate-like structures than in *Irgm1* KO cells. The percentage of lysosomes that co-localize with Irgb10 was quantified in IFNγ-induced *Irgm1* KO DDCs and IFNγ-induced *Irgm1/Irga6* KO DDCs (Figure 21C). In *Irgm1* KO DDCs, about 27 percent of the lysosomes were Irgb10 coated, while in *Irgm1/Irga6* KO DDCs, about 22 percent of the lysosomes were Irgb10 coated. Thus, it seems that Irgb10 proteins do not spread to more lysosomes in the absence of Irga6.

Taken together, these data indicate that Irga6 is not an irreplaceable factor in GKS aggregate localization to the lysosomes. Even though Irga6 and Irgb10 are the predominant proteins in lysosome localization, the presence of Irga6 on the lysosome is not a prerequisite for lysosomal localization of Irgb6, which is also shown for the loading of these two proteins onto the PVM of *T. gondii* in IFNγ-induced cells, although in that case Irgb6 is the leading protein.

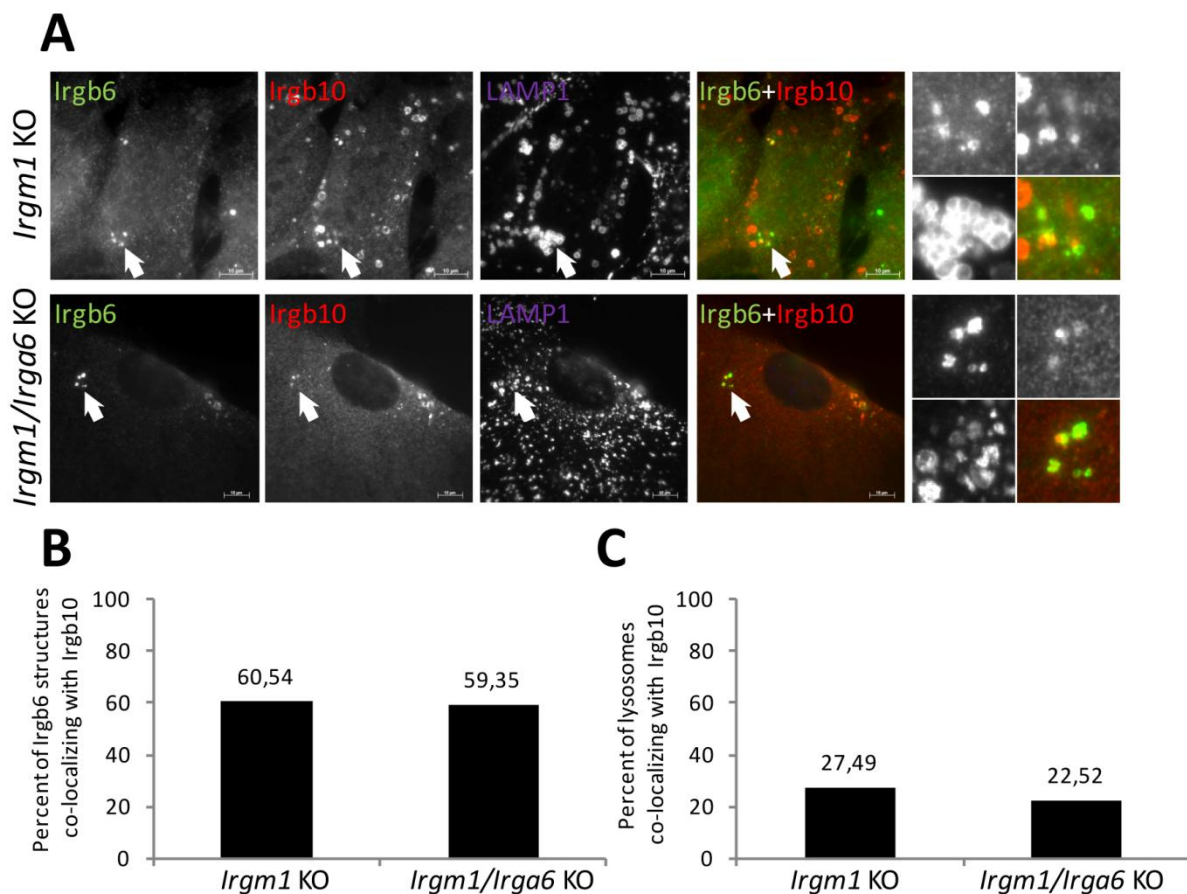**Figure 21. Irgb6 and Irgb10 lysosomal localization in *Irgm1/Irga6* KO DDCs A)** *Irgm1* KO DDCs and *Irgm1/Irga6* KO DDCs were induced with 200 U/ml IFNγ for 24 hours, fixed and stained for Irgb6, Irgb10 and LAMP1. Representative microscopic images of GKS structures and LAMP1 are shown. Arrows point at the GKS structures which are magnified at the end of each panel (zoom in the following order: upper left: Irgb6, upper right: Irgb10, lower left: LAMP1, lower right: overlay of Irgb6 and Irgb10). Scale bar represents 10µM. **B)** Quantification of 21A, showing percent of Irgb6 structures that co-localize with Irgb10. 50 cells per sample were blind counted. **C)** Quantification of 21A, showing percent of LAMP1 structures that co-localize with Irgb10. 50 cells per sample were blind counted.

3.3. Lysosomal function is impaired in IFNγ-induced *Irgm1* KO MEFs

A role of Irgm1 in autophagy regulation has been suggested in a couple of different contexts (Chapter 1.6.4.). Irgm1 has been proposed to mediate autophagic degradation of bacterial phagosomes (Deretic, 2011). However, it has been also shown that induced *Irgm1* KO lymphocytes have increased the number of autophagosomes and undergo autophagic cell death, suggesting the role of Irgm1 as an autophagy inhibitor (Feng et al., 2008b). Thus, the role of Irgm1 in autophagic degradation is not fully understood and remains to be investigated.

To complete the autophagic cycle, autophagosomes have to undergo fusion with lysosomes and to finally be degraded in these organelles (Feng et al., 2014) (Klionsky et al., 2012). Since GKS proteins accumulate at the lysosomes in *Irgm1* KO MEFs, we questioned whether these GKS coated lysosomes can fuse with and process autophagosomes in IFNγ-induced Irgm1 deficient cells.

3.3.1. The amount of autophagosomal protein LC3-II is increased in IFNγ-induced *Irgm1* KO MEFs

To test whether the autophagic flux is altered in *Irgm1* KO MEFs, lipidation of microtubule associated protein 1 light chain 3 (LC3), which is an essential step in autophagosome maturation, was monitored. In cooperation with Dr Susanne Bohlen (Institute for Medical microbiology, immunology and hygiene, University of Cologne), the turnover of non-lipidated LC3-I protein to lipidated LC3-II protein was analyzed by Western Blot. Thus, WT, *Irgm1* KO, *Irgm3* KO and *Irgm1/Irgm3* KO MEFs were treated either with IFNγ, and/or an LC3 turnover inducer Rapamycin (RAP), and/or an inhibitor of lysosome acidification Bafilomycin A1 (BAF), or left untreated. The cell lysates were separated by SDS-PAGE followed by Western Blots that were probed with anti-LC3 and anti-β-actin antibodies (Figure 22A, B, C, D). The intensities of the protein bands specific for LC3 staining and for the loading control actin were quantified by "Quantity one" software and the ratio of LC3-II band to Actin band was calculated (Figure 22E).

. In accordance with previous reports, when cells were treated with the LC3 turnover stimulator Rapamycin, the intensity of the LC3-II band was increased and the intensity of the LC3-I band was decreased (Klionsky et al., 2012). When Bafilomycin was added to the cells,

lysosomal acidification and autophagosome processing were impaired and the intensity of the LC3-II band was increased without a decrease of LC3-I (Klionsky et al., 2012). In four independent experiments, no difference in LC3-II band intensity was observed between non-treated or IFNγ-induced WT, *Irgm3* KO or *Irgm1/Irgm3* KO MEFs, but in IFNγ-induced *Irgm1* KO MEFs, the LC3-II band intensity was increased 3 to 8 fold in comparison to non-treated *Irgm1* KO cells.
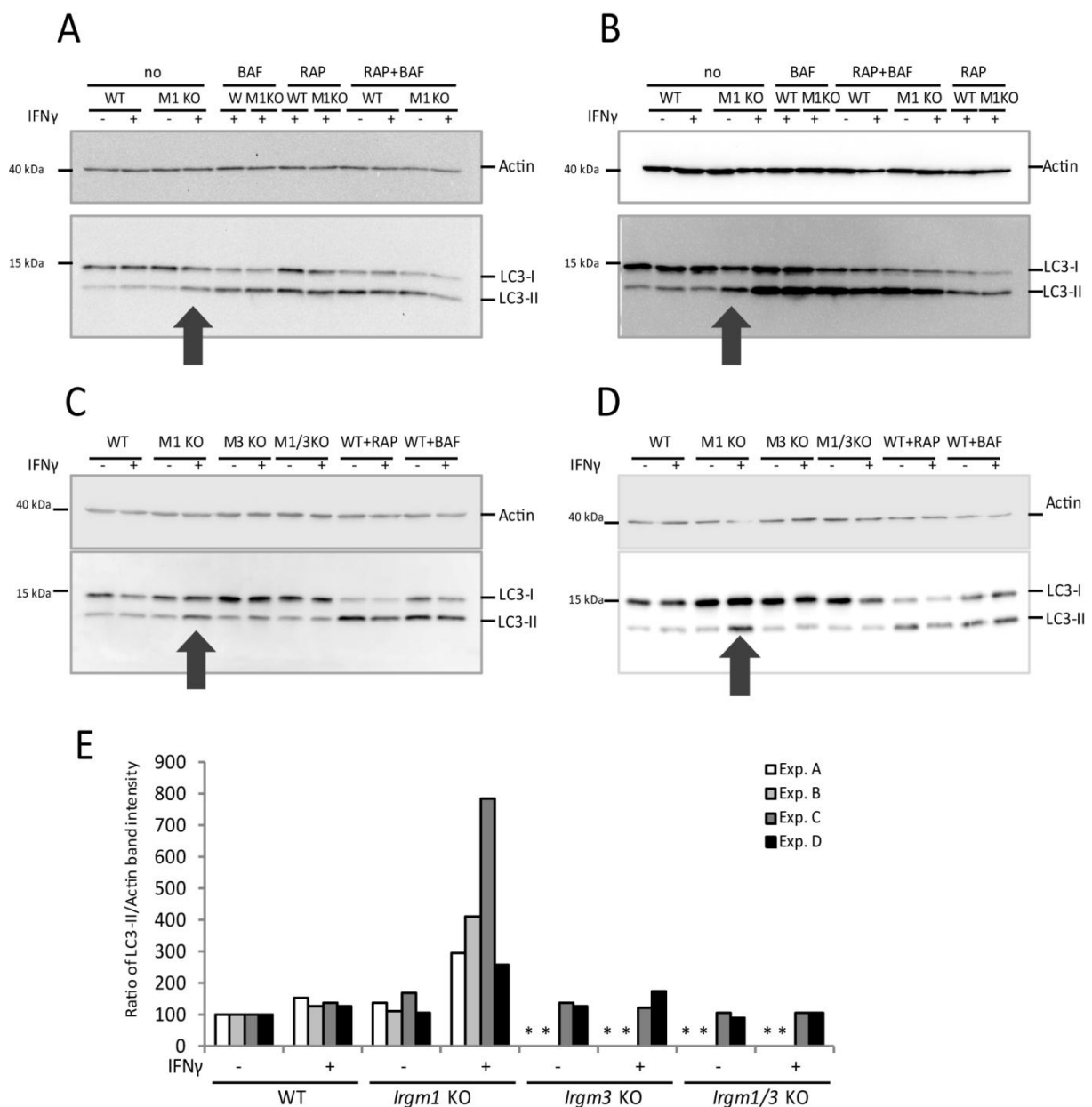

Figure 22. LC3-II signal is increased in IFNγ induced *Irgm1* KO MEFs WT **(A, B, C, D)**, *Irgm1* KO **(A, B, C, D)**, *Irgm3* KO **(C,D)** and *Irgm1/Irgm3* KO **(C,D)** MEFs were induced with 200 U/ml IFNγ for 24 hours, 40 µg/ml Rapamycin (RAP) and/or 200 nM Bafilomycin (BAF) for 2 hours or left untreated. Equal amounts of cell lysates were analyzed by SDS-PAGE and Western Blot. Membrane was probed with anti-LC3 and anti-Actin antibodies. **E)** Quantification of 22A, 22B, 22C and 22D, representing ratios between LC3-II and Actin band intensities for each sample. Results of four independent experiments are shown. Asterisk marks samples that were not included in the particular experiment.

In IFNγ treated *Irgm1* KO MEFs, even though the intensity of LC3-II was increased, intensity of LC3-I was not reduced. Thus, LC3-II increase could be an outcome of two possible scenarios: either autophagy induction might be enhanced in IFNγ treated *Irgm1* KO cells, or autophagosome processing might be impaired in these cells and LC3-II could not be further processed and degraded. Since the LC3-I level was not reduced in this sample, it seems that impairment of autophagic flux would be a more plausible scenario.

3.3.2. The number of LC3 punctae is increased in IFNγ-induced *Irgm1* KO MEFs

To better understand the changes in autophagic flux that might cause the LC3-II increase in IFNγ-induced *Irgm1* KO cells, microscopical analysis of the LC3 pattern in these cells was performed. WT MEFs and *Irgm1* KO MEFs were treated with IFNγ and/or RAP or left untreated. Cells were fixed and stained with LC3 immunoreagent, which labels both the LC3-I and LC3-II (Figure 23A). Immunofluorescence pictures were taken and the number of LC3 punctae per cell was blind counted (Figure 23B).

In the non-treated or IFNγ-treated WT cells, a small number of punctae could be observed. When WT cells were treated with RAP, large numbers of LC3-positive punctae were seen in the cell, confirming previous reports on LC3 behaviour in autophagy (Klionsky et al., 2012). Similarly, non-treated *Irgm1* KO cells had only few LC3-punctae and when *Irgm1* KO cells were treated with RAP, they showed a large amount of LC3-positive punctae. Unlike wild type cells, when *Irgm1* KO cells were treated with IFNγ, a large number of LC3 punctae were seen.

Taken together, these data, together with Western Blot results from chapter 3.3.1., show that the number of autophagosomes in IFNγ-induced *Irgm1* KO cells is increased.
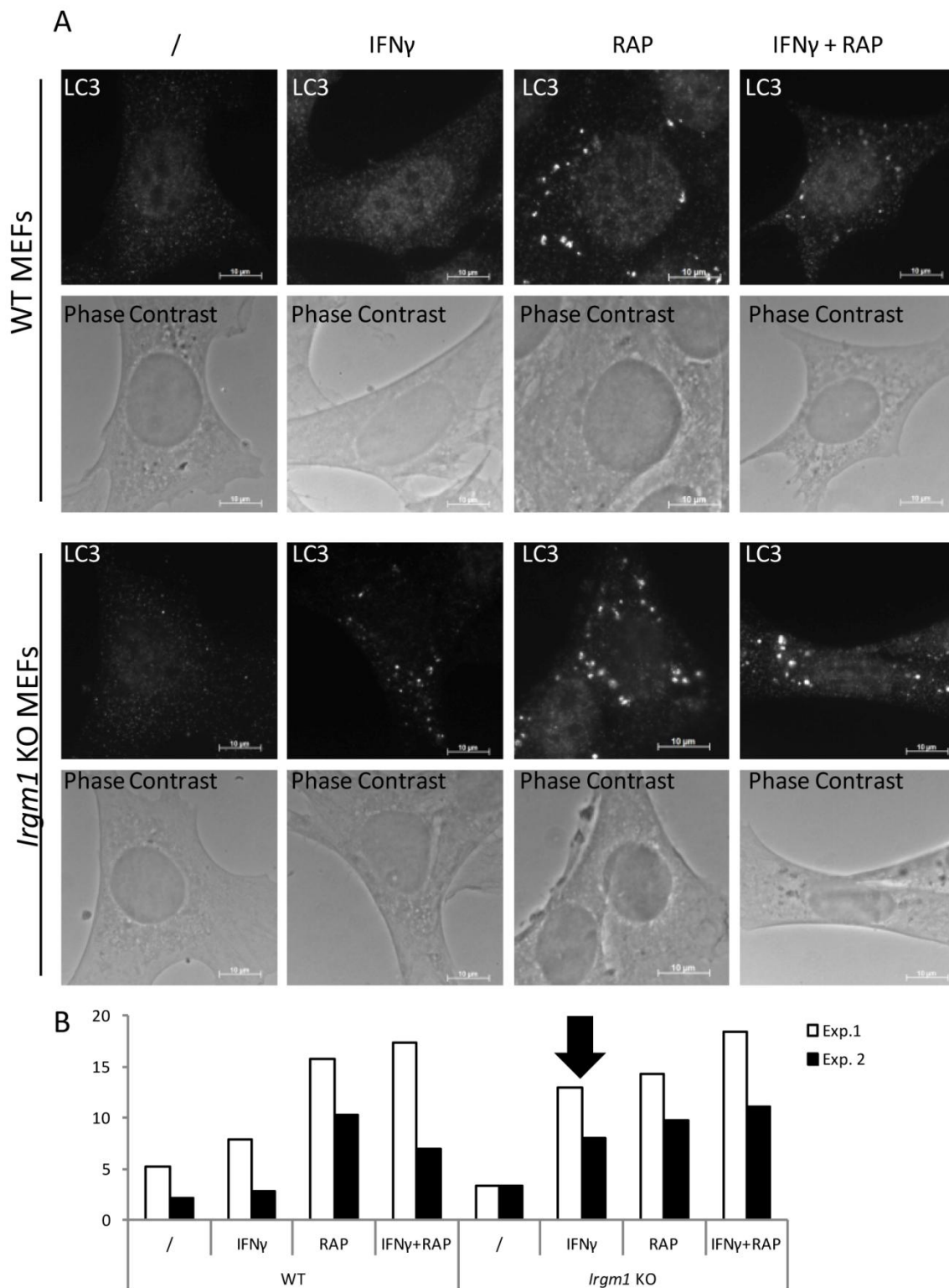
Figure 23. Number of LC3 punctae is increased in IFNγ induced *Irgm1* KO MEFs A) WT and *Irgm1* KO MEFs were induced with 200 U/ml IFNγ for 24 hours and/or 40µg/ml RAP for 2 hours or left untreated. Cells were fixed and stained with the immunoreagent against LC3. Representative microscopic images of LC3 punctae and Phase Contrast are shown. Scale bars represent 10µm. **B)** Quantification of 23A, showing average number of LC3 punctae per cell. Arrow points at the unusually high number of LC3 punctae in IFNγ-induced *Irgm1* KO cells. 50 cells per sample were blind counted and the results of two independent experiments are shown.

3.3.3. Autophagosomes are trapped in lysosomes in IFNγ-induced *Irgm1* KO MEFs

As proposed earlier, an increase in the LC3 punctae number and the LC3-II levels in IFNγ-induced *Irgm1* KO MEFs could be a consequence of the autophagy induction in *Irgm1* KO cells (Feng et al., 2008b). However, as discussed in chapter 3.3.1., these results could also suggest that the processing of autophagosome is impaired in *Irgm1* KO cells. Previously, it was shown that the lysosomes, which should process the autophagosomes, are coated with GKS aggregates in IFNγ-induced *Irgm1* KO cells (chapter 3.1.2.). It was therefore possible that autophagosome processing could be impaired in these cells. To better understand autophagosome/lysosome fusion and processing, co-localization of autophagic LC3 punctae with the lysosomal marker LAMP1 was analyzed.

WT MEFs and *Irgm1* KO MEFs were treated with IFNγ for 24 hours and/or RAP for 2 hours or left untreated. The cells were fixed and stained with immunoreagents against LC3 and against LAMP1 (Figure 24). The percent of LC3 structures that co-localize with LAMP1 was quantified. As expected, in WT cells, whether they were non-treated, IFNγ-treated, RAP-treated or IFNγ- and RAP-treated, less than 15 percent of LC3 positive structures co-localized with lysosomes (Figure 25), presumably reflecting efficient processing of autophagosomes. In non-treated and RAP-treated *Irgm1* KO cells, only a few of the LC3-punctae co-localized with the lysosomes. In contrast in IFNγ or IFNγ and RAP treated *Irgm1* KO cells, a 60 to 80 percent of LC3 punctae co-localized with lysosomes.

This phenomenon was not dependent on the number of LC3 punctae in the cell. Thus, abundant autophagosomes in *Irgm1* KO cells that were only treated with RAP did not co-localize with lysosomes. It seems that this phenomenon is IFNγ-dependent and that co-localization of autophagosomes with lysosomes is enhanced whenever IFNγ alone or together with RAP was added to *Irgm1* KO MEFs.

These findings strongly indicate that, in IFNγ-induced *Irgm1* KO cells, once lysosomes and autophagosomes fuse, the autophagosomes cannot be further processed and stay trapped in the lysosomes. Hence, autophagic flux of IFNγ-induced *Irgm1* KO MEFs is probably impaired.
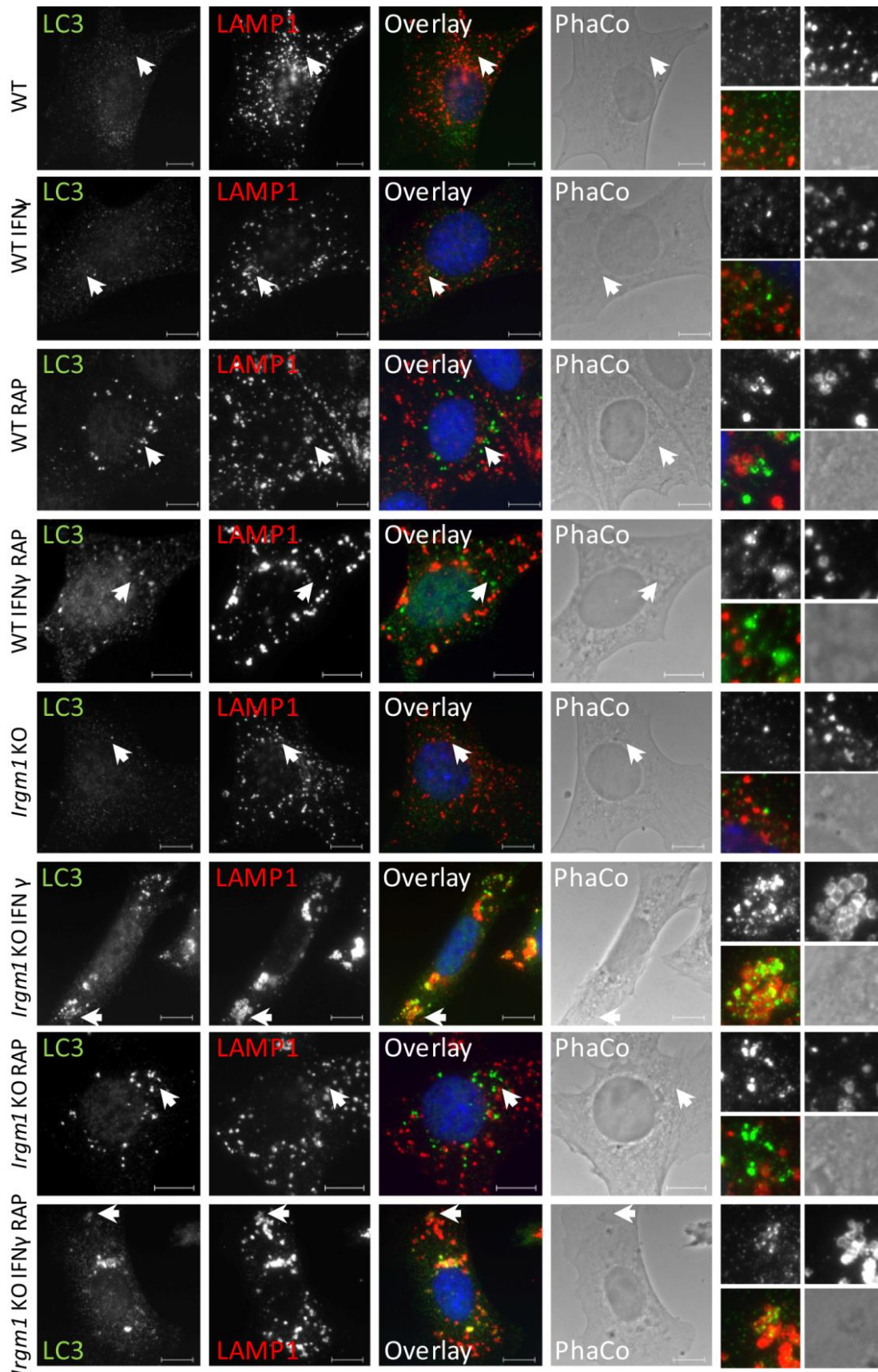
Figure 24. LC3 punctae co-localize with LAMP1 in IFNγ induced *Irgm1* KO MEFs WT and *Irgm1* KO MEFs were induced with 200 U/ml IFNγ for 24 hours, 40µg/ml RAP for 2 hours or left untreated. Cells were fixed and stained with the immunoreagents against LC3 and LAMP1. Representative microscopic images of LC3 and LAMP1 are shown. Arrows point at the LC3 structures which are magnified at the end of each panel (zoom in the following order: upper left: LC3, upper right: LAMP1, lower left: overlay, lower right: phase contrast). Scale bars represent 10 µM.
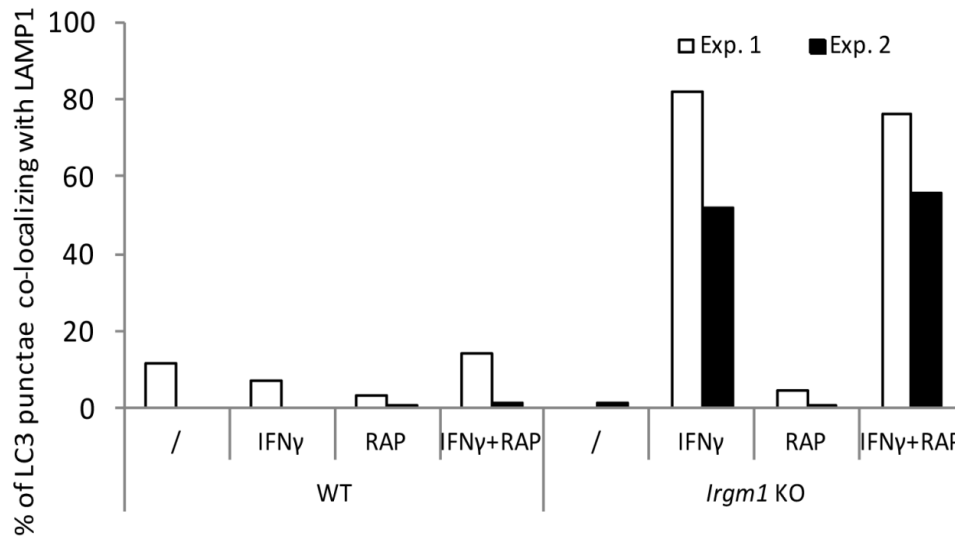
Figure 25. LC3 punctae co-localize with LAMP1 in IFNγ induced *Irgm1* KO MEFs. Quantification of Figure 23 that shows percent of LC3 structures that co-localize with LAMP1. 50 cells per sample were quantified and the results of two independent experiments are shown.

3.3.4. GKS coated lysosomes cannot process autophagosomes

The accumulation of GKS proteins at the lysosomes could be the cause of the autophagic flux impairment in *Irgm1* KO MEFs. If so, it is possible that the lysosomes that are unable to process LC3 are the same ones that are coated with GKS aggregates

To examine this question, *Irgm1* KO MEFs were induced with IFNγ and triple-stained for LC3, LAMP1 and Irga6 (Figure 26A). Immunofluorescence microscopy images of these cells were taken and co-localization of LC3 with LAMP1 and of LC3 with LAMP1 and Irga6 was quantified (Figure 26C). In accordance with results from chapter 3.3.3., about 60 percent of the LC3 structures co-localized with LAMP1 in IFNγ-induced *Irgm1* KO MEFs. However, only 33 percent of LC3 and LAMP1 positive structures also co-localized with Irga6.

As shown in chapter 3.1.7., Irga6 and Irgb10 are the leading GKS proteins which can localize to the lysosomes without the presence of the other GKS proteins. However, Irga6 and Irgb10 do not always localize to the same lysosomes. Hence, it was hypothesized that the lysosomes that trap autophagosomes and are not coated with Irga6, are actually Irgb10 coated. Hence, *Irgm1* KO MEFs were again induced with IFNγ but this time, due to antibody incompatibility, transfected with EGFP-LC3. These cells were stained for Irga6 and Irgb10 together in the red channel and LAMP1 in the far red channel (Figure 26B). Immunofluorescence images were taken and LC3 structures co-localizing with LAMP1 and with Irga6, Irgb10 and LAMP1 were quantified (Figure 26D). As in the previous experiment, 70 to 90 percent of the LC3 co-localized with LAMP1 in IFNγ-induced *Irgm1* KO cells. About

80 percent of LC3 and LAMP1 positive structures also co-localized with Irga6 and/or Irgb10. Thus, at least 80 percent of the autophagosomes are indeed trapped in the lysosomes that are GKS coated. To this end, GKS protein accumulations at the lysosomes in IFNγ-induced *Irgm1* KO MEFs probably do affect the ability of these lysosomes to process autophagosomes.
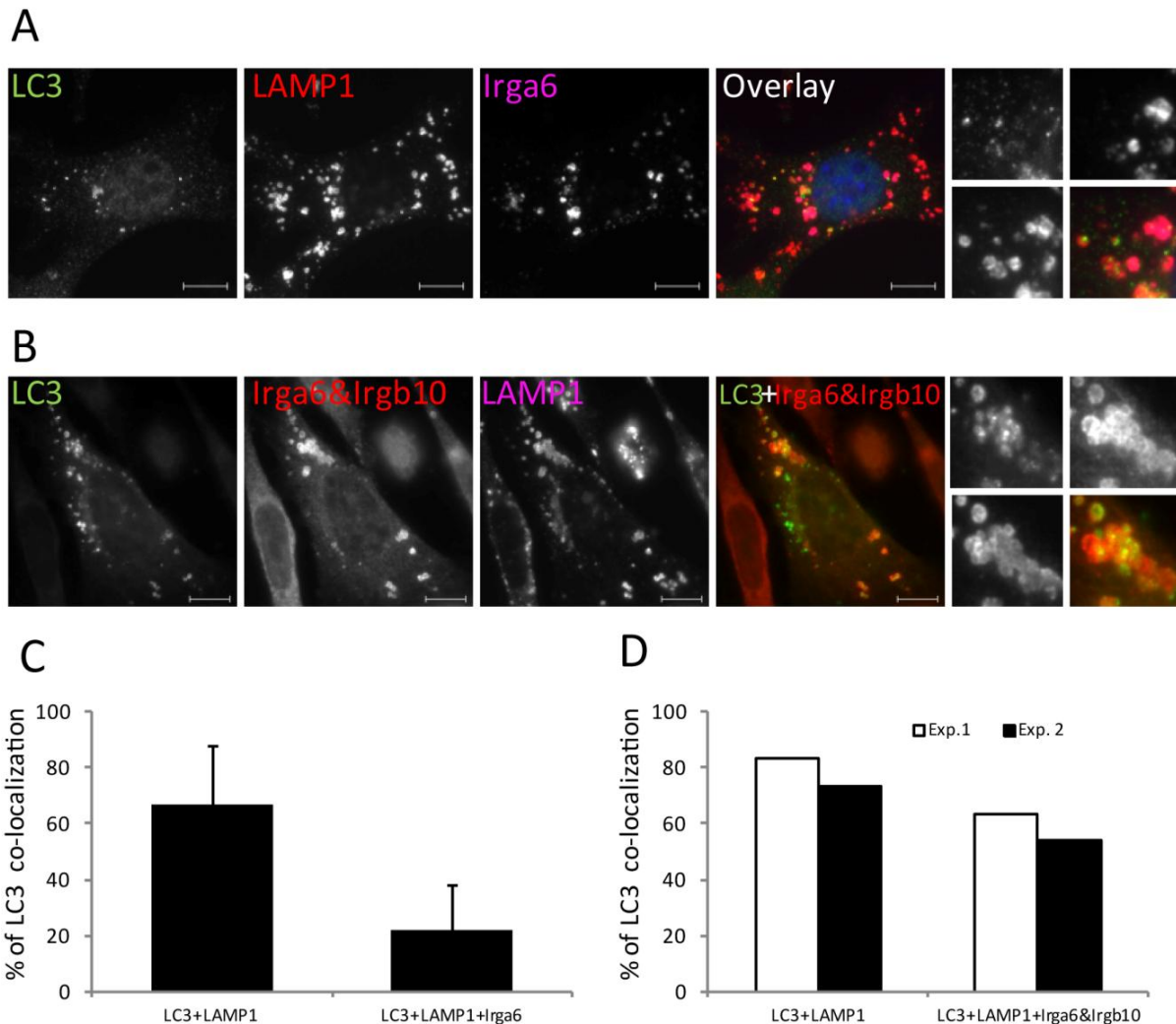

Figure 26. LC3 punctae co-localize with GKS covered lysosomes A) *Irgm1* KO MEFs were induced with 200 U/ml IFNγ for 24 hours or left untreated. Cells were fixed and stained against LC3, LAMP1 and Irga6 (165/3). Representative microscopic images of LC3, LAMP1 and Irga6 are shown. Arrows point at the LC3 structures which are magnified at the end of each panel (zoom in the following order: upper left: LC3, upper right: Irga6, lower left: LAMP1, lower right: overlay of Irga6, LC3 and LAMP1). Scale bars represent 10 µM. **B)** WT and *Irgm1* KO MEFs were transfected with EGFP-LC3 and induced with 200 U/ml IFNγ for 24 hours or left untreated. Cells were fixed and stained against LAMP1, Irga6 (165/3) and Irgb10 (940/6). Representative microscopic images of LC3, LAMP1 and Irga6&Irgb10 are shown **C)** Quantification of 26A, showing percent of LC3 structures that co-localize with LAMP1 or with Irga6 and LAMP1. 50 cells per sample were quantified and the means of three independent experiments +/- SD are shown. **D)** Quantification of 26B, showing percent of LC3 structures that co-localize with LAMP1 or with Irga6, Irgb10 and LAMP1. 50 cells per sample were quantified and the results of two independent experiments are shown.

3.3.5. GKS coated lysosomes are not acidic

In IFNγ-induced *Irgm1* KO MEFs, autophagosomes were reported to be trapped in the GKS covered lysosomes (chapter 3.3.4.). Since lysosomes play an important role in degradation or activation of many crucial cellular components (De Duve, 1963), it was questioned whether degradation impairment of GKS covered lysosomes is autophagosome specific, or whether the processing of all lysosomal substrates is actually impaired in these cells. Hence, the lysosomal acidity status in IFNγ-induced *Irgm1* KO MEFs was assessed.

Irgm1 KO MEFs were induced with IFNγ and simultaneously transfected with EGFP-Irga6-ctag1. After 24 hours, live non fixed cells were incubated with the pH sensitive lysosomal dye Lysotracker red. Pictures of live cells were taken (Figure 27A) and EGFP-Irga6 structures that co-localized with Lysotracker were quantified (Figure 27B). Only about a quarter (3,1 out of 11,7) of EGFP-Irga6 structures per cell were Lysotracker positive. The possibility that EGFP-Irga6 aggregate-like structures do not accumulate at the lysosomes can be excluded due to clear co-localization of EGFP-Irga6 and LAMP1 in IFNγ-induced *Irgm1* KO MEFs, which is shown in chapter 3.1.2.b. Thus, it seems that the pH of GKS-coated lysosomes in IFNγ-induced *Irgm1* KO cells is increased and these lysosomes cannot be detected with pH sensitive Lysotracker dye. Therefore, processing abilities of GKS-coated lysosomes are probably impaired not only during autophagy, but also during other important lysosome-dependent processes in the cell.
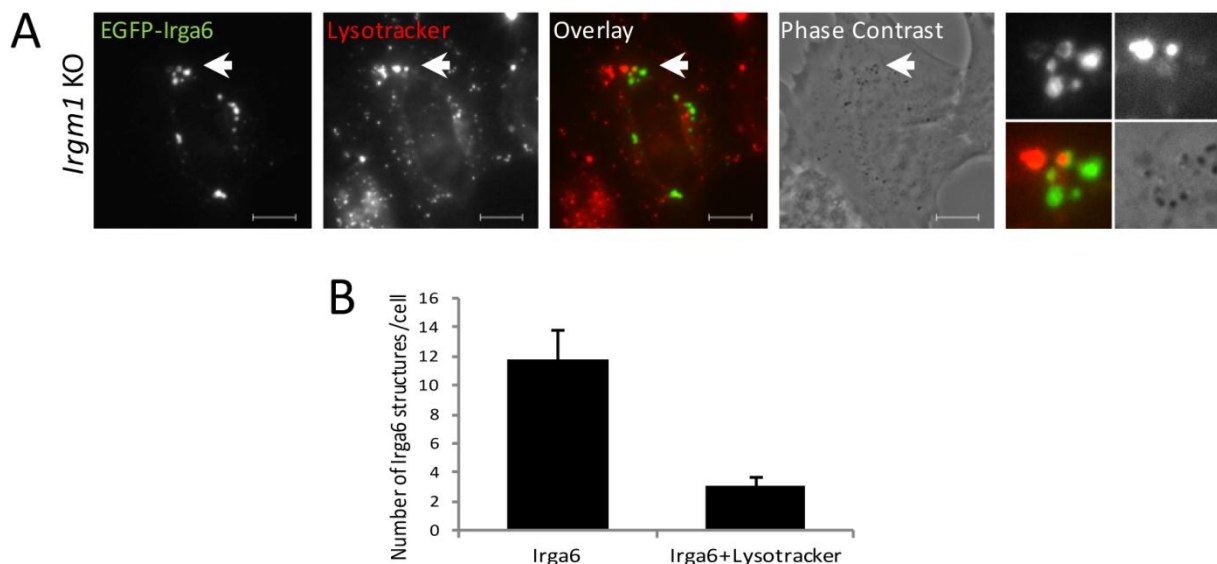

Figure 27. Acidity of GKS-coated lysosomes is impaired A) *Irgm1* KO MEFs were transfected with pEGFP-Irga6-ctag and simultaneously induced with 200 U/ml IFNγ for 24 hours. Non-fixed cells were incubated with 50 nM Lysotracker for 15 minutes and pictures of live cells were taken. Representative microscopic images of Irga6 and lysotracker are shown. Arrows point at the Irga6 structures which are magnified at the end of each panel (zoom in the following order: upper left: Irga6, upper right: lysotracker, lower left: overlay, lower right: phase contrast). Scale bars represent 10 µM. **B)** Quantification of 27A that shows number of Irga6 structures that co-localizes with Lysotracker. 25 cells per sample were quantified and means of three independent experiments +/- standard deviation are shown.

3.3.6. Lysosomes are not permeabilized in IFNγ-induced *Irgm1* KO MEFs

When it was observed that GKS proteins localize to LAMP1 structures (chapter 3.1.2.), we first hypothesized that these proteins can disrupt the lysosomal membrane in a similar manner as they mediate disruption of *T. gondii* PVM. Thus, lysosomal membrane permeablilization (LMP) could cause lysosomal enzyme leakage and induce cell death (Boya and Kroemer, 2008) (Repnik et al., 2014). To test the possibility that GKS proteins might permeabilize lysosomal membranes, LMP was assessed by cathepsin B staining in collaboration with intern Jessie Zhang.

Cathepsin B is an enzyme that is transported from Golgi to lysosomes through endosomes as inactive pro-cathepsin B. Once pro-cathepsin B reaches the acidic environment of the lysosome, it is truncated into the active cathepsin B form (Dean, 1979) (Barrett and Kirschke, 1981). The immunofluorescence microscopy images of the resting WT cells stained with anti-cathepsin B antibody show marginal extra-lysosomal staining of the immature pro-cathepsin B and outstanding cathepsin B punctae (Tholen et al., 2014).

To monitor the lysosomal membrane permeabilization, WT MEFs were treated with a reagent which induces lysosomal membrane permeabilization named H-Leu-Leu-OMe·HBr (shortly LeuLeuOMe) (Mizuta et al., 2002) (Uchimoto et al., 1999). The non-treated and LeuLeuOMe-treated WT MEFs were stained with anti-cathepsin B and anti-LAMP1 antibodies. Indeed, in non-treated cells, cathepsin B stained punctae co-localized with non-permeabilized LAMP1 stained lysosomes. However, when lysosomes were treated with LeuLeuOMe, and presumably permeabilized, cathepsin B was released into the cytosol and the number of punctae was reduced (data not shown).

In order to establish a concentration of LeuLeuOMe that can induce LMP without killing the cell, *Irgm1* KO MEFs were treated with different concentrations of this reagent for 24 hours. Cell death was measured with PI/Hoechst staining assay as described in chapter 3.4. 3.75mM was the highest tested concentration of LeuLeuOMe that did not strongly affect the cell survival (Figure 28A).

It was further microscopically tested whether the degree of LMP is correlated to the number of cathepsin B punctae. To induce LMP, *Irgm1* KO MEFs were treated with 2mM, 3mM or 4mM of LeuLeuOMe or left untreated for 24 hours. Cells were fixed and stained with the anti-cathepsin B antibody. Pictures of the samples were taken and cathepsin B punctae in the cells were manually blind counted (Figure 28B). Samples treated with higher concentrations of LeuLeuOMe had fewer cathepsin B punctae per cell, indicating that

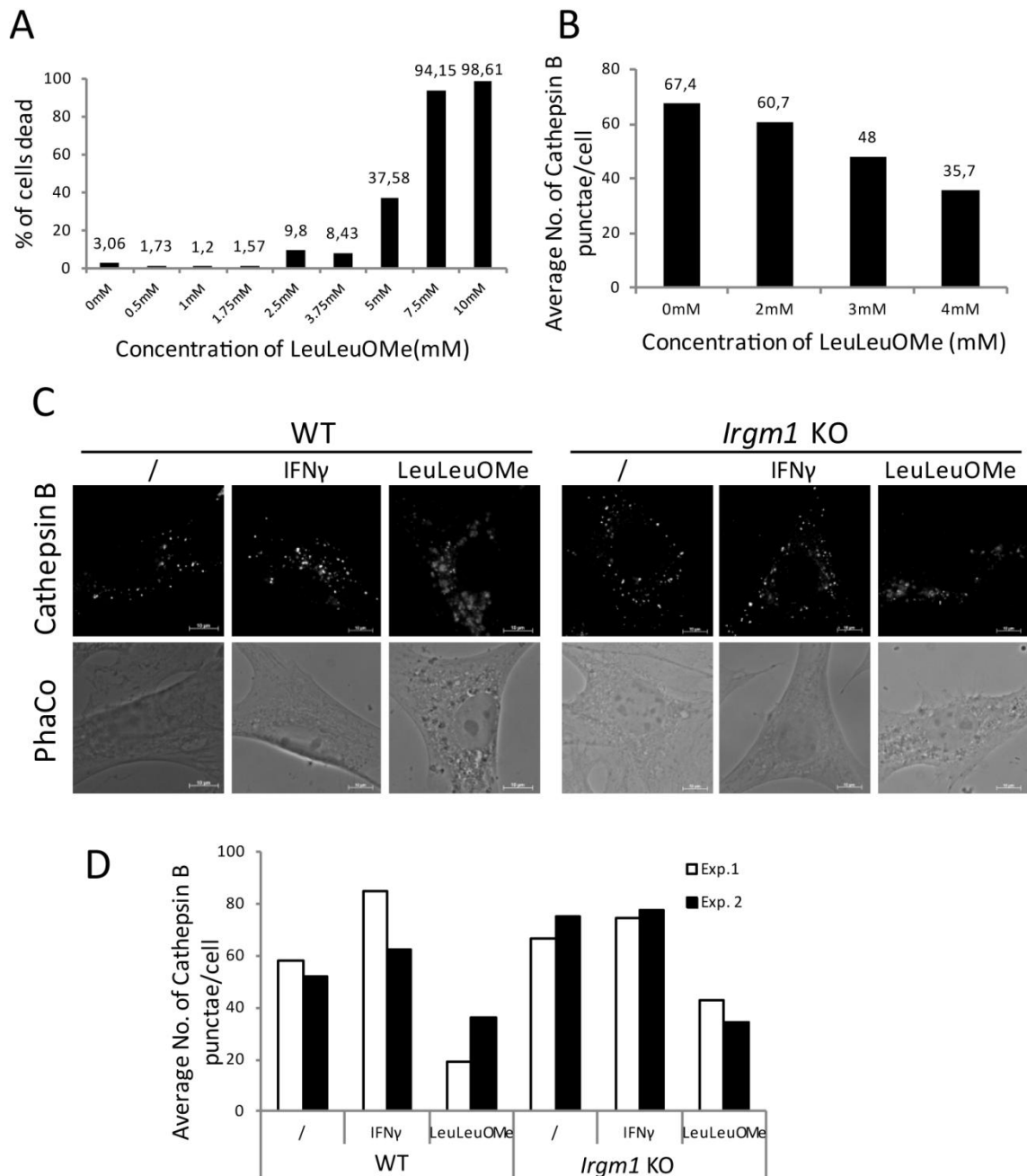cathepsin B punctae staining corresponds to the extent of the LMP in dose-dependent manner.

Figure 28. Cathepsin B punctae quantification in *Irgm1* KO MEFs A) *Irgm1* KO MEFs were treated with different concentrations of lysosomal permeabilization agent LeuLeuOMe or left untreated for 24 hours. Cells were stained with Propidium Iodide and Hoechst dye and analyzed as in chapter 3.4. Percent of PI positive cells is shown. 5000-10000 cells per sample were quantified. **B)** *Irgm1* KO MEFs were treated with 2mM, 3mM or 4mM of LeuLeuOMe or left untreated for 24 hours. Cells were fixed and stained with anti-cathepsin B antibody AF965. Average number of cathepsin B positive punctae per cell is shown. 50 cells per sample were blind counted. **C)** WT MEFs and *Irgm1* KO MEFs were treated with 200 U/ml IFNγ, 3 mM LeuLeuOMe or left un-treated for 24 hours. Cells were fixed and stained with anti-cathepsin B antibody. Representative images of cathepsin B staining and Phase contrast are shown. **D)** Quantification of 28C, showing number of cathepsin B punctae per cell. 100 cells per sample blind counted and results of two independent experiments are shown.

To analyze LMP in the cells of interest, WT MEFs and *Irgm1* KO MEFs were left un-treated, induced with IFNγ or treated with 3mM LeuLeuOMe. Cells were fixed and stained with the antibody against cathepsin B. Immunofluorescence images of cathepsin B staining were taken (Figure 28C) and the number of cathepsin B punctae per cell was blind manually counted (Figure 28D). Both, LeuLeuOMe-treated WT and LeuLeuOMe-treated *Irgm1* KO cells had fewer cathepsin B punctae than non-treated cells. However, the amount of punctae in IFNγ-induced *Irgm1* KO MEFs was very similar to untreated *Irgm1* KO MEFs as well as treated and untreated WT MEFs. Taken together, these data indicate that GKS proteins, which are localized to lysosomes, probably do not mediate lysosomal membrane permeabilization in IFNγ-induced *Irgm1* KO cells.

3.4. IFNγ does not induce death of *Irgm1* KO MEFs and BMDMs

Previously, it has been reported that *Irgm1* KO lymphocytes and hematopoetic stem cells (HSCs) undergo cell death upon induction (Feng et al., 2008b) (Feng et al., 2008a) (King et al., 2011) (chapter 1.6.3.). However, it has been also shown that *Irgm1* KO Bone marrow derived macrophages (BMDMs) do not die upon induction with IFNγ (Henry et al., 2007). Thus, it had to be clarified which Irgm1 cell types undergo cell death upon induction.

WT and *Irgm1* KO MEFs were induced with IFNγ, high concentration of LeuLeuOMe or left non-induced. After 24, 48 or 72 hours, non-fixed cells were stained with permeable DNA binding Hoechst dye, which stains nuclei of live and dead cells, and impermeable Propidium Iodide (PI), which stains only nuclei of dead cells (Figure 29A). Pictures of the cells were taken and PI positive and Hoechst positive cells were detected and enumerated with Volocity software. The percentage of PI-positive cells was calculated (Figure 29B). In LeuLeuOMe-induced cells, more than 80 percent of the Hoechst stained cells were also PI positive. In all other samples in this analysis, less than 10 percent of the cells were PI positive, indicating that IFNγ does not induce cell death in *Irgm1* KO MEFs.

Further, cell death was again tested in primary BMDMs. WT BMDMs and *Irgm1* KO BMDMs were left untreated, induced with IFNγ or induced with LeuLeuOMe. In addition, these cells were also stimulated with the combination of IFNγ and Lipopolysaccharide (LPS). (Figure 29C).
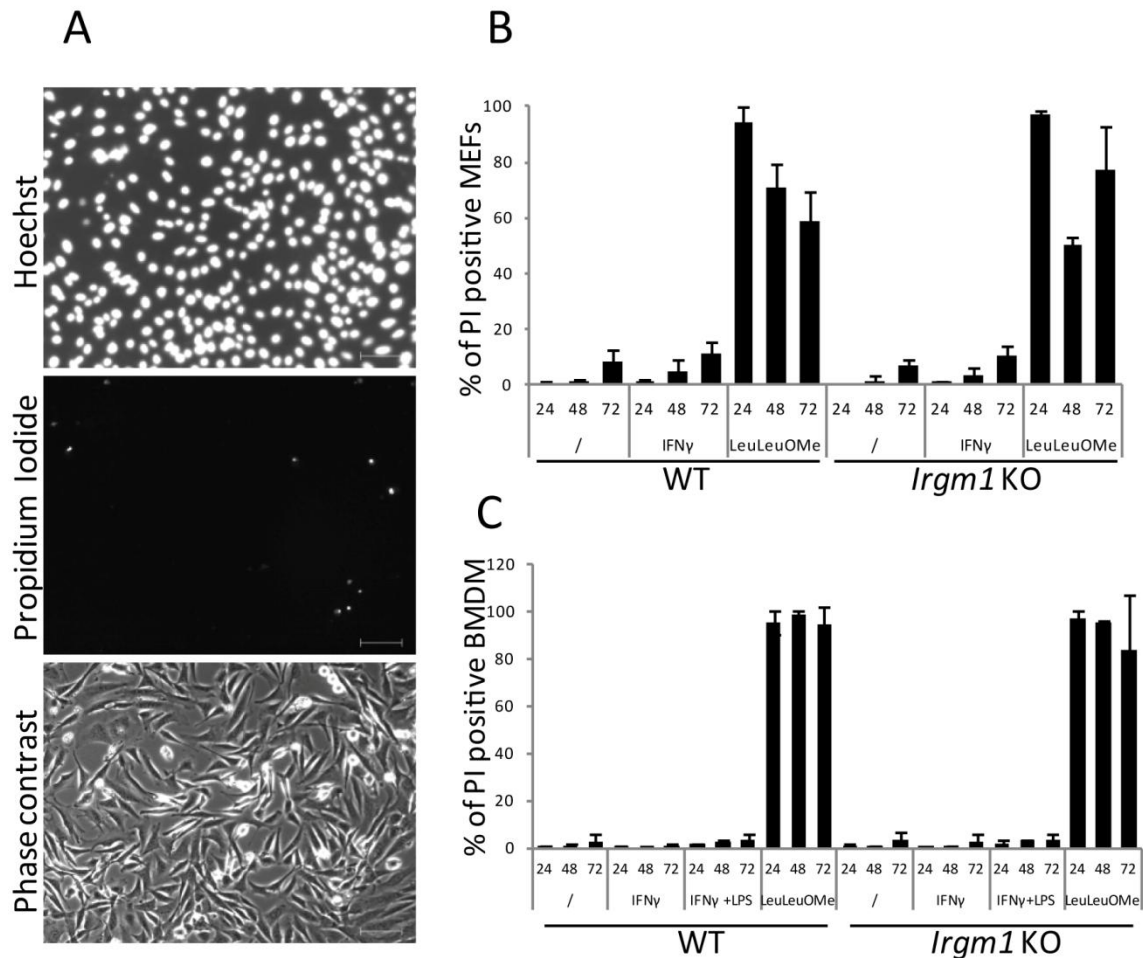
Figure 29. Cell death of IFNγ induced *Irgm1* KO MEFs and BMDMs A) WT and *Irgm1* KO MEFs were induced with 200 U/ml IFNγ or treated 10 mM LeuLeuOMe for 24, 48 and 72 hours or left untreated. Cells were stained with nuclear dyes Hoechst and Propidium iodide and pictures of the cells were taken. Representative microscopic images of Hoechst staining, PI staining and Phase Contrast are shown. Scale bars represent 10µM. **B)** Quantification of 29A that shows percent of PI positive MEFs. Dye stained nuclei were quantified with Volocity software. 10 pictures (5000-10000 cells) per sample were quantified and the means of three independent experiments +/- standard deviation are shown. **C)** WT and *Irgm1* KO BMDM cells were induced with 200 U/ml IFNγ, 500 ng/ml LPS, 5 mM LeuLeuOMe for 24, 48 and 72 hours or left untreated. Experiment was performed as in 29A, B. 10 pictures (5000-10000 cells) per sample were quantified and the means of three independent experiments +/- standard deviation are shown.

Similarly to the analysis of cell death in MEFs, more than 80 percent of LeuLeuOMe treated WT and *Irgm1* KO BMDMs were PI positive. Again, no difference in the percent of dead cells was observed between non-induced, IFNγ-induced or IFNγ and LPS induced WT and *Irgm1* KO BMDMs.

Taken together, the results of the cell death assay show that neither immortalized *Irgm1* KO MEFs, nor primary *Irgm1* KO BMDMs, undergo cell death after IFNγ-induction. Therefore, IFNγ-mediated cell death is probably characteristic for the particular sets of cells of the *Irgm1* KO mouse, like, for example *Irgm1* KO lymphocytes and HSCs (Feng et al., 2008b) (Feng et al., 2008a) (King et al., 2011).

3.5. Irga6 aggregate-like structures are detergent soluble

Initially, the GKS protein structures that are formed in the absence of GMS proteins were described as aggregates (Martens et al., 2004). However, after detailed analysis of Irga6 ring-like structures that localize to lysosomes in *Irgm1* KO MEFs, it seems that so called GKS aggregates are more similar to GTP-bound GKS proteins at the PVM (Figure S1). To better characterize these GKS aggregate-like structures, their solubility was assessed. Thus, Filter Trap assay, a method for the isolation and analysis of aggregates optimized for Dendritic Cell Aggresome Like Structures (DALIS) (Kettern et al., 2011), was adjusted for GKS aggregate-like structure analysis in collaboration with Dr Nadja Kettern (Institute for Cell Biology, University of Bonn).

To establish the method, the filter trap assay was first performed on DALIS. RAW309 macrophages were left untreated or treated with LPS for 12 hours, a time point in which DALIS formation reaches its peak. Macrophages were lysed in RIPA buffer and filtered though the nitrocellulose membrane. Under vacuum force, detergent soluble proteins were filtered though the membrane, and non-soluble DALIS were retained on the membrane. Since DALIS are highly ubiquitinated, nitrocellulose membrane was probed with anti-ubiquitin antibody FK2 (Figure 30A). A clear difference in the intensity of FK2 staining between LPS-induced and LPS non-induced sample could be observed.

To have an insight into the solubility of the GKS aggregate like structures, a filter trap assay used on DALIS was adjusted for GKS aggregate analysis. Irga6 stable transfected Gene Switch (GS) 3T3 cells express only Irga6 when induced with Mifepristone (MIF) (chapter 3.1.2.c). In the absence of GMS regulatory proteins, Irga6 forms aggregates in these cells. IFNγ-induced GS 3T3 Irga6 cells express the full set of IRG proteins and GMS proteins control GKS protein aggregation. Therefore, even though Irga6 is present in these cells, it does not form and should not accumulate on the membrane.

GS 3T3 Irga6 cells were induced with MIF, IFNγ or left untreated for 24 hours. The cells were lysed in different lysis buffers composed of a variety of ionic and non-ionic detergents: 0,5 % Thesit (Figure 30B), RIPA buffer, 1% TritonX-100, 80mM n-Octyl β-D-glucopyranoside or 1% Digitonin (data not shown) and filtered through nitrocellulose membrane. The membrane was probed with the antibody against Irga6 (10E7) (Figure 30B). Even though multiple Filter trap analysis attempts were performed with several detergents, no difference between Irga6 staining in MIF-induced, IFNγ-induced or non-induced cells could be observed. Therefore, it was hypothesized that GKS aggregate-like structures are actually detergent soluble.
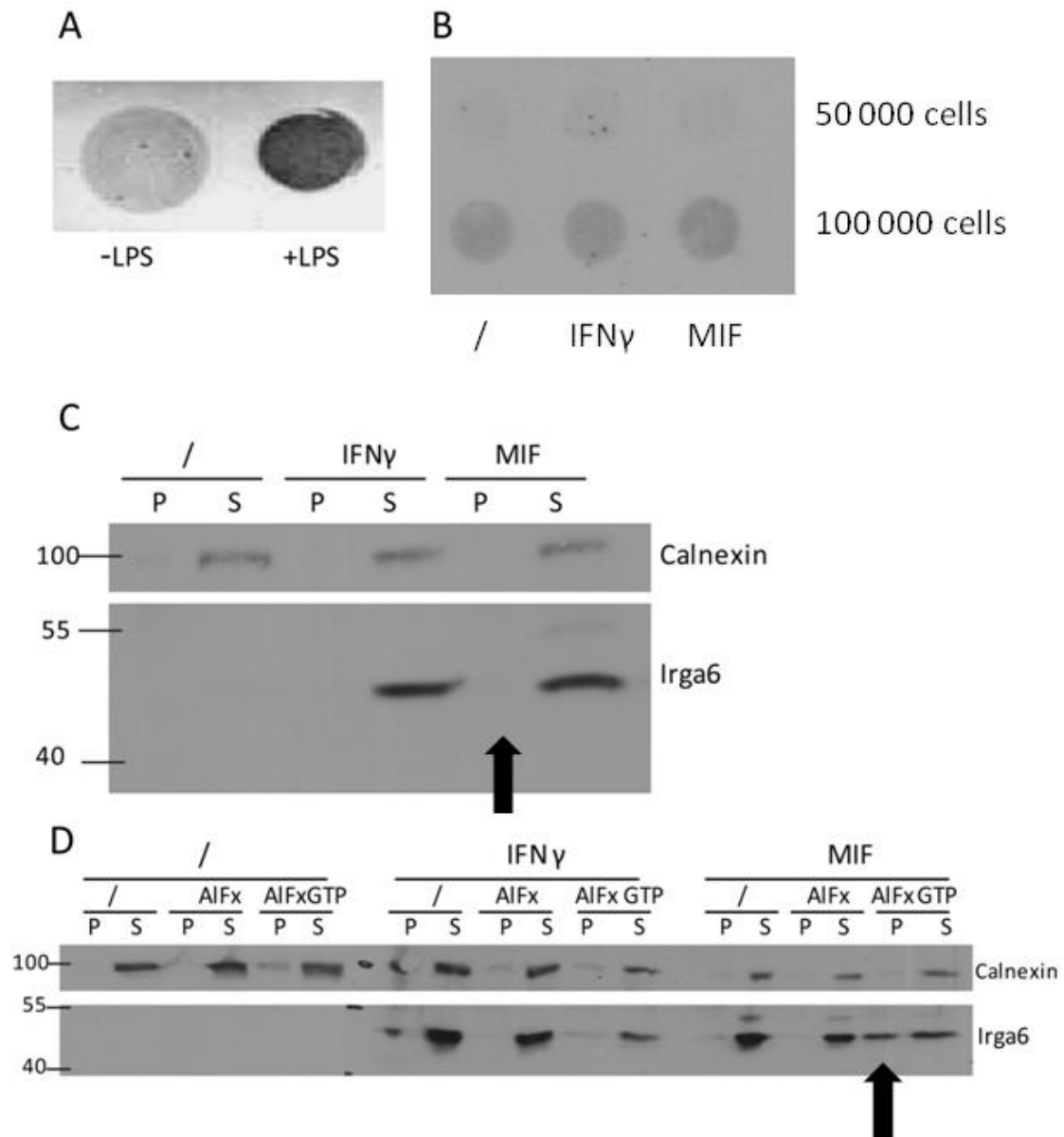
Figure 30. Irga6 aggregate-like structures are detergent soluble A) RAW309 macrophages were left untreated or stimulated with 500ng/ml LPS for 12 hours to induce formation of dendritic cell aggresome like structures (DALIS). Cells were lysed in RIPA buffer and 50mg of each cell lysate were vacuum filtered through a nitrocellulose membrane on a dot-blotter. Detergent insoluble ubiquitin conjugates were detected on the membrane with the FK2 antibody. **B)** GS 3T3 Irga6 cells were induced with IFNγ, MIF or left untreated for 24 hours. 50000 or 100000 cells were lysed in 0,5 % Thesit, filtered through a nitrocellulose membrane and probed with Irga6 (10E7) antibody. **C)** GS 3T3 Irga6 cells were treated as in 30B. 30000 cells were lysed in 0,5 % Thesit and centrifuged at 45000 rpm for 30 minutes. Supernatant and the pellet were separated, analyzed by SDS-PAGE/Western Blot and probed with anti-Irga6 (10E7) and anti-Calnexin reagents. Arrow points at the pellet fraction of MIF-induced GS 3T3 Igra6 cell lysates, in which insoluble Irga6 could not be isolated. **D)** GS 3T3 Irga6 cells were induced with IFNγ, MIF and/or left untreated for 24 hours. Following, cells were treated with $AlCl_3$, NaF and/or GTP or left un-treated for 1 hour. 30000 cells were lysed in 0,5 % Thesit and centrifuged at 13000 rpm for 30 minutes. Supernatant and the pellet were separated, analyzed by SDS-PAGE/Western blot analysis and probed with anti-Irga6 and anti-Calnexin reagents. Arrow points at the pellet fraction of GS 3T3 Igra6 cell lysates that were pre-treated with MIF, AlFx and GTP, in which insoluble Irga6 is isolated.

To further test the solubility of Irga6 aggregates, cell lysates prepared with 0,5 % Thesit (Figure 30C), 80mM n-Octyl β-D-glucopyranoside or 1% Digitonin (Figure S3), as described in previous experiment, were utracentrifuged at 45000 rpm for 30 minutes. The pellet and supernatant were separated and analyzed by SDS-PAGE/Western Blot analysis probed with anti-Irga6 and anti-calnexin immunoreagents (Figure 30C). Calnexin, which is detergent soluble, was detected only in supernatant fraction. Irga6 could also be detected only in the supernatant fraction and not in the insoluble pellet of MIF-induced cells, indicating that the complete Irga6 in this sample is detergent soluble.

Previously, it has been shown that Irga6 forms transient oligomers that can be permanently preserved by addition of Aluminium fluoride (AlFx) and excess of GTP (Papic et al., 2008) (chapter 1.4.4.). Aluminum fluoride (AlFx) is the substance that locks the GTPases in the transition state and therefore prevents the shifts between GTP- and GDP-bound states (Wittinghofer, 1997). To this end, GS 3T3 Irga6 were treated with IFNγ or MIF for 24 hours or left untreated. In addition, these cells were treated with AlFx and GTP or left untreated. The samples were lysed with 0,5 percent Thesit and ultracentrifuged at 45000 rpm. The pellet and supernatant were separated, analyzed with SDS-PAGE/Western Blot and probed with the antibody against Irga6 (10E7). Indeed, addition of AlFx and GTP yielded Irga6-positive band in the pellet fraction of MIF-induced cells (Figure 30D). Thus, the ultracentrifugation method can capture naturally or artificially formed GKS aggregates if they exist.

Taken together, Irga6 proteins probably form membrane-bound structures similar to the GTP-bound Irga6 accumulations at the PVM. Once the membranes are dissolved in detergent, these structures are also dispersed.

4. DISCUSSION

4.1. How do GKS proteins function in the absence of GMS proteins?

The role of regulatory Immunity-related GTPases (IRGs), called GMS proteins is to keep the effector IRG proteins, called GKS proteins in the inactive, GDP-bound state and prevent them from activating on endomembranes (Hunn et al., 2008). The presence of GMS proteins on endomembranes but not on vacuolar membranes surrounding certain classes of pathogens enables GKS proteins to target the pathogen vacuolar membranes preferentially (Martens, 2004) (Hunn and Howard, 2010) (Howard et al., 2011) (Haldar et al., 2013) (Coers, 2013) (da Fonseca Ferreira-da-Silva et al., 2014).

In this study, it was shown that GKS localization at the particular membranes is dependent on the presence of particular GMS proteins. GKS proteins can accumulate only on the membranes that are not GMS-coated (Figure 31). Namely, in IFNγ-induced *Irgm1* KO cells, more than 90 percent of Irga6 and other GKS proteins accumulate at the lysosomes, which are normally coated with Irgm1 (chapters 3.1.2. and 3.1.6.). In accordance with that, in IFNγ-induced *Irgm3* KO cells, more than 90 percent of Irga6 accumulates on the endoplasmic reticulum (ER), which is normally coated with Irgm3 (chapter 3.1.3.). The Golgi apparatus, which is coated with Irgm1 and Irgm2, is not coated with Irga6 in *Irgm1* KO or *Irgm3* KO cells (chapter 3.1.4.). As shown by (Haldar et al., 2013), in IFNγ-induced *Irgm1/Irgm3* KO cells, GKS proteins accumulate on the lipid droplets (LDs), which are otherwise coated with Irgm1 and Irgm3 (Bougneres et al., 2009) (Haldar et al., 2013), but do not accumulate on the ER and lysosomes, which should also be GMS-free in these cells (chapter 3.1.5.). Taken together, GKS proteins accumulate at the membranes that are not GMS-coated, but probably prefer one type of membranes over another, when given a choice (further discussed in chapters 4.2. and 4.3.)

The consequences of GKS accumulation on the lysosomes in IFNγ-induced *Irgm1* KO cells were investigated. The hypothesis that GKS proteins disrupt the lysosomal membrane is probably not correct since lysosomal membrane permeabilization (LMP) and consequent cell death could not be observed in IFNγ-induced *Irgm1* KO mouse embryonic fibroblasts (MEFs) (chapters 3.3.6. and 3.4.). However, the autophagic flux in these cells is impaired and the number of autophagosomes is increased (chapters 3.3.1. and 3.3.2). The impairment of the autophagic flux is probably caused by the inability of GKS-coated lysosomes to process autophagosomes after lysosomal fusion (chapters 3.3.3. and 3.3.4.). Finally, it was shown that the pH of GKS-coated lysosomes is unusually increased (chapter

3.3.5.), indicating that the substrate processing in these lysosomes must be impaired (further discussed in chapter 4.4.).
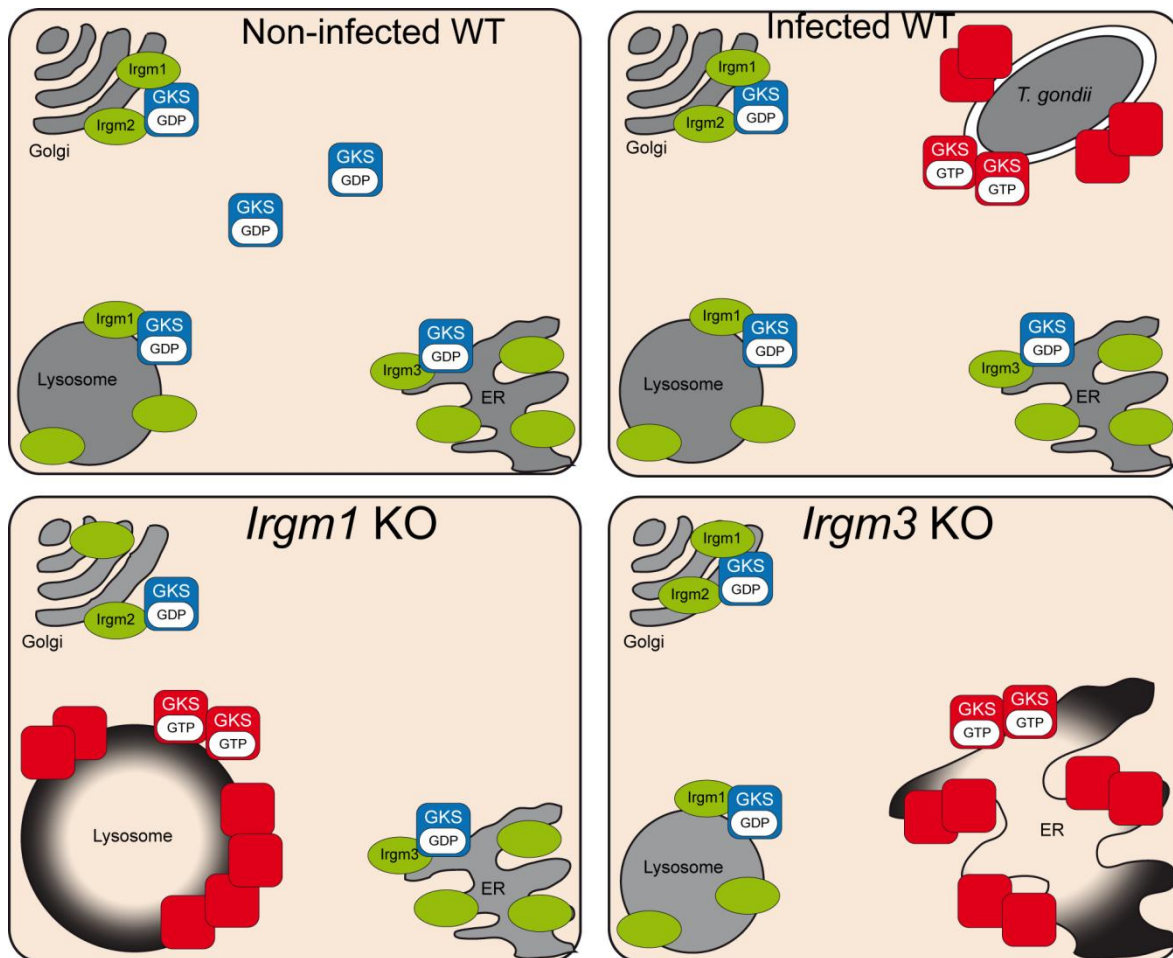

Figure 31. Model of cytotoxic effect of dysregulated GKS proteins A) GMS proteins localize to different cellular endomembranes, like the ER, the Golgi and lysosomes, and keep GKS proteins in an inactive GDP-bound state **B)** When *T. gondii* enters the cell, GKS proteins accumulate and activate at the PVM, because of the absence of GMS proteins on PVM membrane. GKS proteins turn into active GTP-bound form and mediate membrane disruption **C)** In *Irgm1* KO cells, GMS protein do not protect lysosomal membranes. Therefore, GKS proteins become activated, form GTP-bound structures and accumulate on the lysosome. Acidification and digestive abilities of these lysosomes are impaired. Thus, the lysosomes cannot properly process autophagosomes after lysosome/autophagosome fusion. Hence, autophagic flux of IFNγ induced *Irgm1* KO cells is impaired **D)** In *Irgm3* KO cells the ER cisternae are not protected by GMS proteins. GKS proteins accumulate on the ER, possibly cause ER deformation, which does not have as severe consequences for the cell as lysosomal impairment in *Irgm1* KO cells.

The connection between lysosomal failure in IFNγ-induced *Irgm1* KO cells and the striking lymphopenia that causes death of the *Irgm1* KO mice after infection remains to be further investigated. In this study, it was shown and reproduced that *Irgm1* KO MEFs and BMDMs do not die after IFNγ-induction (chapter 3.4.). Thus, it seems that the death of the *Irgm1* KO mice is caused by a failure of specific subsets of cells, like lymphocytes and hematopoetic stem cells (HSCs), which do die upon induction (Feng et al., 2008b) (Feng et al., 2008a) (King et al., 2011) (further discussed in chapters 4.5. and 4.6.).

Finally, it was shown that up to now called GKS aggregates, which appear when GKS proteins are overexpressed in the absence of GMS proteins, are actually detergent soluble. Detergent solubility, together with the possibility to eliminate these accumulations with the addition of GMS proteins (Hunn and Howard, 2010) and discovery that they are in the GTP-bound conformation (Papic et al., 2008), indicate that GKS protein accumulations rather resemble active GTP-bound structures, similar to the GKS proteins at the PVM of *T. gondii*, than the insoluble accumulations of missfolded inactive protein aggregates (further discussed in chapter 4.7.).

4.2. How do IRG proteins recognize their targets?

As previously described (chapter 1.1.), host organisms can recognize their pathogens by different mechanisms: by recognition of "microbial non-self", by recognition of "induced or altered self" and by recognition of "missing self". Host recognition of pathogens by the "missing self" principle relies on the detection of gene products and products of metabolic pathways that are unique to host and absent from the pathogen. Therefore, host immunity effectors can target for destruction the structures which are not labeled as self for destruction (Medzhitov and Janeway, 2002).

Even though the IRG response to *T. gondii* is relatively well described (chapter 1.5.1), the mechanism by which IRG proteins recognize the PVM and distinguish it from the other cellular membranes is not yet understood. One hypothesis for the IRG mechanism of action suggests that GKS proteins recognize the PVM by the "missing self" principle (Martens, 2004) (Hunn and Howard, 2010) (Haldar et al., 2013) (Coers, 2013). By this principle, regulatory GMS proteins would label all the endocellular membranes and GKS proteins would accumulate to the only membranes in the cell that are not GMS-labeled, the parasitophorous vacuolar membrane (PVM) (da Fonseca Ferreira-da-Silva et al., 2014).

In this study, the simplistic model of the host distinction between self and non-self membranes was shown to be partially true. In IFNγ-induced *Irgm1* KO cells, lysosomes are not GMS-coated and GKS proteins accumulate on them (chapters 3.1.2. and 3.1.6.). In IFNγ-induced *Irgm3* KO cells, where the ER is not GMS coated, Irga6 localizes to the ER (chapter 3.1.3.).

However, certain findings from this and other studies indicate that the model by which GKS proteins can accumulate to any GMS-free membrane is not fully correct and that GKS proteins select the GMS-undefended membranes with certain preference.

Firstly, in IFNγ-induced *Irgm1/Irgm3* KO cells, lipid droplets (LDs), lysosomes and ER are not coated with GMS proteins. GKS proteins were indeed reported to accumulate to LDs (Haldar et al., 2013) (chapter 3.1.5.), but no accumulation of GKS proteins onto lysosomes or the ER could be observed in these cells (chapters 3.1.2., 3.1.3. and 3.1.6.). Therefore, it seems that GMS proteins do not accumulate on every GMS-free membrane when given more options.

Secondly, it seems that Irga6, when expressed in the absence of all GMS proteins, also prefers particular endomembranes. Namely, in the GS 3T3 Irga6 cells, which express Irga6 upon induction with Mifepristone (MIF), GMS proteins are not present. Hence, all endocellular membranes in these cells are not GMS-coated and all should be potential targets for the GKS proteins. However, in MIF-induced GS 3T3 Irga6 cells, less than 5 percent of Irga6 structures accumulated to the lysosomes and Golgi apparatus (chapters 3.1.2. and 3.1.4.), indicating that Irga6 probably prefers another compartment, possibly lipid droplets or ER, when given more options. In contrast, when Irgm2 and Irgm3 were co-transfected in these cells, GMS-free membranes were probably limited to the lysosomes and thus in these cells more than 70 % of Irga6 structures accumulated at the lysosomes.

Thirdly, when Irga6 and Golgi co-localization was analyzed in the GMS-transfected MIF-induced GS 3T3 Irga6 cells (chapter 3.1.4.), it was observed that in the sample with cells that were not GMS-coated, and even in the sample with cells that were transfected with Irgm3, Irga6 clearly did not accumulate to the Golgi, even though this compartment is GMS-free.

Finally, one of the strongest arguments against the hypothesis that GKS proteins accumulate at any membrane that is not GMS-coated is the fact that neither GKS nor GMS proteins localize to the host plasma membrane of IFNγ-induced wild type mouse cell.

Recently, it has been proposed that another hypothetical unknown protein, named factor Y, could localize at the plasma membrane and protect it from the off-target activation of GKS proteins (da Fonseca Ferreira-da-Silva et al., 2014). The pathogens that are targeted by the GKS proteins all have unusual non-phagocytic entry mechanism into cell, which involves the formation of the PVM from heavily modified plasma membrane (Ling et al., 2006) (Hybiske and Stephens, 2007) (Bohne et al., 2011). Therefore, it has been proposed that the hypothetic factor Y is excluded from the plasma membrane during formation of the PVM of these pathogens. Thus, the PVM, but not the plasma membrane, can be targeted by GKS proteins. Pathogens like *M. tuberculosis* and *L. monocytogenes*, which are taken up by phagocytosis, probably do not exclude factor Y from the phagosomal membrane, and cannot be targeted by GKS proteins (da Fonseca Ferreira-da-Silva et al., 2014).

Another possibility, which could explain why the plasma membrane is not targeted by GKS proteins, could be that GKS proteins have a preference for membranes of particular lipid composition. As previously discussed, in IFNγ-induced *Irgm1/Irgm3* KO cells, GKS proteins accumulate at LDs, even though lysosomes and ER are also not GMS coated. Similarly, it could be that GKS proteins have low affinity to accumulate at the plasma membrane.

Membrane binding mechanisms and lipid preferences of IRG proteins are not clarified up to date. It has been shown that myristoylation of Irga6 is important for its membrane binding (Papic et al., 2008). However, it is still not clear if Irga6 can bind membranes of any lipid composition. Moreover, Golgi membrane targeting of Irgm1 is shown to require by the αK helix of this protein (Martens et al., 2004) (Martens and Howard, 2006) (Zhao et al., 2010). It has been reported that Irgm1 can bind lipid samples of phosphatidylinositol-3,4-biphosphate (PitIns(3,4)P_2), phosphatidylinositol-3,4,5-triphosphate (PitIns(3,4,5)P_3) and diphosphatydil-glycerol (DPG), but cannot bind many other lipid samples (Tiwari et al., 2009). However, the significance of these results *in vivo* is not clear, because PitIns(3,4)P_2 and PitIns(3,4,5)P_3, were not found in the lysosomes or Golgi apparatus, the compartments to which Irgm1 normally localizes in WT cells (Kutateladze, 2010). However, DPG can be found in mitochondria, the compartments to which Irgm1 also localizes (Tiwari et al., 2009). Thus, the preference of the IRG proteins for membranes of particular lipid composition should be further investigated.

Taken together, GMS proteins indeed protect endocellular membranes from GKS accumulation and probably help the host to distinguish between self membranes and the pathogen. However, GKS proteins probably do not accumulate on every membrane that is not GMS coated and show some preference when choosing their targets.

4.3. Is there hierarchy in GKS localization to the lysosomes?

Irga6, Irgb6, Irgb10 and Irgd were shown to accumulate at the same PVMs of *T. gondii* after infection. It was proposed that they do so in cooperative and hierarchical manner (Khaminets et al., 2010). Co-staining for Irga6 and Irgb6 had shown that Irgb6 could be found at the PVM alone or together with Irga6 (Figure 32A). However, Irga6 could only rarely be present at the PVM without Irgb6. Similarly, Irgb10 could be detected at the PVM alone or with Irga6, but Irga6 could not be at the PVM without Irgb10. Irgb6 and Irgb10 could be detected at the PVM together or independently. In addition, time lapse microscopy analysis had shown that, when Irga6 and Irgb6 are co-transfected into cell, Irgb6 was always the first

one to start PVM accumulation and it was followed by Irga6. Taken together, these data indicate that Irgb6 and Irgb10 are the leading GKS proteins that localize to the PVM of *T. gondii* (Khaminets et al., 2010).

Similarly, in IFNγ-induced *Irgm1* KO cells, not only Irga6, but also Irgb6, Irgb10 and Irgd accumulate to the lysosomes (chapters 3.1.2.and 3.1.6.). However, the hierarchy of GKS loading to the lysosomes differs from the hierarchy of GKS loading to the PVM of *T. gondii* (chapter 3.1.7.) (Figure 32B). When IFNγ-induced *Irgm1* KO cells were stained for combinations of two GKS-proteins and for LAMP1, it was observed that Irga6 and Irgb10 could localize to the lysosomes alone or together with other GKS proteins. Contrary, Irgb6 and Irgd could be detected at the lysosome only if Irga6 or Irgb10 were also there. Therefore, Irga6 and Irgb10 are probably the leading GKS proteins in the hierarchy of lysosomal accumulation in *Irgm1* KO cells.
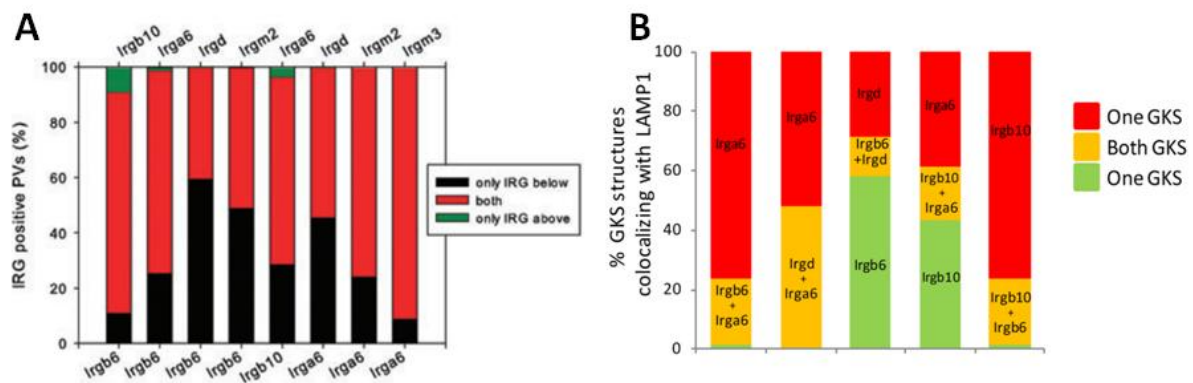

Figure 32. Hierarchical loading of different IRG proteins onto the PVM of *T. gondii* and onto the lysosomes in *Irgm1* KO cells. A) IRG proteins loaded onto the PVM of *T. gondii* were detected by co-staining with pairs of specific antibodies directed against IRG proteins. Vacuoles containing one or two IRG proteins were quantified. Vacuoles not loaded with IRG proteins of interest were not included in the analysis (Modified from (Khaminets et al., 2010)). **B)** *Irgm1* KO MEFs were induced with 200 U/ml IFNγ and immunostained with pairs of specific antibodies directed against IRG proteins and an antibody against LAMP1. Lysosomes containing one or both IRG proteins were quantified. Lysosomes that are not loaded with either IRG protein of interest were not included into analysis (modified from figure 18).

Another interesting similarity between GKS accumulation onto lysosomes and onto the PVM is that some vacuoles and some lysosomes are never coated with up to now tested IRG proteins. Namely, after infection with avirulent strains of *T. gondii*, a majority of the PVMs are fully coated with the GKS proteins. However, certain fraction of PVMs are always GKS-free (Khaminets et al., 2010) no matter the time point of analysis. Similarly, certain percentages of the lysosomal membranes in *Irgm1* KO cells are not GKS coated. Even though, one cannot exclude the possibility that other GKS proteins, for example Irga4 or Irga8, which cannot be immunostained with existing antibodies, could accumulate at the

remaining lysosomes and PVMs, two other models were discussed to explain the difference between strongly loaded and non-loaded PVMs of *T. gondii*.

First it was suggested that non-coated PVMs represent the membranes of *T. gondii* that got damaged or malfunctioned during cellular invasion. Therefore, there was not need to activate the IRG defence system against organisms that are not dangerous for the cell (Howard lab, personal communication).

The second proposal suggests that discrimination of particular membranes is a consequence of the cooperativity and homo-/hetero-oligomer formation during PVM loading. According to this model, the first activated IRG protein molecule on the parasite membrane would encourage cooperative activation and oligomerization of further IRGs on the same membrane. Therefore, following GKS molecules would rather accumulate at the already "conquered" membranes and not to the GKS-free membranes (Khaminets et al., 2010). Assuming that lysosomes cannot be divided to "functional" and "failed", the proposal which suggests easier cooperative loading of the GKS proteins to already coated membranes may be more plausible.

It was possible that the absence of Irga6, which is, together with Irgb10, one of the leading proteins in lysosomal accumulation, would affect subsequent GKS accumulation at the lysosomes in *Irgm1* KO cells and possibly also the phenotypic outcome of infected *Irgm1* KO mice.

Unlike in *Irgm1* KO cells, when IFNγ-induced *Irgm1/Irga6* KO cells were stained with Irgb6 and Irgb10, it was observed that Irgb6 could localize to the lysosomes that were not Irgb10 stained and obviously not Irga6 positive (chapter 3.2.2.). In addition, preliminary data had shown that in MIF-induced GS 3T3 Irgb6 cells, which were also transfected with Irgm2 and Irgm3, Irgb6 could form aggregates and accumulate at the lysosomes, even though Irga6 and Irgb10 were not expressed in the cell (Figure S4). Even though Irgb6 and Irgb10 are the leading proteins in the hierarchy of PVM loading (Khaminets et al., 2010), in MIF-induced GS 3T3 Irga6 cells, which were transfected with Irgm1, Irgm2 and Irgm3, Irga6 could accumulate at the PVM of *T. gondii* (Hunn et al., 2008).

These results indicate that the leading GKS proteins, like Irga6 and Irgb10 at the lysosomes, are not a prerequisite for the other GKS proteins, like Irgb6, to accumulate at these endocellular membranes. Similarly, presence of Irgb6 and Irgb10 is not a prerequisite for Irga6 to accumulate to the PVM of *T. gondii*. However, there is evidence that the presence of Irga6 stabilises the binding of Irgb6 to the *T. gondii* PVM. Even though the

efficiency of the loading and the ability of Irga6 to independently disrupt the PVM remain to be investigated, these observations indicate that the hierarchy of GKS loading is not qualitatively required for the accumulation of GKS proteins.

In accordance with the successful loading of the other GKS proteins in IFNγ-induced *Irgm1/Irga6* KO cells, the phenotype of *Irgm1/Irga6* KO mice is similar to the phenotype of *Irgm1* KO mice. Firstly, the weight reduction, which is characteristic for *Irgm1* KO mice grown in non-sterile conditions, was also observed in *Irgm1/Irga6* KO mice (chapter 3.2.1). Secondly, *Irgm1/Irga6* KO mice were equally susceptible to *L. monocytogenes* infection and succumbed within 5 days, as *Irgm1* KO mice did (chapter 3.2.1.).

Taken together, these results indicate that the absolute hierarchy, which was considered to be important in the GKS loading to the PVM, is not a prerequisite for successful accumulation of these proteins. However, it seems that cooperativity between GKS proteins is important and that accumulation of these proteins is enhanced when other GKS proteins are already there.

4.4. Does GKS coating impair functionality of lysosomes?

When GKS proteins were observed to accumulate to the lysosomes in IFNγ-induced *Irgm1* KO cells, it was questioned whether this phenomenon could have severe consequences for the GKS-coated lysosomes, for the *Irgm1* KO cells and for the *Irgm1* KO mice.

GKS proteins, which accumulate at the lysosomes, showed a shape and pattern that strongly resembles the ring-like appearance of GKS-oligomers at the PVM of *T. gondii.* Therefore, it was initially hypothesised that activated GKS proteins could disrupt the lysosomal membrane in a similar manner as they mediate the disruption of the PVM. Lysosomal membrane permeabilization (LMP) (reviewed in (Boya and Kroemer, 2008)), a process which includes the rupture of the lysosomal membrane, cytosolic release of lysosomal enzymes, and finally cell death, could be the cause of the lymphocyte death, lymphopenia and the death of the *Irgm1* KO mice.

However, quantification of cathepsin B-positive punctae, which are a marker for undisrupted lysosomes, showed that there is no difference in the punctae number between induced and non-induced WT cells or *Irgm1* KO cells, suggesting that there is no lysosomal rupture and enzyme release in these cells (chapter 3.3.6.). The cell death of IFNγ-induced

Irgm1 KO MEFs and BMDMs was also not increased in comparison to uninduced cells, indicating that LMP is highly unlikely to occur in these cells (chapter 3.4.).

Another hypothesis proposed that Irgm1 is directly or indirectly involved in the regulation of the autophagic pathway (Feng et al., 2008a) (Deretic, 2011) (King et al., 2011) (Haldar et al., 2013).

Firstly, it was proposed that Irgm1 is an autophagy inducing factor (Gutierrez et al., 2004) (Singh et al., 2006) (Deretic, 2011). This hypothesis was based on the observation that the turnover of the autophagic protein LC3 is increased in Irgm1-transfected cells that were not induced with interferon (Gutierrez et al., 2004) (Singh et al., 2006). It has been also shown that autophagic induction increased the fusion of Mycobacterial phagosomes with lysosomes and enhanced *Mycobacterium tuberculosis* clearance (Gutierrez et al., 2004). However, since these tests were performed with transfected Irgm1, in the absence of GKS proteins and other GMS proteins, they do not properly describe the consequences of the Irgm1 interaction with its targets, the GKS proteins.

Secondly, opposing data had shown that LC3 turnover and autophagy are induced in stimulated *Irgm1* KO lymphocytes, hematopoetic stem cells (HSC) and Paneth cells (Feng et al., 2008b) (King et al., 2011) (Liu et al., 2013). In addition, electron microscopy (EM) images of induced *Irgm1* KO lymphocytes had revealed enlarged multi-lamellar round structures that resemble enlarged autophagosomes (Feng et al., 2008b).

The termination of the autophagic cycle requires that mature autophagosomes fuse with the lysosomes, where they get processed and degraded (Feng et al., 2014). Lysosomes that are GKS coated appear to be enlarged and swollen in IFNγ-induced *Irgm1* KO cells (chapter 3.1.2.). Therefore, it was questioned whether the fusion of the lysosomes with autophagosomes and autophagosomal processing are still functional in these cells. The analysis of the autophagy protein LC3 revealed that the number of LC3-labeled autophagosomes and the level of the mature lipidated form of LC3, called LC3-II are both increased in IFNγ-induced *Irgm1* KO cells, indicating that that there is a change of autophagic flux in these cells (chapters 3.3.1. and 3.3.2.). The increase in LC3-II levels, without the decrease in LC3-I levels, indicated that it is more likely that the autophagic flux is arrested, than that autophagy induction is enhanced in these cells.

Analysis of autophagosome and lysosome co-localization in IFNγ-induced *Irgm1* KO cells revealed that 60-80 % of the LC3-labeled autophagosomes co-localizes with LAMP1 lysosomal marker (chapter 3.3.3.). In comparison, less than 10 % of autophagosomes co-localized with lysosomes in induced and non-induced WT cells, and less than 5 percent did so in non-induced *Irgm1* KO MEFs. In immunofluorescence microscopy images, it appeared

that autophagosome structures were "trapped" inside lysosomal membranes. Hence, it was proposed that certain lysosomes in induced *Irgm1* KO cells are unable to process the autophagosomes once they fuse with them. Thus, autophagic flux could be inhibited after fusion, and LC3-II levels could increase without decreasing LC3-I levels. It was further shown that the lysosomes that cannot process autophagosomes are exactly the same lysosomes that are coated with Irga6 or Irgb10 (chapter 3.3.4.). Therefore, the impairment of autophagic flux probably is the consequence of the GKS loading to the lysosomes.

Apart from autophagosome degradation, lysosomes are also involved in degradation or activation of the variety of intra- and extracellular substrates. Not only autophagosomes, but also bacterial phagosomes and many enzymes are processed in the lysosomes (Feng et al., 2014). Thus, it was questioned whether the processing problems of the GKS-coated lysosomes affect only autophagosomes, or also other lysosomal substrates. The analysis of live in IFNγ-induced *Irgm1* KO cells showed that Irga6-EGFP, which were previously shown to co-localize with LAMP1 structures (chapter 3.1.2.), did not co-localize with the acidotropic marker Lysotracker red, indicating that Irga6-coated lysosomes do not have as low pH, as other lysosomes in the cell (chapter 3.3.5.). Therefore, these non-acidic lysosomes probably cannot process autophagosomes and other lysosomal substrates in the cell.

The early claim that Irgm1 plays an active role in the acidification of the mycobacterial phagosome was based on the observation that phagosomal acidification is impaired in IFNγ-induced *Irgm1* KO cells (MacMicking et al., 2003). This observation can be explained by the fact that Irga6 and other GKS accumulations prevent normal acidification of lysosomes in these cells.

Taken together, in IFNγ-induced *Irgm1* KO cells, GKS proteins that localize to the lysosomes inhibit lysosomal acidity. Non-acidic lysosomes cannot process autophagosomes and cause the arrest in the autophagic flux. How does lysosomal dysfunction and autophagy impairment influence the resistance of *Irgm1* KO mice, remains to be investigated.

4.5. How does lysosome impairment induce leukopenia and death of the in *Irgm1* KO mice?

As previously discussed, *Irgm1* KO mice undergo striking leukopenia and death not only after infection with a variety of pathogens, but also in non-pathogen induced inflammation (chapters 1.6.1. and 1.6.2.). Almost any described cause that leads to IFNγ induction and with it to IRG protein expression is probably fatal for the *Irgm1* KO mouse

(Chapters 1.6.1., 1.6.2.). Hematopoetic stem cells (HSCs), which constitutively express GKS proteins, also show a variety of proliferation and replenishment defects (King et al., 2011) (Ivanova et al., 2002). Hypothetically, in every cell of the *Irgm1* KO mouse which responds to IFNγ stimulation and produces other IRG proteins, the GKS proteins should accumulate at the lysosomes and cause an impaired lysosomal function.

It is not understood how do GKS accumulation at the lysosomes, impairment of lysosomal functionality and autophagic flux arrest lead to leukopenia and death of *Irgm1* KO mice. It is not clear why the particular sets of *Irgm1* KO cells die after these events, while other sets of cells survive and continue to proliferate equally well as WT cells. Up to now, it has been reported that isolated *Irgm1* KO lymphocytes, HSCs and intestinal cells undergo cell death and show proliferation defects upon induction (Feng et al., 2008b) (King et al., 2011) (Liu et al., 2013). However, the proliferation and survival of induced *Irgm1* KO BMDMs (Henry et al., 2009) (chapter 3.4.) and *Igrm1* KO MEFs (chapter 3.4. and unpublished data) are not affected. In accordance to the selective death of the *Irgm1* KO cells, *Irgm1* KO mice are dying from striking leukopenia.

The connection between autophagic flux inhibition and lymphocyte death remains to be better understood. However, it is clear that, after infection and IFNγ induction, lysosomes are stimulated to rapidly activate and proliferate. Since the resources for their expansion have to be rapidly processed, autophagy and lysosomal degradation probably have to be fully functional. Therefore, it can be proposed that fast dividing lymphocytes with impairment in the autophagic flux and lysosomal processing are stressed and especially prone to cell death and delay in proliferation. In addition, it seems that other fast dividing cells, like hematopoetic stem cells (HSC) and induced Paneth cells, also suffer from a variety of morphology, proliferation and cell survival defects in *Irgm1* KO mice (Liu et al., 2013).

Thus, it can be proposed that fast proliferating *Irgm1* KO cells are indeed the cells whose survival is mostly affected by lysosomal malfunction and autophagic flux impairment.

4.6. Why *Irgm3* KO and *Irgm1/Irgm3* KO mice survive infections that are fatal for *Irgm1* KO mice?

Unlike *Irgm1* KO mice, *Irgm3* KO mice can survive and fully recover from infections with *L. monocytogenes*, *M. tuberculosis* and other pathogens. In this study it was shown that Irga6 co-localizes with the ER marker calreticulin in IFNγ-induced *Irgm3* KO MEFs (chapter 3.1.3). The consequences of the accumulation of activated GKS proteins onto the ER remain

to be investigated. When Irga6 was transfected in the NIH 3T3 mouse fibroblasts, in the absence of GMS proteins, it accumulated at the ER in the activated, GTP-bound state and the ER appeared to be enlarged and distorted in electron microscopy pictures (Figure 33.) (Kaiser, 2005) (Hunn et al., 2008). Thus, in IFNγ-induced *Irgm3* KO cells, GKS accumulations probably also cause deformation of the ER structure. However, ER deformation and distortion might not have such severe consequences for proliferating *Irgm3* KO cells, as lysosomal processing impairment does for proliferating *Irgm1* KO cells. Therefore, lysosomal impairment could be the reason why infected *Irgm1* KO mice undergo lymphopenia and death and *Irgm3* KO mice do not.
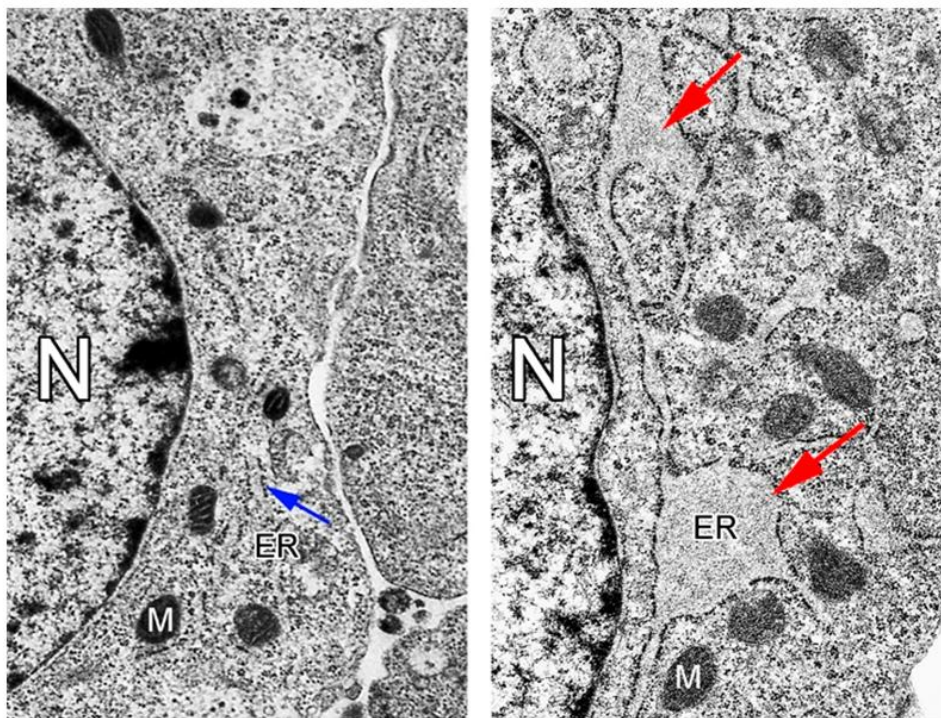
Figure 33. Non-regulated Irga6 induces endoplasmic reticulum deformation. Electron microscopy images of the endoplasmic reticulum in NIH 3T3 mouse fibroblasts that are not Irga6 transfected (left panel, blue arrow shows ER) or transfected with Irga6 (right panel, red arrow shows swollen ER). (Modified from (Kaiser, 2005)).

The causes of the surprising phenotype of *Irgm1/Irgm3* KO mouse are also not fully understood. After infection with pathogens that are directly targeted by the GKS proteins, like *T. gondii*, the *Irgm1/Irgm3* KO mice die (Chapter 1.6.1.). However, when *Irgm1/Irgm3* KO mice are infected with the pathogens which are not directly targeted by GKS proteins, like, for example, *Salmonella typhimurium*, these mice can fully recover (Henry et al., 2009).

Considering that *Irgm1* KO mice succumb to infection with a number of pathogens, which do not kill *Irgm3* KO and *Irgm1/Irgm3* KO mice, it was first hypothesised that Irgm3 is toxic for the cell and that it is negatively regulated by Irgm1. Thus, when Irgm3 is present in the cell without Irgm1, it can perform its toxic actions. When Irgm3, or both Irgm1 and Irgm3,

are absent, the mice do not encounter Irgm3-caused problems (Henry et al., 2009). The discovery that GMS proteins rather inhibit GKS protein activation and not each other, indicates that this hypothesis probably is not correct (Hunn et al., 2008).

It has been proposed that activated GKS aggregate-like structures, as many other aggregates, are toxic for the cell and perform their toxic actions in the cell in dose dependent manner (Hunn and Howard, 2010). Namely, a Western Blot analysis of IFNγ-induced induced *Irgm1* KO, *Irgm3* KO and *Irgm1/Irgm3* KO macrophages had revealed that these cells contain overall lower levels of Irgb6, and somewhat lower level of Irga6. *Igrm1* KO and *Irgm3* KO macrophages expressed less of Irgb6 than the wild type cells, but *Irgm1/Irgm3* KO cells had even lower levels than the single knock-outs (Henry et al., 2009). Hence, it has been proposed that, due to lower level of GKS aggregates, *Irgm1/Irgm3* KO cells can survive the infection, IFNγ-induction and uncontrolled GKS expression (Hunn and Howard, 2010). .

The report that different GMS KO cells contain different levels of GKS proteins has to be reproduced and analyzed into more details. The preliminary results in this study showed that Irgb6 levels are indeed reduced in all GMS KO MEFs, but the levels of Irga6, one of the leading GKS proteins in lysosomal accumulation, are not changed (Figure S5). The levels of Irgb10 and Irgd were also never investigated in GMS KO cells. Even if the levels of all GKS proteins are reduced in *Irgm1/Irgm3* double KO cells in comparison to *Irgm1* KO and *Irgm3* KO cells, this fact does not offer an explanation why *Irgm1* KO mice and *Irgm3* KO mice, that have very similar levels of GKS proteins after induction, show two opposing phenotypes.

As in *Irgm3* KO mice, the different localization of GKS accumulations might be the reason for essentially normal phenotype of *Irgm1/Irgm3* KO mice. In *Irgm1/Irgm3* KO MEFs, GKS proteins do not localize to the lysosomes, but rather to lipid droplets. Thus the levels of LC3-II in *Irgm1/Irgm3* KO cells are not increased and the autophagic flux is normal. This suggests that the full recovery of the *Irgm1/Irgm3* KO mice after infection could very well be related to the fact that lysosomes in these cells are not GKS coated and hence fully functional.

As previously discussed, in IFNγ-induced *Irgm1/Irgm3* KO cells, GKS proteins Irga6, Irgb6 and Irgb10 accumulate at lipid droplets instead at lysosomes (Haldar et al., 2013) (chapter 3.1.5.). The events that follow GKS accumulation to the LDs are not fully understood. It has been reported that GKS-covered LDs are common targets of the autophagy protein p62 and that the overall mass of the lipid droplets is reduced in IFNγ-induced *Irgm1/Irgm3* KO cells. Therefore, it has been hypothesised that these LDs are targeted for autophagic degradation (Haldar et al., 2013). Even though the outcome of GKS

action at the LDs is not clear, the consequences of this accumulation are probably not as severe as the lysosomal failure and autophagic flux arrest.

Taken together, *Irgm3* KO mice and *Irgm1/Irgm3* KO mice probably can survive the infections that kill *Irgm1* KO mice, due to the fact that the lysosomes in their cells are not coated with GKS proteins. Therefore, autophagic flux and lysosomal function are presumably not impaired, and fast dividing cells probably can proliferate without major difficulties.

4.7. Are GKS protein structures conventional aggregates?

When GKS proteins are expressed in the absence of GMS proteins, distinct GKS accumulations can be observed at the subcellular level. In the first description, these GKS accumulations were named aggregates (Martens et al., 2004). These accumulations were reported not to load to the PVM of *T. gondii* and thus aggregated GKS proteins cannot perform their function (Martens et al., 2004). Hence, the first hypothesis was that Irga6 structures are simply clusters of missfolded aggregated non-functional IRG proteins, which are, like most aggregates, toxic for the cell (Martens et al., 2004).

However, a couple of years after those first observations, it was reported that aggregation of GKS proteins is inhibited by GMS proteins and that expression of three GMS proteins in the cell is sufficient to prevent GKS accumulation (Hunn et al., 2008). Staining with the Irga6 10D7 antibody, which exclusively binds to the activated form of Irga6, had shown that these aggregates are GTP-bound (Papic et al., 2008). It was shown that Irga6 aggregate-like structures are formed only transiently and that they can be isolated from the cell only when locked in the GTP-bound conformation (Papic et al., 2008).

The first experiments in this study had revealed that GKS aggregate-like structures have different shape and localize to the different endocellular membranes in the absence of different GMS proteins (chapter 3.1.). The GKS accumulations look like the GKS protein rings that form at the PVM of *T. gondii* (chapter 3.1.). In this study, it was shown that GKS aggregate-like structures are detergent soluble and cannot be captured and isolated with Filter trap assay or with Ultracentrifugation assay (chapter 3.5.). Once the membrane is dissolved with the detergent, these aggregate-like oligomers are fully dispersed. However, when GKS proteins were treated with GTP and AlFx, the insoluble complexes could be captured by ultracentrifugation (chapter 3.5.).

Taken together, it was proposed that previously called GKS aggregates actually represent activated oligomerized GTP-bound proteins that are very similar to the GKS oligomers at the PVM of *T. gondii.*

The GBP proteins were also shown to form the aggregates in the absence of GMS proteins in IFNγ-induced mouse cells (Traver et al., 2011). Therefore, there is a possibility that GMS proteins also regulate activation of the GBPs. Whether GBP aggregation is regulated in the same manner as the GKS protein aggregation remains to be investigated. Recently, it has been published that GBP proteins indeed accumulate at the same lipid droplets together with the GKS proteins in IFNγ-induced *Irgm1/Irgm3* KO cells (Haldar et al., 2013). It would be interesting to test whether mouse GBP proteins also co-localize with the lysosomes in the *Irgm1* KO cells and contribute to the failure of lysosomal functionality.

If GBP protein aggregation is regulated by the GMS proteins in mice, it is not clear which proteins would substitute GMS-regulatory role in humans. Even though it is tempting to propose that the only remaining GMS homologue in humans, IRGM protein, could be responsible for GBP protein regulation, this proposal should be taken with reserve. There are indications that non-IFN-inducible truncated human IRGM protein with non-functional G-domain might play very different role than the mouse Irgm1 (Bekpen et al., 2005).

It has also been reported that GKS proteins form the aggregates in the absence of autophagy proteins Atg5 and Atg3 (Khaminets et al., 2010) (Traver et al., 2011) (Haldar et al., 2014). These aggregates are also GTP-bound and unable to accumulate at the PVM of *T. gondii* or at the inclusions of *C. trachomatis* (Khaminets et al., 2010) (Haldar et al., 2014). GBP aggregates are also formed in *Atg5* KO and *Atg3* KO mouse cells (Traver et al., 2011) (Haldar et al., 2014). In IFNγ-induced *Atg7* KO and *Atg16L* KO cells, Irgb6 and GBP proteins were not able to load to the *T. gondii* PVM probably also due to aggregate formation (Ohshima et al., 2014). However, *Atg9a* KO and *Atg14* KO cells did not encounter this problem (Ohshima et al., 2014). Interestingly, Atg3, Atg5, Atg7 and Atg16 all play a role in the LC3-I to LC3-II turnover, while Atg9a and Atg14 are involved in the earlier stage of autophagy, the vesicle elongation, giving a hint that the late stages of autophagosome formation may be important for IRG control.

The formation of GKS protein aggregates in Atg-deficient cells could indicate that GKS proteins are degraded by the autophagic pathway. It has been proposed that the failure of autophagy is blocking proper GKS protein degradation, and hence, these proteins accumulate in aggregate-like structures (Traver et al., 2011) (Haldar et al., 2014). Another hypothesis had proposed is that GMS proteins are regulated by the autophagic pathway, and

the failure in the GMS regulation leads to aggregate formation in Atg deficient cells (Khaminets et al., 2010).

The preliminary results of live cell imaging microscopy revealed that, in EGFP-Irga6-transfected non-induced WT MEFs, the number, the size and the shape of particular Irga6 aggregate-like structures did not greatly change over a 12 hour analysis. New aggregate structures were also not formed during this period (data not shown). Thus, even if Irga6 aggregate formation and degradation are dynamic processes, it is highly unlikely that whole accumulations of the aggregates are captured in autophagosomes and degraded.

4.8. Why is *Irgm1* the most conserved *IRG* gene?

IRG genes are extremely polymorphic and their presence largely varies among the species (Bekpen et al., 2005) (Hunn et al., 2008) (Lilue et al., 2013). The copy number and the sequence of the particular *IRG* genes can also greatly vary within different wild mouse strains (Lilue et al., 2013).

The polymorphisms in GKS genes in mice are proposed to be related to the efficiency of the immune responses to virulent and avirulent strains of *T. gondii* and probably to other pathogens (Lilue et al., 2013). GKS proteins are directly involved in the response to certain intracellular pathogens, and are probably directly challenged to co-evolve together with the pathogen itself and combat pathogen virulence factors. In accordance to that, a recent study had shown that certain wild mice have a particular set of GKS proteins that makes them greatly resistant to otherwise very virulent strains of *T. gondii* (Lilue et al., 2013).

The sequences of all GMS genes that were analyzed in the variety of wild and laboratory mouse strains are relatively conserved in comparison to those of the GKS genes. *Irgm1* represents the most conserved *IRG* gene in mice and its sequence does not differ between wild mouse strains which, except for Irga6, otherwise have very polymorphic *GKS* gene sequences (Lilue et al., 2013). Thus, it could be that GMS proteins are not directly involved in interaction with the pathogen and hence not directly challenged to co-evolve with it.

The conserved sequence and conformation of mouse GMS proteins is probably crucial for GMS interaction with GKS proteins, GKS inactivation and GMS localization to the particular intracellular membranes. Polymorphisms in *Irgm1* sequence could, in some cases, result in the Irgm1 protein that cannot inhibit GKS protein activation, or Irgm1 which cannot properly bind to lysosomal membranes. In both cases, Irgm1 polymorphisms would cause

GKS protein off-target activation and its accumulation at the lysosomes. As previously explained, GKS proteins at the lysosomes would lead to lysosomal dysfunction, autophagic flux arrest, leukopenia and death of the mouse. Hence, the risks brought with Irgm1 malfunction might cause that Irgm1 stays the most conserved IRG protein in mice.

Even though *IRG* gene presence greatly varies between the species, *IRGM* gene remained present in many animals that have lost other IRGs (Hunn, 2008) (Bekpen et al., 2005). Almost every species, in which the homologues of GKS proteins are reported, also has a homologue of *IRGM*. *IRGM* is also present in species which do not have representatives of "real" GKS gene homologues but only non-inducible *IRGC* and quasi-IRG protein *IRGQ*, like for example in humans (Hunn, 2008) (Bekpen et al., 2005). Therefore, it could be speculated that the role of Irgm1 homologues in the other species is also to keep remaining GKS proteins inactive.

However, the function of IRGM homologues in other organisms but mice is not clarified up to date. Whether they also prevent the activation of GKS homologues remains to be investigated. Human IRGM is extremely truncated, its G-domain is not functional and it is only 51 percent homologous to the mouse Irgm1 (chapter 1.4.1.). IRGM is not IFNγ-inducible, but constitutively expressed. Instead of 2 alternative splicing isoforms present in mouse, 5 different 3' isoforms can be formed in human. Therefore, human IRGM is unlikely to play a role in IRG or GBP protein regulation.

As previously discussed (chapter 1.4.1.), it has been proposed that *IRGM* gene was disrupted due to the shift open reading frame (ORF) about 40 million years ago. Thus, the species like old and new world monkeys do not have *IRGM*. However, according to this proposal, the new change in ORF had caused the "resurrection" of the truncated *IRGM* about 20 million years ago (Bekpen et al., 2009). Whether the function of IRGM remained the same before and after "resurrection" remains to be investigated. Recently, whole genome association studies had shown that specific *IRGM* haplotypes associate with increased risk of Crohn's disease in humans (Fisher et al., 2008) (Parkes et al., 2007). However, it has been also demonstrated that 20,1 kb deletion upstream of IRGM also associates with Crohn's disease and hence, these results need to be further researched (Bekpen et al., 2009).

5. REFFERENCES

AL-ZEER, M. A., AL-YOUNES, H. M., BRAUN, P. R., ZERRAHN, J. & MEYER, T. F. 2009. IFN-gamma-inducible Irga6 mediates host resistance against Chlamydia trachomatis via autophagy. *PLoS One,* 4, e4588.

ANTONY, V. B., OWEN, C. L. & HADLEY, K. J. 1989. Pleural mesothelial cells stimulated by asbestos release chemotactic activity for neutrophils in vitro. *Am Rev Respir Dis,* 139, 199-206.

BAFICA, A., FENG, C. G., SANTIAGO, H. C., ALIBERTI, J., CHEEVER, A., THOMAS, K. E., TAYLOR, G. A., VOGEL, S. N. & SHER, A. 2007. The IFN-inducible GTPase LRG47 (Irgm1) negatively regulates TLR4-triggered proinflammatory cytokine production and prevents endotoxemia. *J Immunol,* 179, 5514-22.

BALCH, W. E., MORIMOTO, R. I., DILLIN, A. & KELLY, J. W. 2008. Adapting proteostasis for disease intervention. *Science,* 319, 916-9.

BARRETT, A. J. & KIRSCHKE, H. 1981. Cathepsin B, Cathepsin H, and cathepsin L. *Methods Enzymol,* 80 Pt C, 535-61.

BEKPEN, C., HUNN, J. P., ROHDE, C., PARVANOVA, I., GUETHLEIN, L., DUNN, D. M., GLOWALLA, E., LEPTIN, M. & HOWARD, J. C. 2005. The interferon-inducible p47 (IRG) GTPases in vertebrates: loss of the cell autonomous resistance mechanism in the human lineage. *Genome Biol,* 6, R92.

BEKPEN, C., MARQUES-BONET, T., ALKAN, C., ANTONACCI, F., LEOGRANDE, M. B., VENTURA, M., KIDD, J. M., SISWARA, P., HOWARD, J. C. & EICHLER, E. E. 2009. Death and resurrection of the human IRGM gene. *PLoS Genet,* 5, e1000403.

BLACK, M. W. & BOOTHROYD, J. C. 2000. Lytic cycle of Toxoplasma gondii. *Microbiol Mol Biol Rev,* 64, 607-23.

BOEHM, U., GUETHLEIN, L., KLAMP, T., OZBEK, K., SCHAUB, A., FUTTERER, A., PFEFFER, K. & HOWARD, J. C. 1998. Two families of GTPases dominate the complex cellular response to IFN-gamma. *J Immunol,* 161, 6715-23.

BOEHM, U., KLAMP, T., GROOT, M. & HOWARD, J. C. 1997. Cellular responses to interferon-gamma. *Annu Rev Immunol,* 15, 749-95.

BOHNE, W., BOTTCHER, K. & GROSS, U. 2011. The parasitophorous vacuole of Encephalitozoon cuniculi: biogenesis and characteristics of the host cell-pathogen interface. *Int J Med Microbiol,* 301, 395-9.

BOOTHROYD, J. C. & GRIGG, M. E. 2002. Population biology of Toxoplasma gondii and its relevance to human infection: do different strains cause different disease? *Curr Opin Microbiol,* 5, 438-42.

BORDEN, E. C., SEN, G. C., UZE, G., SILVERMAN, R. H., RANSOHOFF, R. M., FOSTER, G. R. & STARK, G. R. 2007. Interferons at age 50: past, current and future impact on biomedicine. *Nat Rev Drug Discov,* 6, 975-90.

BOUGNERES, L., HELFT, J., TIWARI, S., VARGAS, P., CHANG, B. H., CHAN, L., CAMPISI, L., LAUVAU, G., HUGUES, S., KUMAR, P., KAMPHORST, A. O., DUMENIL, A. M., NUSSENZWEIG, M., MACMICKING, J.

D., AMIGORENA, S. & GUERMONPREZ, P. 2009. A role for lipid bodies in the cross-presentation of phagocytosed antigens by MHC class I in dendritic cells. *Immunity,* 31, 232-44.

BOYA, P. & KROEMER, G. 2008. Lysosomal membrane permeabilization in cell death. *Oncogene,* 27, 6434-51.

BRASS, A. L., HUANG, I. C., BENITA, Y., JOHN, S. P., KRISHNAN, M. N., FEELEY, E. M., RYAN, B. J., WEYER, J. L., VAN DER WEYDEN, L., FIKRIG, E., ADAMS, D. J., XAVIER, R. J., FARZAN, M. & ELLEDGE, S. J. 2009. The IFITM proteins mediate cellular resistance to influenza A H1N1 virus, West Nile virus, and dengue virus. *Cell,* 139, 1243-54.

BUTCHER, B. A., GREENE, R. I., HENRY, S. C., ANNECHARICO, K. L., WEINBERG, J. B., DENKERS, E. Y., SHER, A. & TAYLOR, G. A. 2005. p47 GTPases regulate Toxoplasma gondii survival in activated macrophages. *Infect Immun,* 73, 3278-86.

CARLOW, D. A., TEH, S. J. & TEH, H. S. 1998. Specific antiviral activity demonstrated by TGTP, a member of a new family of interferon-induced GTPases. *J Immunol,* 161, 2348-55.

CHANG, C. P., YANG, M. C. & LEI, H. Y. 2011. Concanavalin A/IFN-gamma triggers autophagy-related necrotic hepatocyte death through IRGM1-mediated lysosomal membrane disruption. *PLoS One,* 6, e28323.

CHENG, Y. S., COLONNO, R. J. & YIN, F. H. 1983. Interferon induction of fibroblast proteins with guanylate binding activity. *J Biol Chem,* 258, 7746-50.

CHENG, Y. S., PATTERSON, C. E. & STAEHELI, P. 1991. Interferon-induced guanylate-binding proteins lack an N(T)KXD consensus motif and bind GMP in addition to GDP and GTP. *Mol Cell Biol,* 11, 4717-25.

CHOUDHRY, N., KORBEL, D. S., ZAALOUK, T. K., BLANSHARD, C., BAJAJ-ELLIOTT, M. & MCDONALD, V. 2009. Interferon-gamma-mediated activation of enterocytes in immunological control of Encephalitozoon intestinalis infection. *Parasite Immunol,* 31, 2-9.

COERS, J. 2013. Self and non-self discrimination of intracellular membranes by the innate immune system. *PLoS Pathog,* 9, e1003538.

COERS, J., BERNSTEIN-HANLEY, I., GROTSKY, D., PARVANOVA, I., HOWARD, J. C., TAYLOR, G. A., DIETRICH, W. F. & STARNBACH, M. N. 2008. Chlamydia muridarum evades growth restriction by the IFN-gamma-inducible host resistance factor Irgb10. *J Immunol,* 180, 6237-45.

COERS, J., GONDEK, D. C., OLIVE, A. J., ROHLFING, A., TAYLOR, G. A. & STARNBACH, M. N. 2011. Compensatory T cell responses in IRG-deficient mice prevent sustained Chlamydia trachomatis infections. *PLoS Pathog,* 7, e1001346.

COLLAZO, C. M., YAP, G. S., SEMPOWSKI, G. D., LUSBY, K. C., TESSAROLLO, L., VANDE WOUDE, G. F., SHER, A. & TAYLOR, G. A. 2001. Inactivation of LRG-47 and IRG-47 reveals a family of interferon gamma-inducible genes with essential, pathogen-specific roles in resistance to infection. *J Exp Med,* 194, 181-8.

COTTER, T. W. & BYRNE, G. I. 1996. Immunity to Chlamydia: comparison of human infections and murine models. *Res Immunol,* 147, 587-95.

DA FONSECA FERREIRA-DA-SILVA, M., SPRINGER-FRAUENHOFF, H. M., BOHNE, W. & HOWARD, J. C. 2014. Identification of the Microsporidian Encephalitozoon cuniculi as a New Target of the IFNgamma-Inducible IRG Resistance System. *PLoS Pathog,* 10, e1004449.

DE DUVE, C. 1963. The lysosome. *Sci Am,* 208, 64-72.

DE SOUZA, A. P., TANG, B., TANOWITZ, H. B., FACTOR, S. M., SHTUTIN, V., SHIRANI, J., TAYLOR, G. A., WEISS, L. M. & JELICKS, L. A. 2003. Absence of interferon-gamma-inducible gene IGTP does not significantly alter the development of chagasic cardiomyopathy in mice infected with Trypanosoma cruzi (Brazil strain). *J Parasitol,* 89, 1237-9.

DEAN, R. T. 1979. Lysosomes and protein degradation. *Ciba Found Symp*, 139-49.

DEGRANDI, D., KONERMANN, C., BEUTER-GUNIA, C., KRESSE, A., WURTHNER, J., KURIG, S., BEER, S. & PFEFFER, K. 2007. Extensive characterization of IFN-induced GTPases mGBP1 to mGBP10 involved in host defense. *J Immunol,* 179, 7729-40.

DEGRANDI, D., KRAVETS, E., KONERMANN, C., BEUTER-GUNIA, C., KLUMPERS, V., LAHME, S., WISCHMANN, E., MAUSBERG, A. K., BEER-HAMMER, S. & PFEFFER, K. 2013. Murine guanylate binding protein 2 (mGBP2) controls Toxoplasma gondii replication. *Proc Natl Acad Sci U S A,* 110, 294-9.

DERETIC, V. 2011. Autophagy in immunity and cell-autonomous defense against intracellular microbes. *Immunol Rev,* 240, 92-104.

DI PAOLO, C., HEFTI, H. P., MELI, M., LANDIS, H. & PAVLOVIC, J. 1999. Intramolecular backfolding of the carboxyl-terminal end of MxA protein is a prerequisite for its oligomerization. *J Biol Chem,* 274, 32071-8.

DIDIER, E. S. 2005. Microsporidiosis: an emerging and opportunistic infection in humans and animals. *Acta Trop,* 94, 61-76.

DUBEY, J. P. 1995. Duration of immunity to shedding of Toxoplasma gondii oocysts by cats. *J Parasitol,* 81, 410-5.

DUBEY, J. P. & FRENKEL, J. K. 1972. Cyst-induced toxoplasmosis in cats. *J Protozool,* 19, 155-77.

DUBEY, J. P., SPEER, C. A., SHEN, S. K., KWOK, O. C. & BLIXT, J. A. 1997. Oocyst-induced murine toxoplasmosis: life cycle, pathogenicity, and stage conversion in mice fed Toxoplasma gondii oocysts. *J Parasitol,* 83, 870-82.

EVANS, D. T., SERRA-MORENO, R., SINGH, R. K. & GUATELLI, J. C. 2010. BST-2/tetherin: a new component of the innate immune response to enveloped viruses. *Trends Microbiol,* 18, 388-96.

FELLENBERG, F., HARTMANN, T. B., DUMMER, R., USENER, D., SCHADENDORF, D. & EICHMULLER, S. 2004. GBP-5 splicing variants: New guanylate-binding proteins with tumor-associated expression and antigenicity. *J Invest Dermatol,* 122, 1510-7.

FENG, C. G., COLLAZO-CUSTODIO, C. M., ECKHAUS, M., HIENY, S., BELKAID, Y., ELKINS, K., JANKOVIC, D., TAYLOR, G. A. & SHER, A. 2004. Mice deficient in LRG-47 display increased susceptibility to mycobacterial infection associated with the induction of lymphopenia. *J Immunol,* 172, 1163-8.

FENG, C. G., WEKSBERG, D. C., TAYLOR, G. A., SHER, A. & GOODELL, M. A. 2008a. The p47 GTPase Lrg-47 (Irgm1) links host defense and hematopoietic stem cell proliferation. *Cell Stem Cell,* 2, 83-9.

FENG, C. G., ZHENG, L., JANKOVIC, D., BAFICA, A., CANNONS, J. L., WATFORD, W. T., CHAUSSABEL, D., HIENY, S., CASPAR, P., SCHWARTZBERG, P. L., LENARDO, M. J. & SHER, A. 2008b. The immunity-related GTPase Irgm1 promotes the expansion of activated CD4+ T cell populations by preventing interferon-gamma-induced cell death. *Nat Immunol,* 9, 1279-87.

FENG, C. G., ZHENG, L., LENARDO, M. J. & SHER, A. 2009. Interferon-inducible immunity-related GTPase Irgm1 regulates IFN gamma-dependent host defense, lymphocyte survival and autophagy. *Autophagy,* 5, 232-4.

FENG, Y., HE, D., YAO, Z. & KLIONSKY, D. J. 2014. The machinery of macroautophagy. *Cell Res,* 24, 24-41.

FISCHER, J., TRAN, D., JUNEAU, R. & HALE-DONZE, H. 2008. Kinetics of Encephalitozoon spp. infection of human macrophages. *J Parasitol,* 94, 169-75.

FISHER, S. A., TREMELLING, M., ANDERSON, C. A., GWILLIAM, R., BUMPSTEAD, S., PRESCOTT, N. J., NIMMO, E. R., MASSEY, D., BERZUINI, C., JOHNSON, C., BARRETT, J. C., CUMMINGS, F. R., DRUMMOND, H., LEES, C. W., ONNIE, C. M., HANSON, C. E., BLASZCZYK, K., INOUYE, M., EWELS, P., RAVINDRARAJAH, R., KENIRY, A., HUNT, S., CARTER, M., WATKINS, N., OUWEHAND, W., LEWIS, C. M., CARDON, L., LOBO, A., FORBES, A., SANDERSON, J., JEWELL, D. P., MANSFIELD, J. C., DELOUKAS, P., MATHEW, C. G., PARKES, M. & SATSANGI, J. 2008. Genetic determinants of ulcerative colitis include the ECM1 locus and five loci implicated in Crohn's disease. *Nat Genet,* 40, 710-2.

GAO, S., VON DER MALSBURG, A., DICK, A., FAELBER, K., SCHRODER, G. F., HALLER, O., KOCHS, G. & DAUMKE, O. 2011. Structure of myxovirus resistance protein a reveals intra- and intermolecular domain interactions required for the antiviral function. *Immunity,* 35, 514-25.

GAO, S., VON DER MALSBURG, A., PAESCHKE, S., BEHLKE, J., HALLER, O., KOCHS, G. & DAUMKE, O. 2010. Structural basis of oligomerization in the stalk region of dynamin-like MxA. *Nature,* 465, 502-6.

GAZZINELLI, R. T., MENDONCA-NETO, R., LILUE, J., HOWARD, J. & SHER, A. 2014. Innate resistance against Toxoplasma gondii: an evolutionary tale of mice, cats, and men. *Cell Host Microbe,* 15, 132-8.

GHOSH, A., UTHAIAH, R., HOWARD, J., HERRMANN, C. & WOLF, E. 2004. Crystal structure of IIGP1: a paradigm for interferon-inducible p47 resistance GTPases. *Mol Cell,* 15, 727-39.

GILLY, M., DAMORE, M. A. & WALL, R. 1996. A promoter ISRE and dual 5' YY1 motifs control IFN-gamma induction of the IRG-47 G-protein gene. *Gene,* 179, 237-44.

GUTIERREZ, M. G., MASTER, S. S., SINGH, S. B., TAYLOR, G. A., COLOMBO, M. I. & DERETIC, V. 2004. Autophagy is a defense mechanism inhibiting BCG and Mycobacterium tuberculosis survival in infected macrophages. *Cell,* 119, 753-66.

HACKSTADT, T., SCIDMORE, M. A. & ROCKEY, D. D. 1995. Lipid metabolism in Chlamydia trachomatis-infected cells: directed trafficking of Golgi-derived sphingolipids to the chlamydial inclusion. *Proc Natl Acad Sci U S A,* 92, 4877-81.

HALDAR, A. K., PIRO, A. S., PILLA, D. M., YAMAMOTO, M. & COERS, J. 2014. The E2-like conjugation enzyme Atg3 promotes binding of IRG and Gbp proteins to Chlamydia- and Toxoplasma-containing vacuoles and host resistance. *PLoS One,* 9, e86684.

HALDAR, A. K., SAKA, H. A., PIRO, A. S., DUNN, J. D., HENRY, S. C., TAYLOR, G. A., FRICKEL, E. M., VALDIVIA, R. H. & COERS, J. 2013. IRG and GBP host resistance factors target aberrant, "non-self" vacuoles characterized by the missing of "self" IRGM proteins. *PLoS Pathog,* 9, e1003414.

HALLER, O. & KOCHS, G. 2002. Interferon-induced mx proteins: dynamin-like GTPases with antiviral activity. *Traffic,* 3, 710-7.

HALLER, O. & KOCHS, G. 2011. Human MxA protein: an interferon-induced dynamin-like GTPase with broad antiviral activity. *J Interferon Cytokine Res,* 31, 79-87.

HALLER, O., STAEHELI, P. & KOCHS, G. 2007. Interferon-induced Mx proteins in antiviral host defense. *Biochimie,* 89, 812-8.

HALONEN, S. K., TAYLOR, G. A. & WEISS, L. M. 2001. Gamma interferon-induced inhibition of Toxoplasma gondii in astrocytes is mediated by IGTP. *Infect Immun,* 69, 5573-6.

HE, S., WANG, C., DONG, H., XIA, F., ZHOU, H., JIANG, X., PEI, C., REN, H., LI, H., LI, R. & XU, H. 2012. Immune-related GTPase M (IRGM1) regulates neuronal autophagy in a mouse model of stroke. *Autophagy,* 8, 1621-7.

HENRY, S. C., DANIELL, X., INDARAM, M., WHITESIDES, J. F., SEMPOWSKI, G. D., HOWELL, D., OLIVER, T. & TAYLOR, G. A. 2007. Impaired macrophage function underscores susceptibility to Salmonella in mice lacking Irgm1 (LRG-47). *J Immunol,* 179, 6963-72.

HENRY, S. C., DANIELL, X. G., BURROUGHS, A. R., INDARAM, M., HOWELL, D. N., COERS, J., STARNBACH, M. N., HUNN, J. P., HOWARD, J. C., FENG, C. G., SHER, A. & TAYLOR, G. A. 2009. Balance of Irgm protein activities determines IFN-gamma-induced host defense. *J Leukoc Biol,* 85, 877-85.

HERTZOG, P., FORSTER, S. & SAMARAJIWA, S. 2011. Systems biology of interferon responses. *J Interferon Cytokine Res,* 31, 5-11.

HINSON, E. R. & CRESSWELL, P. 2009. The antiviral protein, viperin, localizes to lipid droplets via its N-terminal amphipathic alpha-helix. *Proc Natl Acad Sci U S A,* 106, 20452-7.

HOWARD, J. C. 2007. Introduction: cell-autonomous immunity. *Microbes Infect,* 9, 1633-5.

HOWARD, J. C., HUNN, J. P. & STEINFELDT, T. 2011. The IRG protein-based resistance mechanism in mice and its relation to virulence in Toxoplasma gondii. *Curr Opin Microbiol,* 14, 414-21.

HOWE, D. K. & SIBLEY, L. D. 1995. Toxoplasma gondii comprises three clonal lineages: correlation of parasite genotype with human disease. *J Infect Dis,* 172, 1561-6.

HUANG, T., PAVLOVIC, J., STAEHELI, P. & KRYSTAL, M. 1992. Overexpression of the influenza virus polymerase can titrate out inhibition by the murine Mx1 protein. *J Virol,* 66, 4154-60.

HUNN, J. P. 2008. Evolution and Cellular Resistance Mechanisms of the Immunity-Related GTPases. *PhD Thesis. Institute for Genetics, University of Cologne, Cologne, Germany*.

HUNN, J. P. & HOWARD, J. C. 2010. The mouse resistance protein Irgm1 (LRG-47): a regulator or an effector of pathogen defense? *PLoS Pathog,* 6, e1001008.

HUNN, J. P., KOENEN-WAISMAN, S., PAPIC, N., SCHROEDER, N., PAWLOWSKI, N., LANGE, R., KAISER, F., ZERRAHN, J., MARTENS, S. & HOWARD, J. C. 2008. Regulatory interactions between IRG resistance GTPases in the cellular response to Toxoplasma gondii. *Embo J,* 27, 2495-509.

HUTCHISON, W. M. 1965. Experimental transmission of Toxoplasma gondii. *Nature,* 206, 961-2.

HUTT, D. M., POWERS, E. T. & BALCH, W. E. 2009. The proteostasis boundary in misfolding diseases of membrane traffic. *FEBS Lett,* 583, 2639-46.

HYBISKE, K. & STEPHENS, R. S. 2007. Mechanisms of Chlamydia trachomatis entry into nonphagocytic cells. *Infect Immun,* 75, 3925-34.

IVANOVA, N. B., DIMOS, J. T., SCHANIEL, C., HACKNEY, J. A., MOORE, K. A. & LEMISCHKA, I. R. 2002. A stem cell molecular signature. *Science,* 298, 601-4.

JABADO, N., JANKOWSKI, A., DOUGAPARSAD, S., PICARD, V., GRINSTEIN, S. & GROS, P. 2000. Natural resistance to intracellular infections: natural resistance-associated macrophage protein 1 (Nramp1) functions as a pH-dependent manganese transporter at the phagosomal membrane. *J Exp Med,* 192, 1237-48.

KAISER, F. 2005. *Molekulare Charakterisierung und funktionelle Analyse der Interferon-induzierten 47 kDa GTPase IIGP.* Diploma, Teshnische Universität Berlin.

KARRE, K., LJUNGGREN, H. G., PIONTEK, G. & KIESSLING, R. 1986. Selective rejection of H-2-deficient lymphoma variants suggests alternative immune defence strategy. *Nature,* 319, 675-8.

KAWAI, T. & AKIRA, S. 2010. The role of pattern-recognition receptors in innate immunity: update on Toll-like receptors. *Nat Immunol,* 11, 373-84.

KETTERN, N., ROGON, C., LIMMER, A., SCHILD, H. & HOHFELD, J. 2011. The Hsc/Hsp70 co-chaperone network controls antigen aggregation and presentation during maturation of professional antigen presenting cells. *PLoS One,* 6, e16398.

KHAMINETS, A., HUNN, J. P., KONEN-WAISMAN, S., ZHAO, Y. O., PREUKSCHAT, D., COERS, J., BOYLE, J. P., ONG, Y. C., BOOTHROYD, J. C., REICHMANN, G. & HOWARD, J. C. 2010. Coordinated loading of IRG resistance GTPases on to the Toxoplasma gondii parasitophorous vacuole. *Cell Microbiol,* 12, 939-61.

KHAN, I. A. & MORETTO, M. 1999. Role of gamma interferon in cellular immune response against murine Encephalitozoon cuniculi infection. *Infect Immun,* 67, 1887-93.

KIM, B. H., SHENOY, A. R., KUMAR, P., DAS, R., TIWARI, S. & MACMICKING, J. D. 2011. A family of IFN-gamma-inducible 65-kD GTPases protects against bacterial infection. *Science,* 332, 717-21.

KING, K. Y., BALDRIDGE, M. T., WEKSBERG, D. C., CHAMBERS, S. M., LUKOV, G. L., WU, S., BOLES, N. C., JUNG, S. Y., QIN, J., LIU, D., SONGYANG, Z., EISSA, N. T., TAYLOR, G. A. & GOODELL, M. A. 2011. Irgm1 protects hematopoietic stem cells by negative regulation of IFN signaling. *Blood,* 118, 1525-33.

KLAMP, T., BOEHM, U., SCHENK, D., PFEFFER, K. & HOWARD, J. C. 2003. A giant GTPase, very large inducible GTPase-1, is inducible by IFNs. *J Immunol,* 171, 1255-65.

KLIONSKY, D. J., ABDALLA, F. C., ABELIOVICH, H., ABRAHAM, R. T., ACEVEDO-AROZENA, A., ADELI, K., AGHOLME, L., AGNELLO, M., AGOSTINIS, P., AGUIRRE-GHISO, J. A., AHN, H. J., AIT-MOHAMED, O., AIT-SI-ALI, S., AKEMATSU, T., AKIRA, S., AL-YOUNES, H. M., AL-ZEER, M. A., ALBERT, M. L., ALBIN, R. L., ALEGRE-ABARRATEGUI, J., ALEO, M. F., ALIREZAEI, M., ALMASAN, A., ALMONTE-BECERRIL, M., AMANO, A., AMARAVADI, R., AMARNATH, S., AMER, A. O., ANDRIEU-ABADIE, N., ANANTHARAM, V., ANN, D. K., ANOOPKUMAR-DUKIE, S., AOKI, H., APOSTOLOVA, N., ARANCIA, G., ARIS, J. P., ASANUMA, K., ASARE, N. Y., ASHIDA, H., ASKANAS, V., ASKEW, D. S., AUBERGER, P., BABA, M., BACKUES, S. K., BAEHRECKE, E. H., BAHR, B. A., BAI, X. Y., BAILLY, Y., BAIOCCHI, R., BALDINI, G., BALDUINI, W., BALLABIO, A., BAMBER, B. A., BAMPTON, E. T., BANHEGYI, G., BARTHOLOMEW, C. R., BASSHAM, D. C., BAST, R. C., JR., BATOKO, H., BAY, B. H., BEAU, I., BECHET, D. M., BEGLEY, T. J., BEHL, C., BEHRENDS, C., BEKRI, S., BELLAIRE, B., BENDALL, L. J., BENETTI, L., BERLIOCCHI, L., BERNARDI, H., BERNASSOLA, F., BESTEIRO, S., BHATIA-KISSOVA, I., BI, X., BIARD-PIECHACZYK, M., BLUM, J. S., BOISE, L. H., BONALDO, P., BOONE, D. L., BORNHAUSER, B. C., BORTOLUCI, K. R., BOSSIS, I., BOST, F., BOURQUIN, J. P., BOYA, P., BOYER-GUITTAUT, M., BOZHKOV, P. V., BRADY, N. R., BRANCOLINI, C., BRECH, A., BRENMAN, J. E., BRENNAND, A., BRESNICK, E. H., BREST, P., BRIDGES, D., BRISTOL, M. L., BROOKES, P. S., BROWN, E. J., BRUMELL, J. H., et al. 2012. Guidelines for the use and interpretation of assays for monitoring autophagy. *Autophagy,* 8, 445-544.

KUTATELADZE, T. G. 2010. Translation of the phosphoinositide code by PI effectors. *Nat Chem Biol,* 6, 507-13.

LEIPE, D. D., WOLF, Y. I., KOONIN, E. V. & ARAVIND, L. 2002. Classification and evolution of P-loop GTPases and related ATPases. *J Mol Biol,* 317, 41-72.

LEVINE, N. D. 1988. Progress in taxonomy of the Apicomplexan protozoa. *J Protozool,* 35, 518-20.

LI, G., ZHANG, J., SUN, Y., WANG, H. & WANG, Y. 2009. The evolutionarily dynamic IFN-inducible GTPase proteins play conserved immune functions in vertebrates and cephalochordates. *Mol Biol Evol,* 26, 1619-30.

LIEBERMAN, L. A. & HUNTER, C. A. 2002. The role of cytokines and their signaling pathways in the regulation of immunity to Toxoplasma gondii. *Int Rev Immunol,* 21, 373-403.

LIESENFELD, O., PARVANOVA, I., ZERRAHN, J., HAN, S. J., HEINRICH, F., MUNOZ, M., KAISER, F., AEBISCHER, T., BUCH, T., WAISMAN, A., REICHMANN, G., UTERMOHLEN, O., VON STEBUT, E., VON LOEWENICH, F. D., BOGDAN, C., SPECHT, S., SAEFTEL, M., HOERAUF, A., MOTA, M. M., KONEN-WAISMAN, S., KAUFMANN, S. H. & HOWARD, J. C. 2011. The IFN-gamma-inducible GTPase, Irga6, protects mice against Toxoplasma gondii but not against Plasmodium berghei and some other intracellular pathogens. *PLoS One,* 6, e20568.

LILUE, J. 2012. *IRG protein family mediates resistance of mice against virulent strains of Toxoplasma gondii.* University of Cologne.

LILUE, J., MULLER, U. B., STEINFELDT, T. & HOWARD, J. C. 2013. Reciprocal virulence and resistance polymorphism in the relationship between Toxoplasma gondii and the house mouse. *Elife,* 2, e01298.

LINDENMANN, J., LANE, C. A. & HOBSON, D. 1963. The Resistance of A2g Mice to Myxoviruses. *J Immunol,* 90, 942-51.

LING, Y. M., SHAW, M. H., AYALA, C., COPPENS, I., TAYLOR, G. A., FERGUSON, D. J. & YAP, G. S. 2006. Vacuolar and plasma membrane stripping and autophagic elimination of Toxoplasma gondii in primed effector macrophages. *J Exp Med,* 203, 2063-71.

LIU, B., GULATI, A. S., CANTILLANA, V., HENRY, S. C., SCHMIDT, E. A., DANIELL, X., GROSSNIKLAUS, E., SCHOENBORN, A. A., SARTOR, R. B. & TAYLOR, G. A. 2013. Irgm1-deficient mice exhibit Paneth cell abnormalities and increased susceptibility to acute intestinal inflammation. *Am J Physiol Gastrointest Liver Physiol,* 305, G573-84.

LUAN, Z., ZHANG, Y., LIU, A., MAN, Y., CHENG, L. & HU, G. 2002. A novel GTP-binding protein hGBP3 interacts with NIK/HGK. *FEBS Lett,* 530, 233-8.

MACMICKING, J. D. 2012. Interferon-inducible effector mechanisms in cell-autonomous immunity. *Nat Rev Immunol,* 12, 367-82.

MACMICKING, J. D., TAYLOR, G. A. & MCKINNEY, J. D. 2003. Immune control of tuberculosis by IFN-gamma-inducible LRG-47. *Science,* 302, 654-9.

MARTENS, S. 2004. Cell-Biology of Interferon Inducible GTPases. *PhD Thesis. Institute for Genetics, University of Cologne, Cologne*.

MARTENS, S. & HOWARD, J. 2006. The interferon-inducible GTPases. *Annu Rev Cell Dev Biol,* 22, 559-89.

MARTENS, S., PARVANOVA, I., ZERRAHN, J., GRIFFITHS, G., SCHELL, G., REICHMANN, G. & HOWARD, J. C. 2005. Disruption of Toxoplasma gondii parasitophorous vacuoles by the mouse p47-resistance GTPases. *PLoS Pathog,* 1, e24.

MARTENS, S., SABEL, K., LANGE, R., UTHAIAH, R., WOLF, E. & HOWARD, J. C. 2004. Mechanisms regulating the positioning of mouse p47 resistance GTPases LRG-47 and IIGP1 on cellular membranes: retargeting to plasma membrane induced by phagocytosis. *J Immunol,* 173, 2594-606.

MEDZHITOV, R. & JANEWAY, C. A., JR. 2002. Decoding the patterns of self and nonself by the innate immune system. *Science,* 296, 298-300.

MELZER, T., DUFFY, A., WEISS, L. M. & HALONEN, S. K. 2008. The gamma interferon (IFN-gamma)-inducible GTP-binding protein IGTP is necessary for toxoplasma vacuolar disruption and induces parasite egression in IFN-gamma-stimulated astrocytes. *Infect Immun,* 76, 4883-94.

MEUNIER, E., DICK, M. S., DREIER, R. F., SCHURMANN, N., KENZELMANN BROZ, D., WARMING, S., ROOSE-GIRMA, M., BUMANN, D., KAYAGAKI, N., TAKEDA, K., YAMAMOTO, M. & BROZ, P. 2014. Caspase-11 activation requires lysis of pathogen-containing vacuoles by IFN-induced GTPases. *Nature,* 509, 366-70.

MIYAIRI, I., TATIREDDIGARI, V. R., MAHDI, O. S., ROSE, L. A., BELLAND, R. J., LU, L., WILLIAMS, R. W. & BYRNE, G. I. 2007. The p47 GTPases Iigp2 and Irgb10 regulate innate immunity and inflammation to murine Chlamydia psittaci infection. *J Immunol,* 179, 1814-24.

MIZUTA, H., WATANABE, S., SAKURAI, Y., NISHIYAMA, K., FURUTA, T., KOBAYASHI, Y. & IWAMURA, M. 2002. Design, synthesis, photochemical properties and cytotoxic activities of water-soluble caged L-leucyl-L-leucine methyl esters that control apoptosis of immune cells. *Bioorg Med Chem,* 10, 675-83.

MORISAKI, J. H., HEUSER, J. E. & SIBLEY, L. D. 1995. Invasion of Toxoplasma gondii occurs by active penetration of the host cell. *J Cell Sci,* 108 (Pt 6), 2457-64.

MORRISON, R. P. & CALDWELL, H. D. 2002. Immunity to murine chlamydial genital infection. *Infect Immun,* 70, 2741-51.

MOULDER, J. W. 1991. Interaction of chlamydiae and host cells in vitro. *Microbiol Rev,* 55, 143-90.

MÜLLER, U. 2014. *Polymorphism in the IRG resistance system determines virulence of Toxoplasma gondii in mice.*

MURPHY, K., TRAVERS, P., WALPORT, M. & JANEWAY, C. 2012. *Janeway's immunobiology,* New York, Garland Science.

NAIRZ, M., FRITSCHE, G., BRUNNER, P., TALASZ, H., HANTKE, K. & WEISS, G. 2008. Interferon-gamma limits the availability of iron for intramacrophage Salmonella typhimurium. *Eur J Immunol,* 38, 1923-36.

NATHAN, C. & DING, A. 2010. SnapShot: Reactive Oxygen Intermediates (ROI). *Cell,* 140, 951-951 e2.

NATHAN, C. & SHILOH, M. U. 2000. Reactive oxygen and nitrogen intermediates in the relationship between mammalian hosts and microbial pathogens. *Proc Natl Acad Sci U S A,* 97, 8841-8.

NATHAN, C. F., MURRAY, H. W., WIEBE, M. E. & RUBIN, B. Y. 1983. Identification of interferon-gamma as the lymphokine that activates human macrophage oxidative metabolism and antimicrobial activity. *J Exp Med,* 158, 670-89.

NEIL, S. J., ZANG, T. & BIENIASZ, P. D. 2008. Tetherin inhibits retrovirus release and is antagonized by HIV-1 Vpu. *Nature,* 451, 425-30.

NELSON, D. E., VIROK, D. P., WOOD, H., ROSHICK, C., JOHNSON, R. M., WHITMIRE, W. M., CRANE, D. D., STEELE-MORTIMER, O., KARI, L., MCCLARTY, G. & CALDWELL, H. D. 2005. Chlamydial IFN-gamma immune evasion is linked to host infection tropism. *Proc Natl Acad Sci U S A,* 102, 10658-63.

OHSHIMA, J., LEE, Y., SASAI, M., SAITOH, T., SU MA, J., KAMIYAMA, N., MATSUURA, Y., PANN-GHILL, S., HAYASHI, M., EBISU, S., TAKEDA, K., AKIRA, S. & YAMAMOTO, M. 2014. Role of mouse and human autophagy proteins in IFN-gamma-induced cell-autonomous responses against Toxoplasma gondii. *J Immunol,* 192, 3328-35.

OLSZEWSKI, M. A., GRAY, J. & VESTAL, D. J. 2006. In silico genomic analysis of the human and murine guanylate-binding protein (GBP) gene clusters. *J Interferon Cytokine Res,* 26, 328-52.

PAPIC, N., HUNN, J. P., PAWLOWSKI, N., ZERRAHN, J. & HOWARD, J. C. 2008. Inactive and active states of the interferon-inducible resistance GTPase, Irga6, in vivo. *J Biol Chem,* 283, 32143-51.

PARKES, M., BARRETT, J. C., PRESCOTT, N. J., TREMELLING, M., ANDERSON, C. A., FISHER, S. A., ROBERTS, R. G., NIMMO, E. R., CUMMINGS, F. R., SOARS, D., DRUMMOND, H., LEES, C. W., KHAWAJA, S. A., BAGNALL, R., BURKE, D. A., TODHUNTER, C. E., AHMAD, T., ONNIE, C. M., MCARDLE, W., STRACHAN, D., BETHEL, G., BRYAN, C., LEWIS, C. M., DELOUKAS, P., FORBES, A., SANDERSON, J., JEWELL, D. P., SATSANGI, J., MANSFIELD, J. C., CARDON, L. & MATHEW, C. G. 2007. Sequence variants in the autophagy gene IRGM and multiple other replicating loci contribute to Crohn's disease susceptibility. *Nat Genet,* 39, 830-2.

PAWLOWSKI, N., KHAMINETS, A., HUNN, J. P., PAPIC, N., SCHMIDT, A., UTHAIAH, R. C., LANGE, R., VOPPER, G., MARTENS, S., WOLF, E. & HOWARD, J. C. 2011. The activation mechanism of Irga6, an interferon-inducible GTPase contributing to mouse resistance against Toxoplasma gondii. *BMC Biol,* 9, 7.

PFEFFERKORN, E. R. 1984. Interferon gamma blocks the growth of Toxoplasma gondii in human fibroblasts by inducing the host cells to degrade tryptophan. *Proc Natl Acad Sci U S A,* 81, 908-12.

PILLA, D. M., HAGAR, J. A., HALDAR, A. K., MASON, A. K., DEGRANDI, D., PFEFFER, K., ERNST, R. K., YAMAMOTO, M., MIAO, E. A. & COERS, J. 2014. Guanylate binding proteins promote caspase-11-dependent pyroptosis in response to cytoplasmic LPS. *Proc Natl Acad Sci U S A,* 111, 6046-51.

PRAEFCKE, G. J. & MCMAHON, H. T. 2004. The dynamin superfamily: universal membrane tubulation and fission molecules? *Nat Rev Mol Cell Biol,* 5, 133-47.

RAMALHO-SANTOS, M., YOON, S., MATSUZAKI, Y., MULLIGAN, R. C. & MELTON, D. A. 2002. "Stemness": transcriptional profiling of embryonic and adult stem cells. *Science,* 298, 597-600.

RANDOW, F., MACMICKING, J. D. & JAMES, L. C. 2013. Cellular self-defense: how cell-autonomous immunity protects against pathogens. *Science,* 340, 701-6.

REID, A. J., VERMONT, S. J., COTTON, J. A., HARRIS, D., HILL-CAWTHORNE, G. A., KONEN-WAISMAN, S., LATHAM, S. M., MOURIER, T., NORTON, R., QUAIL, M. A., SANDERS, M., SHANMUGAM, D., SOHAL, A., WASMUTH, J. D., BRUNK, B., GRIGG, M. E., HOWARD, J. C., PARKINSON, J., ROOS, D. S., TREES, A. J., BERRIMAN, M., PAIN, A. & WASTLING, J. M. 2012. Comparative genomics of the apicomplexan parasites Toxoplasma gondii and Neospora caninum: Coccidia differing in host range and transmission strategy. *PLoS Pathog,* 8, e1002567.

REPNIK, U., HAFNER CESEN, M. & TURK, B. 2014. Lysosomal membrane permeabilization in cell death: Concepts and challenges. *Mitochondrion*.

RHODE, C. 2007. Genetic and functional studies on the conserved IRG (immunity-related GTPase) protein Irgc (CINEMA)

PhD Thesis. Institute for Genetics, University of Cologne, Cologne, Germany.

ROBERTSEN, B., ZOU, J., SECOMBES, C. & LEONG, J. A. 2006. Molecular and expression analysis of an interferon-gamma-inducible guanylate-binding protein from rainbow trout (Oncorhynchus mykiss). *Dev Comp Immunol,* 30, 1023-33.

RUSINOVA, I., FORSTER, S., YU, S., KANNAN, A., MASSE, M., CUMMING, H., CHAPMAN, R. & HERTZOG, P. J. 2013. Interferome v2.0: an updated database of annotated interferon-regulated genes. *Nucleic Acids Res,* 41, D1040-6.

SADLER, A. J. & WILLIAMS, B. R. 2008. Interferon-inducible antiviral effectors. *Nat Rev Immunol,* 8, 559-68.

SANTIAGO, H. C., FENG, C. G., BAFICA, A., ROFFE, E., ARANTES, R. M., CHEEVER, A., TAYLOR, G., VIEIRA, L. Q., ALIBERTI, J., GAZZINELLI, R. T. & SHER, A. 2005. Mice deficient in LRG-47 display enhanced susceptibility to Trypanosoma cruzi infection associated with defective hemopoiesis and intracellular control of parasite growth. *J Immunol,* 175, 8165-72.

SCHARTON-KERSTEN, T. M., WYNN, T. A., DENKERS, E. Y., BALA, S., GRUNVALD, E., HIENY, S., GAZZINELLI, R. T. & SHER, A. 1996. In the absence of endogenous IFN-gamma, mice develop unimpaired IL-12 responses to Toxoplasma gondii while failing to control acute infection. *J Immunol,* 157, 4045-54.

SCHRODER, K., HERTZOG, P. J., RAVASI, T. & HUME, D. A. 2004. Interferon-gamma: an overview of signals, mechanisms and functions. *J Leukoc Biol,* 75, 163-89.

SHENOY, A. R., KIM, B. H., CHOI, H. P., MATSUZAWA, T., TIWARI, S. & MACMICKING, J. D. 2007. Emerging themes in IFN-gamma-induced macrophage immunity by the p47 and p65 GTPase families. *Immunobiology,* 212, 771-84.

SHENOY, A. R., WELLINGTON, D. A., KUMAR, P., KASSA, H., BOOTH, C. J., CRESSWELL, P. & MACMICKING, J. D. 2012. GBP5 promotes NLRP3 inflammasome assembly and immunity in mammals. *Science,* 336, 481-5.

SHINKAI, Y., RATHBUN, G., LAM, K. P., OLTZ, E. M., STEWART, V., MENDELSOHN, M., CHARRON, J., DATTA, M., YOUNG, F., STALL, A. M. & ET AL. 1992. RAG-2-deficient mice lack mature lymphocytes owing to inability to initiate V(D)J rearrangement. *Cell,* 68, 855-67.

SHWAB, E. K., ZHU, X. Q., MAJUMDAR, D., PENA, H. F., GENNARI, S. M., DUBEY, J. P. & SU, C. 2013. Geographical patterns of Toxoplasma gondii genetic diversity revealed by multilocus PCR-RFLP genotyping. *Parasitology*, 1-9.

SIBLEY, L. D. 2003. Toxoplasma gondii: perfecting an intracellular life style. *Traffic,* 4, 581-6.

SIBLEY, L. D. 2011. Invasion and intracellular survival by protozoan parasites. *Immunol Rev,* 240, 72-91.

SIBLEY, L. D., WEIDNER, E. & KRAHENBUHL, J. L. 1985. Phagosome acidification blocked by intracellular Toxoplasma gondii. *Nature,* 315, 416-9.

SIMS, T. A., HAY, J. & TALBOT, I. C. 1989. An electron microscope and immunohistochemical study of the intracellular location of Toxoplasma tissue cysts within the brains of mice with congenital toxoplasmosis. *Br J Exp Pathol,* 70, 317-25.

SINGH, S. B., DAVIS, A. S., TAYLOR, G. A. & DERETIC, V. 2006. Human IRGM induces autophagy to eliminate intracellular mycobacteria. *Science,* 313, 1438-41.

SPEKKER, K., LEINEWEBER, M., DEGRANDI, D., INCE, V., BRUNDER, S., SCHMIDT, S. K., STUHLSATZ, S., HOWARD, J. C., SCHARES, G., DEGISTIRICI, O., MEISEL, R., SORG, R. V., SEISSLER, J., HEMPHILL, A., PFEFFER, K. & DAUBENER, W. 2013. Antimicrobial effects of murine mesenchymal stromal cells directed against Toxoplasma gondii and Neospora caninum: role of immunity-related GTPases (IRGs) and guanylate-binding proteins (GBPs). *Med Microbiol Immunol,* 202, 197-206.

SPRINGER-FRAUENHOFF, H. M. 2014. *The Immunity-related GTPase (IRG) resistance system against intracellular parasites.*

SPRINGER, H. M., SCHRAMM, M., TAYLOR, G. A. & HOWARD, J. C. 2013. Irgm1 (LRG-47), a regulator of cell-autonomous immunity, does not localize to mycobacterial or listerial phagosomes in IFN-gamma-induced mouse cells. *J Immunol,* 191, 1765-74.

STAEHELI, P., HALLER, O., BOLL, W., LINDENMANN, J. & WEISSMANN, C. 1986. Mx protein: constitutive expression in 3T3 cells transformed with cloned Mx cDNA confers selective resistance to influenza virus. *Cell,* 44, 147-58.

STEINFELDT, T., KONEN-WAISMAN, S., TONG, L., PAWLOWSKI, N., LAMKEMEYER, T., SIBLEY, L. D., HUNN, J. P. & HOWARD, J. C. 2010. Phosphorylation of mouse immunity-related GTPase (IRG) resistance proteins is an evasion strategy for virulent Toxoplasma gondii. *PLoS biology,* 8, e1000576.

STREMLAU, M., OWENS, C. M., PERRON, M. J., KIESSLING, M., AUTISSIER, P. & SODROSKI, J. 2004. The cytoplasmic body component TRIM5alpha restricts HIV-1 infection in Old World monkeys. *Nature,* 427, 848-53.

SUSS-TOBY, E., ZIMMERBERG, J. & WARD, G. E. 1996. Toxoplasma invasion: the parasitophorous vacuole is formed from host cell plasma membrane and pinches off via a fission pore. *Proc Natl Acad Sci U S A,* 93, 8413-8.

SUZUKI, Y., ORELLANA, M. A., SCHREIBER, R. D. & REMINGTON, J. S. 1988. Interferon-gamma: the major mediator of resistance against Toxoplasma gondii. *Science,* 240, 516-8.

TAKAI, Y., SASAKI, T. & MATOZAKI, T. 2001. Small GTP-binding proteins. *Physiol Rev,* 81, 153-208.

TAYLOR, G. A., COLLAZO, C. M., YAP, G. S., NGUYEN, K., GREGORIO, T. A., TAYLOR, L. S., EAGLESON, B., SECREST, L., SOUTHON, E. A., REID, S. W., TESSAROLLO, L., BRAY, M., MCVICAR, D. W., KOMSCHLIES, K. L., YOUNG, H. A., BIRON, C. A., SHER, A. & VANDE WOUDE, G. F. 2000. Pathogen-specific loss of host resistance in mice lacking the IFN-gamma-inducible gene IGTP. *Proc Natl Acad Sci U S A,* 97, 751-5.

TAYLOR, G. A., FENG, C. G. & SHER, A. 2004. p47 GTPases: regulators of immunity to intracellular pathogens. *Nat Rev Immunol,* 4, 100-9.

TAYLOR, G. A., JEFFERS, M., LARGAESPADA, D. A., JENKINS, N. A., COPELAND, N. G. & VANDE WOUDE, G. F. 1996. Identification of a novel GTPase, the inducibly expressed GTPase, that accumulates in response to interferon gamma. *J Biol Chem,* 271, 20399-405.

TAYLOR, G. A., STAUBER, R., RULONG, S., HUDSON, E., PEI, V., PAVLAKIS, G. N., RESAU, J. H. & VANDE WOUDE, G. F. 1997. The inducibly expressed GTPase localizes to the endoplasmic reticulum, independently of GTP binding. *J Biol Chem,* 272, 10639-45.

THOLEN, S., BINIOSSEK, M. L., GANSZ, M., AHRENS, T. D., SCHLIMPERT, M., KIZHAKKEDATHU, J. N., REINHECKEL, T. & SCHILLING, O. 2014. Double deficiency of cathepsins B and L results in massive secretome alterations and suggests a degradative cathepsin-MMP axis. *Cell Mol Life Sci,* 71, 899-916.

TIWARI, S., CHOI, H. P., MATSUZAWA, T., PYPAERT, M. & MACMICKING, J. D. 2009. Targeting of the GTPase Irgm1 to the phagosomal membrane via PtdIns(3,4)P(2) and PtdIns(3,4,5)P(3) promotes immunity to mycobacteria. *Nat Immunol,* 10, 907-17.

TRAVER, M. K., HENRY, S. C., CANTILLANA, V., OLIVER, T., HUNN, J. P., HOWARD, J. C., BEER, S., PFEFFER, K., COERS, J. & TAYLOR, G. A. 2011. Immunity-related GTPase M (IRGM) proteins influence the localization of guanylate-binding protein 2 (GBP2) by modulating macroautophagy. *J Biol Chem,* 286, 30471-80.

TRINCHIERI, G. & SHER, A. 2007. Cooperation of Toll-like receptor signals in innate immune defence. *Nat Rev Immunol,* 7, 179-90.

UCHIMOTO, T., NOHARA, H., KAMEHARA, R., IWAMURA, M., WATANABE, N. & KOBAYASHI, Y. 1999. Mechanism of apoptosis induced by a lysosomotropic agent, L-Leucyl-L-Leucine methyl ester. *Apoptosis,* 4, 357-62.

UTHAIAH, R. C., PRAEFCKE, G. J., HOWARD, J. C. & HERRMANN, C. 2003. IIGP1, an interferon-gamma-inducible 47-kDa GTPase of the mouse, showing cooperative enzymatic activity and GTP-dependent multimerization. *J Biol Chem,* 278, 29336-43.

VERHELST, J., HULPIAU, P. & SAELENS, X. 2013. Mx proteins: antiviral gatekeepers that restrain the uninvited. *Microbiol Mol Biol Rev,* 77, 551-66.

VIRREIRA WINTER, S., NIEDELMAN, W., JENSEN, K. D., ROSOWSKI, E. E., JULIEN, L., SPOONER, E., CARADONNA, K., BURLEIGH, B. A., SAEIJ, J. P., PLOEGH, H. L. & FRICKEL, E. M. 2011. Determinants of GBP recruitment to Toxoplasma gondii vacuoles and the parasitic factors that control it. *PLoS One,* 6, e24434.

WANG, C., DONG, H., WU, X. M., XIA, F., LI, G., JIA, X., HE, S., JIANG, X., LI, H. & XU, H. 2013. Immune-related GTPase Irgm1 exacerbates experimental auto-immune encephalomyelitis by promoting the disruption of blood-brain barrier and blood-cerebrospinal fluid barrier. *Mol Immunol,* 53, 43-51.

WANG, X., HINSON, E. R. & CRESSWELL, P. 2007. The interferon-inducible protein viperin inhibits influenza virus release by perturbing lipid rafts. *Cell Host Microbe,* 2, 96-105.

WHITE, C., LEE, J., KAMBE, T., FRITSCHE, K. & PETRIS, M. J. 2009. A role for the ATP7A copper-transporting ATPase in macrophage bactericidal activity. *J Biol Chem,* 284, 33949-56.

WITTINGHOFER, A. 1997. Signaling mechanistics: aluminum fluoride for molecule of the year. *Curr Biol,* 7, R682-5.

WYNN, T. A., NICOLET, C. M. & PAULNOCK, D. M. 1991. Identification and characterization of a new gene family induced during macrophage activation. *J Immunol,* 147, 4384-92.

XIA, F., LI, R., WANG, C., YANG, S., TIAN, L., DONG, H., PEI, C., HE, S., JIANG, P., CHENG, H., FANG, S., LI, H. & XU, H. 2013. IRGM1 regulates oxidized LDL uptake by macrophage via actin-dependent receptor internalization during atherosclerosis. *Sci Rep,* 3, 1867.

XU, H., WU, Z. Y., FANG, F., GUO, L., CHEN, D., CHEN, J. X., STERN, D., TAYLOR, G. A., JIANG, H. & YAN, S. S. 2010. Genetic deficiency of Irgm1 (LRG-47) suppresses induction of experimental autoimmune encephalomyelitis by promoting apoptosis of activated CD4+ T cells. *Faseb J,* 24, 1583-92.

YAMAMOTO, M., OKUYAMA, M., MA, J. S., KIMURA, T., KAMIYAMA, N., SAIGA, H., OHSHIMA, J., SASAI, M., KAYAMA, H., OKAMOTO, T., HUANG, D. C., SOLDATI-FAVRE, D., HORIE, K., TAKEDA, J. & TAKEDA, K. 2012. A cluster of interferon-gamma-inducible p65 GTPases plays a critical role in host defense against Toxoplasma gondii. *Immunity,* 37, 302-13.

ZERRAHN, J., SCHAIBLE, U. E., BRINKMANN, V., GUHLICH, U. & KAUFMANN, S. H. 2002. The IFN-inducible Golgi- and endoplasmic reticulum- associated 47-kDa GTPase IIGP is transiently expressed during listeriosis. *J Immunol,* 168, 3428-36.

ZHAO, Y. O., KHAMINETS, A., HUNN, J. P. & HOWARD, J. C. 2009b. Disruption of the Toxoplasma gondii parasitophorous vacuole by IFNgamma-inducible immunity-related GTPases (IRG proteins) triggers necrotic cell death. *PLoS Pathog,* 5, e1000288.

ZHAO, Y. O., KONEN-WAISMAN, S., TAYLOR, G. A., MARTENS, S. & HOWARD, J. C. 2010. Localisation and mislocalisation of the interferon-inducible immunity-related GTPase, Irgm1 (LRG-47) in mouse cells. *PLoS One,* 5, e8648.

6. APPENDIX
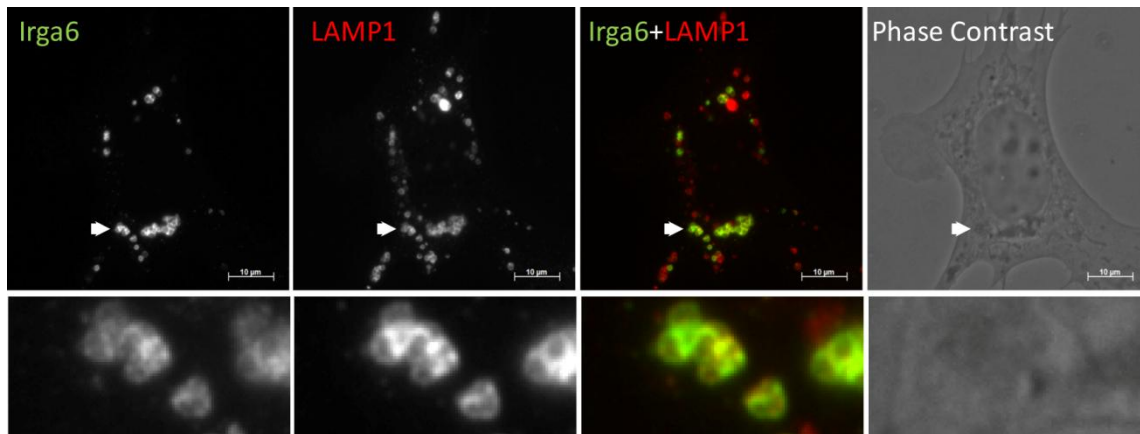
Figure S1. Irga6 structures at the lysosomes are in the GTP-bound state. *Irgm1* KO MEFs were induced with 200 U/ml IFNγ for 24 hours. Cells were fixed and stained with immunoreagents against Irga6 (10D7) and LAMP1. Representative microscopic images of GTP-bound Irga6 and LAMP1 are shown. Arrows point at the Irga6 structures that are magnified below each panel.
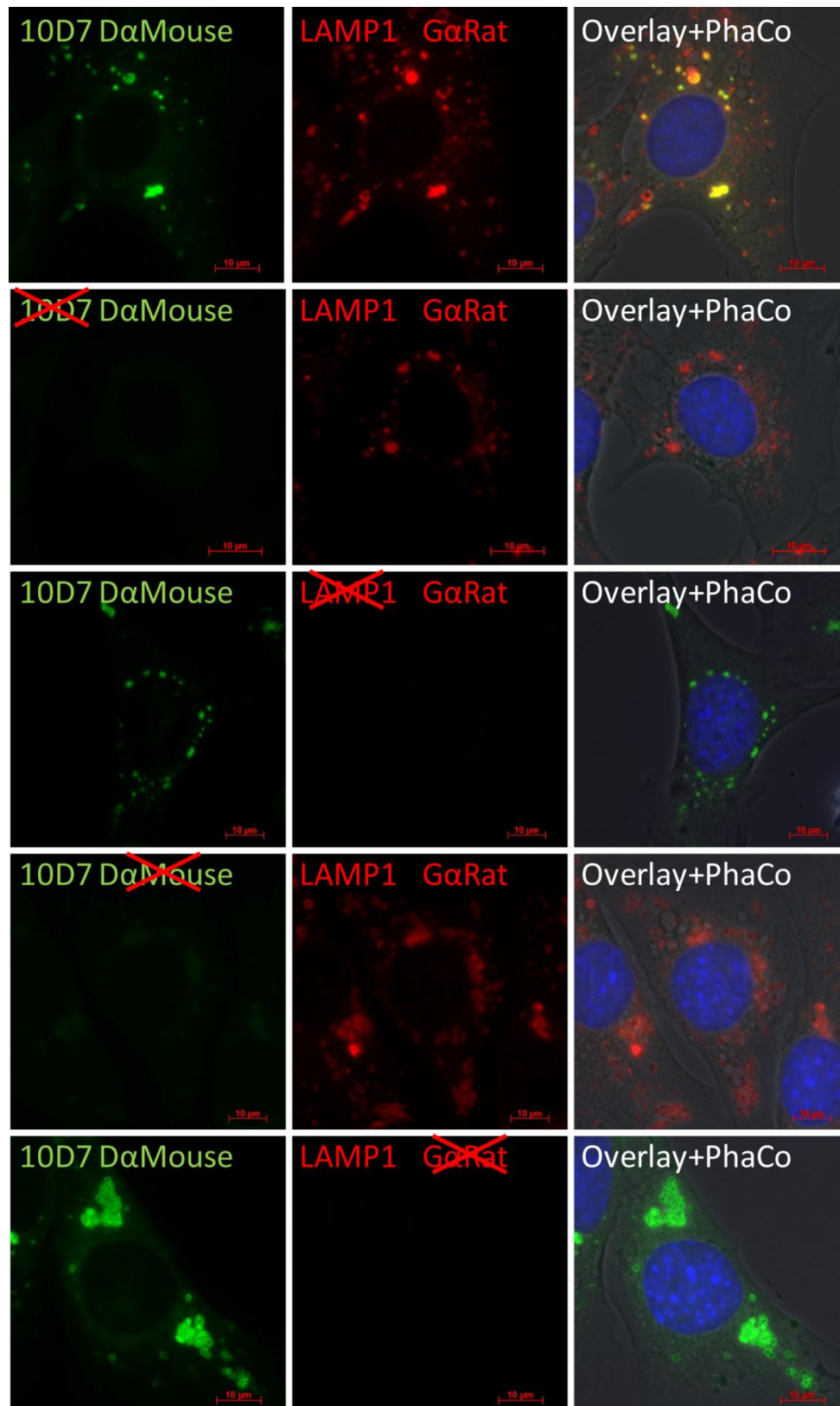
Figure S2. There is no coss-reactivity between 10D7 and 1D4B antibodies. *Irgm1* KO MEFs were induced with 200 U/ml IFNγ for 24 hours. Cells were fixed and stained with mouse antibody 10D7, which stains the Irga6 in GTP-bound state, and rat antibody 1D4B, which stains LAMP1 lysosomal marker. The antibodies were visualised with secondary antibodies Alexa 488 Donkey anti Mouse and Alexa 555 Goat anti rat. To test the cross-reactivity, one of the primary or secondary reagents was omitted in each sample. The images of stained cells were taken. Representative microscopic images of GTP-bound Irga6 and LAMP1 are shown, with omitted antibody being crossed.
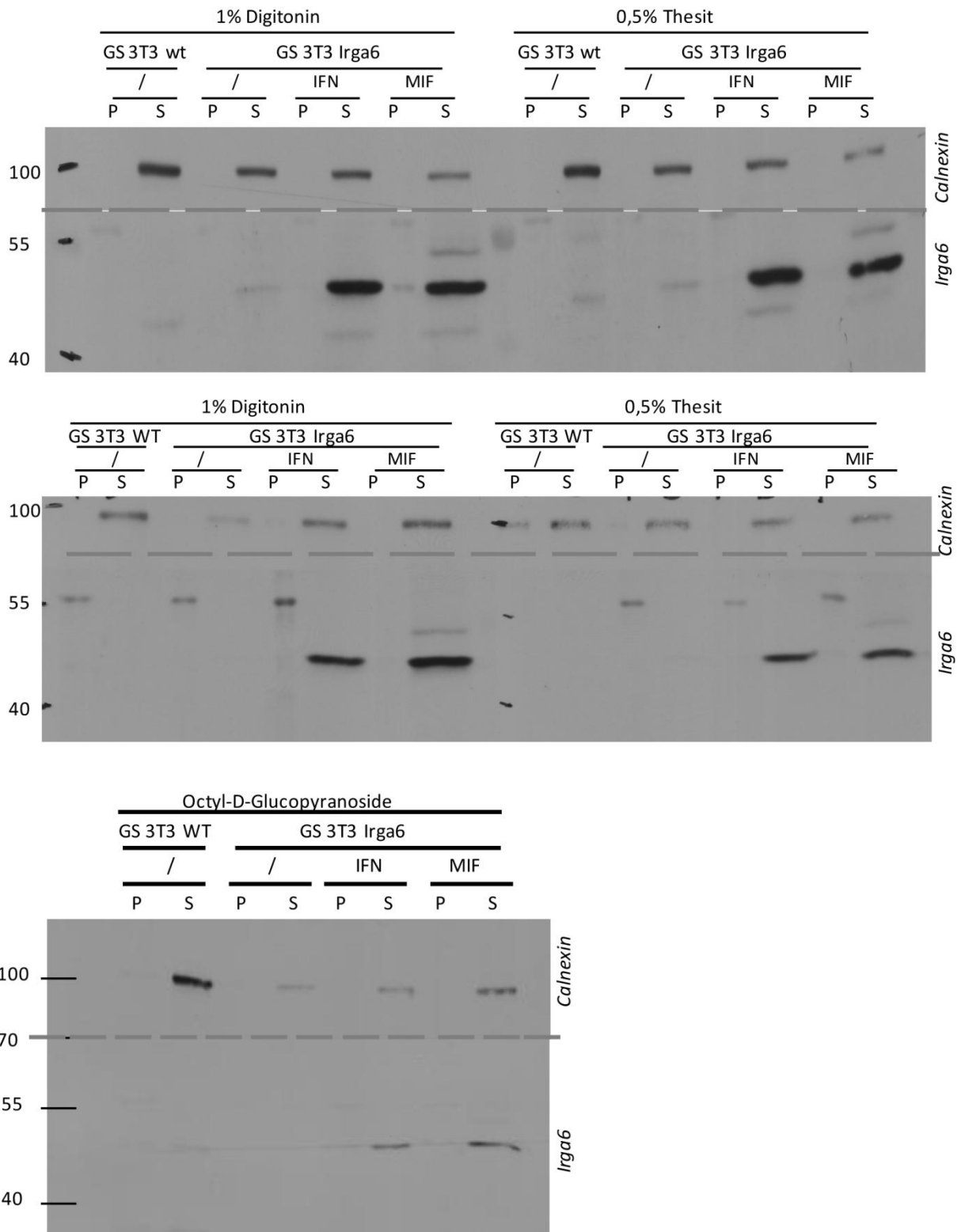
Figure S3. Irga6 aggregate-like structures are detergent soluble. GS 3T3 WT or GS 3T3 Irga6 cells were induced with IFNγ, MIF or left untreated for 24 hours. 30000 cells were lysed in 0,5 % Thesit **(A,B)** , 1% Digitonin **(A,B)** or 80 mM Octyl-D-Glucopyranoside **(C)** and centrifuged at 45000 rpm for 30 minutes. Supernatant and the pellet were separated, analyzed by SDS-PAGE/Western Blot and probed with Irga6 (10E7) and Calnexin antibody. Exposure times: 5-30 seconds.
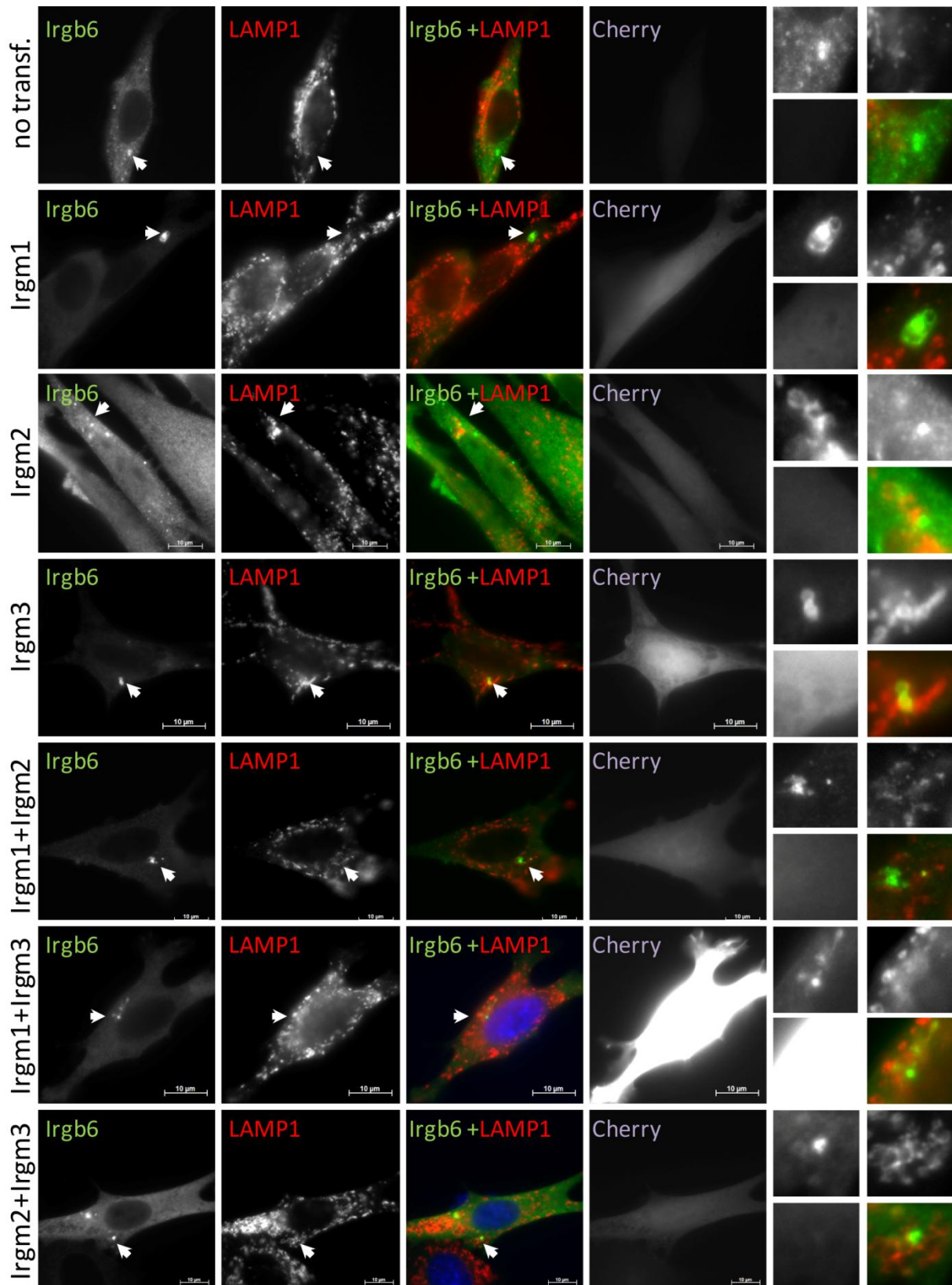
Figure S4. Irgb6 co-localization with LAMP1 in cells transiently transfected with GMS protein A) Gene Switch (GS) 3T3 cells stably transfected with inducible Irgb6 were stimulated with Mifepristone and simultaneously transiently transfected with pGW1H-Irgm1, pGW1H-Irgm2 and pGW1H-Irgm3 and pmCherry for 24 hours. Cells were fixed and stained with anti-Irgb6 antiserum A20 and with anti-LAMP1 antibody. Representative microscopic images of Irgb6, LAMP1 and Cherry are shown. Arrows point at the Irgb6 structures which are magnified at the end of each panel (zoom in the following order: upper left: Irgb6, upper right: LAMP1, lower left: Cherry, lower right: overlay of Irgb6 and LAMP1).
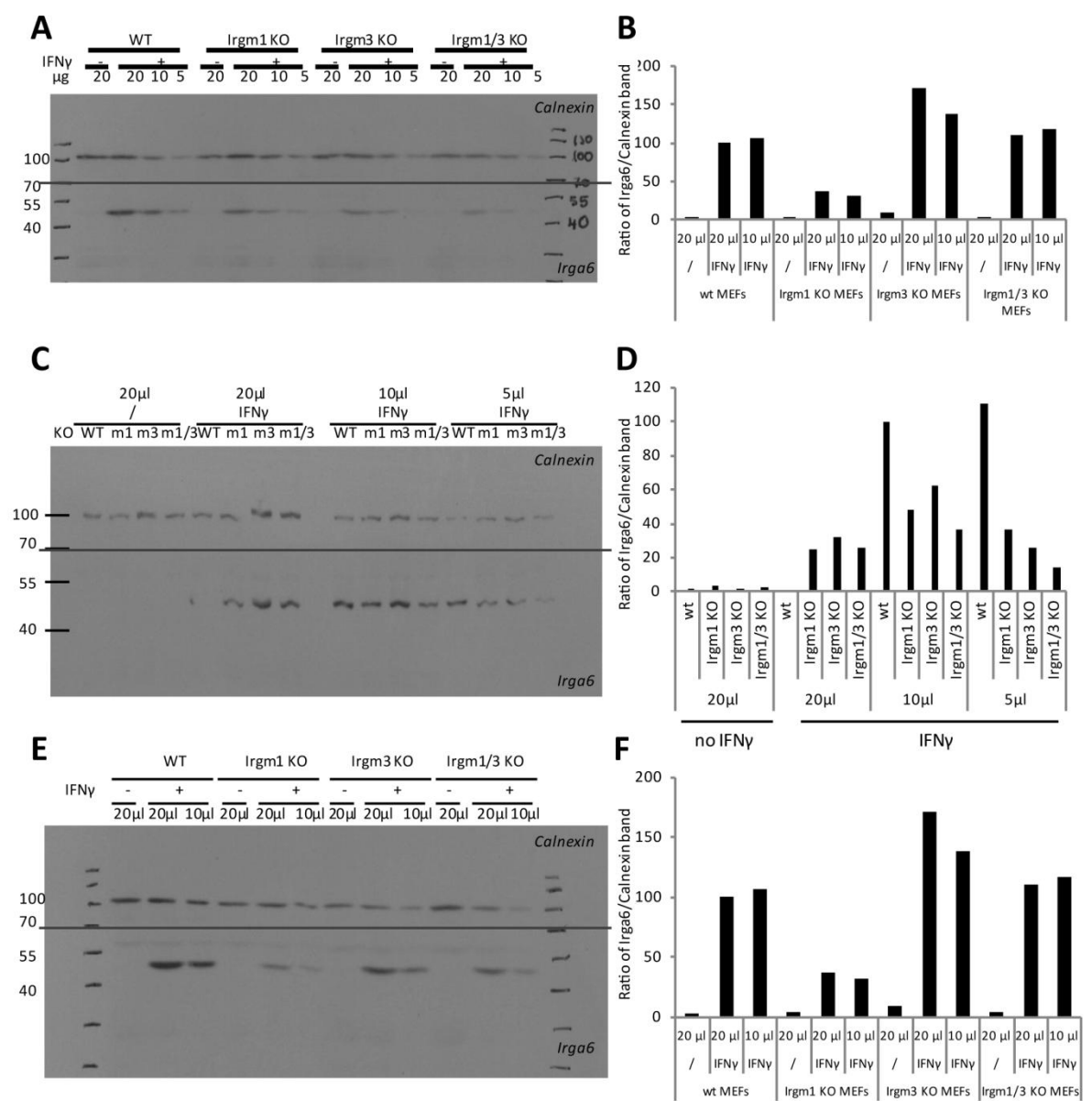
Figure S5. **Irga6 levels in GMS KO cells.** WT, *Irgm1* KO, *Irgm3* KO and *Irgm1/Irgm3* KO MEFs were induced with 200 U/ml IFNγ for 24 h or left untreated. 200 000 cells were lysed in 100µl of 0,5% NP-40 and 5, 10 or 20 µl of the lysate were analyzed by SDS-PAGE/Western blot. Membranes were probed with anti-Irga6 (10E7) and anti-Calnexin immunoreagents. Exposure times are between 5 and 30 seconds. **(A,C,E).** Intensities of Irga6 and Calnexin bands were quantified with appropriate software and ratios of Irga6/Calnexin band intensities are depicted **(B,D,F).** Results of 3 independent experiments **(A,C,E)** are shown.

7. SUMMARY

Immunity-related GTPases (IRGs) play an important role in host immune response to a variety of intracellular pathogens by accumulation at the membranes of the pathogens and their disruption. However, it was never understood how exactly IRG proteins distinguish the membranes of the pathogen from the host membranes.

Previously, it has been reported that regulatory IRG proteins, named GMS proteins, keep the effector IRG proteins, named GKS proteins, in the inactive GDP-bound state. In this study, it has been shown that GMS proteins also play an important role in protection of the endocellular compartments from GKS protein off-target activation. In the absence of the GMS protein Irgm1, which is localized at the lysosomes, GKS proteins Irga6, Irgb6, Irgb10 and Irgd accumulate and activate at these organelles. In the absence of Irgm3, a GMS protein which is localized at the endoplasmic reticulum (ER), GKS protein Irga6 accumulates at the ER. However, in the cells that lack Irgm1 and Irgm3, GKS proteins accumulate only to lipid droplets, but not to lysosomes or ER, indicating that GKS structures do not accumulate at every GMS-free membrane.

In the second part of the study, the consequences Irgm1 accumulation to the lysosomes are investigated. *Irgm1* KO mice undergo leukopenia and succumb after a variety of infections and inflammatory states. The results of this study suggest that the failure of *Irgm1* KO mice is rather an indirect consequence of the off-target action of the GKS proteins, than the direct consequence of the Irgm1 response to a variety of pathogens. The GKS proteins, that accumulate at the lysosomes in *Irgm1* KO cells, affect the acidity of these organelles and therefore lysosomal ability to process autophagosomes. In IFNγ-induced *Irgm1* KO mouse embryonic fibroblasts (MEFs) the mature autophagosome marker LC3-II level is enhanced, the number of autophagosomes is increased and the co-localization between autophagosomes and lysosomes is higher than in the non-induced cells.

Therefore, in this study, it is proposed that the autophagic flux of IFNγ-induced *Irgm1* KO MEFs is impaired. The lymphocytes of the *Irgm1* KO mice, that are stimulated to proliferate as a response to infection, could be the cells that are most affected by autophagic flux arrest and lysosomal acidification impairment. Thus, this effect could be the cause of described defects in lymphocyte proliferation and lymphocyte necrosis, which cause the death of the *Irgm1* KO mouse

8. ZUSAMMENFASSUNG

Die Immun-verwanden GTPasen (Immunity-related GTPases, IRGs) spielen eine wichtige Rolle in der Resistenz gegen intrazelluläre Pathogene, wofür sie vom Zytosol auf bestimmten Membranen der Erreger akkumulieren und jene Zerstörung einleiten. Bisher hat man es jedoch noch nicht wirklich verstanden, wie genau diese Interferon-induzierten IRG-Proteine ihre eigenen zellulären Membranen von Membranen der Pathogenen unterscheiden.

Bislang wurde bekannt, dass die regulatorischen IRG-Proteine, auch GMS-Proteine genannt, die Effektor IRG-Proteine, auch GKS-Proteine genannt, in einem inaktiven GDP-gebundenen Zustand halten. In der vorliegenden Arbeit wurde gezeigt, dass die GMS-Proteine ebenfalls die eigenen Endozellulären-Membranen vor deregulierten GKS-Proteinen schützen. Wenn das GMS-Protein Irgm1 fehlt, das unter anderem an Lysosomen zu finden ist, akkumulieren die GKS-Proteine Irga6, Irgb6, Irgb10 und Irgd an den Lysosomen. Wenn Irgm3 fehlt, ein GMS-Protein an dem Endoplasmatischem Retikulum (ER), lokalisiert das GKS-Protein Irga6 an das ER. Wenn jedoch beide Proteine, Irgm1 und Irgm3, fehlen, finden sich GKS-Proteine nur an den Lipid-Droplet Organellen, jedoch nicht auf den Lysosomen oder dem ER, obwohl diese Organellen auch keine GMS-Proteine tragen. Somit scheinen GKS-Proteine nicht wie erwartet auf jeder GMS-freie Membran zu akkumulieren.

In dem zweiten Teil dieser Arbeit wurden die Folgen von Aggregat-Bildung auf Lysosomen in Zellen der *Irgm1* knock-out Maus. Diese Mäuse leiden unter Leukopenie und sterben bei Infektion mit jeglichen Pathogenen und Entzündungsreaktionen. Die Ergebnisse der vorliegenden Arbeit unterstützen die Hypothese, dass der Tod von *Irgm1* KO Mäuse durch deregulierte Aktivierung der GKS-Proteinen bedingt wird, und nicht eine direkte Folge von einer fehlenden Wirkung von Irgm1 ist. Die GKS-Proteine, die an Lysosomen in *Irgm1* KO Zellen akkumulieren, vermindern den Säuregehalt der Lysosomen und somit den Abbau von Autophagosomen durch Lysosomen. In IFNγ-induzierten *Irgm1* KO Zellen ist LC3-II, ein Marker für reife Autophagosomen, gesteigert, die Anzahl der Autophagosomen ist erhöht und die Kolokalisierung zwischen Autophagosomen und Lysosomen ist auch höher als in nicht-induzierten Zellen.

Deshalb schlagen die Ergebnisse der vorliegenden Arbeit vor, dass der Autophagie-Ablauf in IFNγ-induzierten *Irgm1* KO MEFs gestört ist. Deswegen sind die Lymphozyten der *Irgm1* KO Mäusen, die durch Infektionen stimuliert sich stark vermehren, möglicherweise die Zellen, die am meisten von den Störungen in Autophagie und Lysosome-Säuregehalt betroffen sind. Das könnte die Proliferation der Lymphozyten stören und sogar ihren Zelltod einleiten und schließlich den Tod der *Irgm1* KO Mäuse verursachen.

9. ACKNOWLEDGEMENTS

10. DECLARATION

I hereby declare that I elaborated the entire PhD thesis on my own and that I used only the references listed.

Ich versichere, dass ich die von mir vorgelegte Dissertation selbständig angefertigt, die benutzten Quellen und Hilfsmittel vollständig angegeben und die Stellen der Arbeit − einschließlich Tabellen, Karten und Abbildungen −, die anderen Werken im Wortlaut oder dem Sinn nach entnommen sind, in jedem Einzelfall als Entlehnung kenntlich gemacht habe; dass diese Dissertation noch keiner anderen Fakultät oder Universität zur Prüfung vorgelegen hat; dass sie − abgesehen von unten angegebenen Teilpublikationen − noch nicht veröffentlicht worden ist, sowie, dass ich eine solche Veröffentlichung vor Abschluss des Promotionsverfahrens nicht vornehmen werde. Die Bestimmungen der Promotionsordnung sind mir bekannt. Die von mir vorgelegte Dissertation ist von Prof. Dr. Jonathan Howard betreut worden.

Köln, 17. November 2014

Jelena Maric

11. LEBENSLAUF

Persönliche daten:

Name: Jelena Marić

Addresse: Brüdergasse 15, 53111 Bonn

E-Mail: jelenamaricns@gmail.com

Geburtsdatum/Ort: 11.05.1984. Šabac, Serbien

Nationalität: Serbisch

Ausbildung:

2010-2014   Doktorandin

Institut für Genetik, Mathematisch-Naturwissenschafliche Fakultät

Universität zu Köln

Betreuer: Prof. Dr. Jonathan Howard

Stipendium: DAAD; Mitglied der IGS-DHD

2009-2010   Master von Angewandte pharmazeutsche Wissenschaften

Fakultät Pharmazeutsche Wissenschaften

Gent Universität, Belgien

Abschussarbeit in der Abteilung für Pharmazeutische Biotechnologie;

Betreuer: Prof. Dr. Dieter Deforce; Titel: *Histones are a new substrate for neutrophil elastase: the leukemia model;* mit Auszeichnung bestanden

Stipendium: Basileus, Europäische Komision

2003-2009   Diplom Phamazeutin

Medizinische Fakultät, Universität zu Novi Sad, Serbien

Abschlussarbeit in der Abteilung für Physiologie;

Betreuer. Prof. Dr. Vesna Ivetić;

Titel: *Neurophysiologische Mechanismen der Antiepileptika Wirkung*

Stipendium des Bildungsministeriums, Republik Serbien

1999-2003   Gymnasium Isidora Sekulić, Novi Sad, Serbien

1998-1999   Grundschule Kosta Trifković, Novi Sad, Serbien

1991-1998   Grundschule Stevan Divnin Baba, Žabalj, Serbien